Intrinsic determinants of axon pruning

Antoneta Gavoci

Graduate School of
Systemic Neurosciences
LMU Munich

Dissertation at the
Graduate School of Systemic Neurosciences
Ludwig-Maximilians-Universität München

30th May, 2023

Supervisor
Prof. Dr. med. Thomas Misgeld
Institute of Neuronal Cell Biology
Technical University of Munich

First Reviewer: Prof. Dr. med. Thomas Misgeld
Second Reviewer: Prof. Dr. Carsten Janke
External Reviewer: Prof. Dr. Shaul Yogev

Date of Submission: 30th May, 2023
Date of Defense: 14th September, 2023

Contents

List of Figures

List of Tables

1 Abstract

Developmental neuronal remodeling includes loss of axon branches or dendritic spines and is essential to shape neural circuits. The cytoskeleton plays a central role in this process, as branch-specific microtubule loss is an early indicator of axon dismantling. The underlying regulatory mechanisms driving these cytoskeletal re-arrangements are partially mediated by the microtubule severase Spastin's recruitment to polyglutamylated microtubules. However, whether polyglutamylation plays an instructive role during synapse elimination remains elusive. Here, we show that the enzymes responsible for the removal and addition of polyglutamylation, deglutamylases (CCP), and glutamylases (TTLL), rheostatically regulate pruning through Spastin-mediated severing of microtubules.

Motor neurons lacking CCP1/6 accelerate axon dismantling, while the deletion of TTLL1, a chain-elongating glutamylase on α-tubulin, delayed the remodeling of both PNS and CNS. Surprisingly, deleting TTLL7, which 'seeds' the first glutamate residue to β-tubulin tails, did not affect polyglutamylation or pruning, which suggests a functional divergence of glutamylses to selectively modify either of the tubulin dimers. Further measurements of polyglutamylation, microtubule mass, and dynamics corroborate the predicted branch-specific regulation of microtubule stability. However, axon pruning outcome might be achieved through different modalities downstream of the two enzyme families: CCP1/6 deletion mainly affected MT dynamics of young motor axons, while our preliminary ultrastructural analysis hints that TTLL1 might affect organelle redistribution along the axon. My data further show that synaptic activity coordinates glutamylases and deglutamylases since blocking neurotransmission to simulate punishment signals reduces microtubule mass and modulates polyglutamylation, simi-

lary to CCP1/6 deletion. Indeed, polyglutamylation levels are reestablished to wild-type levels when the effector, Spastin, is also absent in motor axons. Thus, the 'tubulin code,' by endowing the microtubule scaffold with specific and local functionality, could control morphogenic events during the nervous system development through mechanisms conserved across the central and peripheral nervous systems. Future work will focus on finding parallels between physiological axonal pruning and neurodegeneration, as CCP1 mutations are linked to human infantile-onset neurodegeneration and affect the cerebellum, spinal motor neurons, and peripheral nerves. Our data show that adult mice lacking functional CCP1/6 in motor neurons present axonal swellings and display axonal transport defects. Consequently, these degenerating neurons have impaired organelle trafficking and accumulate mito-lysosomes in distal axons.

In conclusion, our findings highlight the importance of elucidating the molecular underpinnings of polyglutamylation and its effects on axon stability during physiological and disease-related remodeling.

2 Introduction

2.1 Developmental synaptic pruning

The mature human brain consists of about 100 billion nerve cells and up to 100 trillion synaptic connections[1]. An immature neuron has to connect with its own specific partners, while navigating a complex entangled and immature environment, crammed with guidance cues. Even more astounding, the immature brain starts with a surplus of synaptic connections that are later removed or "pruned" in an activity dependent manner[2]. Synaptic pruning is a large scale recessive event, as exemplified by studies of the neuromuscular junction (NMJ) of mice, where a ten-fold excess of synapses is rapidly lost in the two first postnatal weeks in mice and two postnatal years in humans[3,4] (Figure 2.1). Thus, a first phase of exuberant connections with temporary targets established during early embryonic development is pruned back at a second stage to leave only functional connections and a mature nervous system.

This counter-intuitive and seemingly “wasteful” process consisting of the generation of superfluous synapses to only discard them at the later stage, might be instead a fundamental biological strategy to refine and correct misguided connections based on experience and preserve only the appropriate connections[5]: which in case of the NMJs, then serve for the rest of the organisms’ life. A fascinating example of a deliberate and elegant development strategy to generate only a few general guidance programs instead of several for each particular connection. A crucial question still remains unanswered: how is this fine orchestration of signals achieved?
Intuitively, the level of accuracy of brain wiring depends on the accuracy of the regulation. Improper wiring are linked to deficits such as those observed

2.1 Developmental synaptic pruning

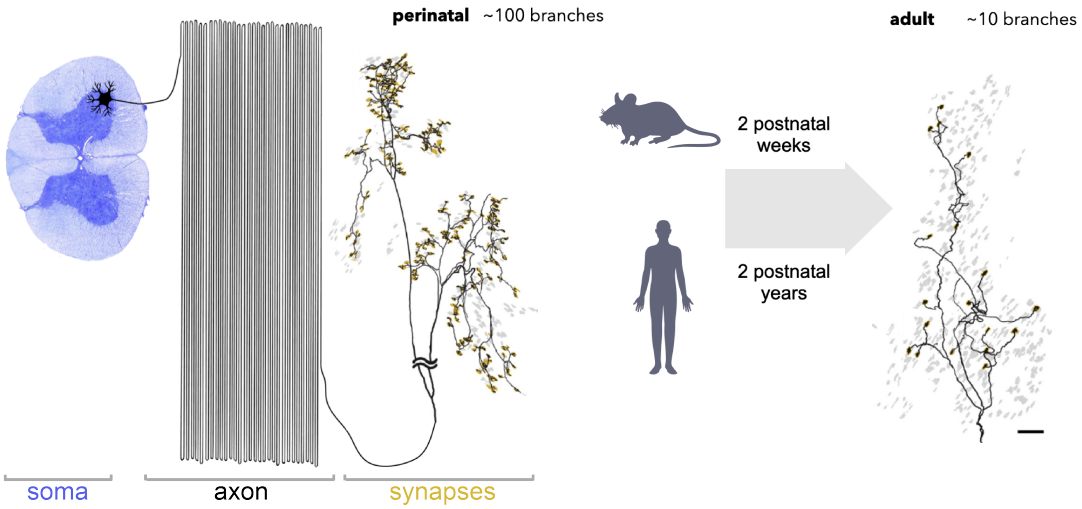

Figure 2.1: ***Developmental axon pruning at NMJ is extensive.*** *Schematic representation of extremely polarized geometry of motoneurons, with somata in the ventral horn of spinal cord, and highly branched axonal arbor, which undergoes 10-fold loss of synapses (yellow spots) during the transition from perinatal to adult stages. Scale bar = 100µm. Modified from Tapia et al. (2012)*

in autism spectrum disorders (underpruning) and schizophrenia (overpruning)[6,7].

The importance of these elimination programs is also evinced by the pervasive presence in several location of the central and peripheral nervous system including thalamus, cerebellum, hippocampus, autonomic ganglia and the most extensively researched, the NMJ[8–10]. The NMJ is the system I have mainly utilized for my PhD project, thanks to the several advantages it presents in terms of ease of accessibility, big size and possibility to execute relatively effortless *in vivo* and *ex-vivo* preparations that conserve the 3D structure and endogenous processes[11], as well as the similarities between structure, function and development with CNS[12].

2.2 Activity driven synapse elimination at the mammalian NMJ

Mammalian NMJ is a cholinergic tripartite synapse consisting of axon terminal, Schwann cell and skeletal muscle[12]. The synthesis of the neurotransmitter Acetylcholine in presynaptic nerve cells is mediated by the enzyme Choline-acetyltransferase (Chat). Signal transduction downstream of neurotransmitter release from nerve terminals occurs through binding to postsynaptic Nicotinic acetylcholine receptors (nAChRs), found in abundance in junctional folds. Each motoneuron soma, located in the ventral horn of spinal cord, extends a highly branched axon and each of its terminal branch makes a contact with an individual muscle fiber (Figure 2.1). Several fibers are thus in contact with branches from the same neuron, and fire together (motor unit), which allows for precise and coordinated muscle contraction. At the end of the embryonic development, the NMJ post-synapse receives up to 10 concomitant inputs from different motor neurons, a phenomenon termed poly-innervation[3,13,14] (Figure 2.2a). Therefore, the resolution of the poly-innervation status that is a characteristic of the immature NMJ, induces a shrinkage of the motor unit size as the circuitry becomes more refined[12].

Axonal branches undergo selective dismantling in activity-dependent fashion[15,16], ultimately leaving a one-to-one connectivity between each muscle fiber and innervating input at maturation[4,12,17]. The level of precision is such that no muscle fibers are left denervated when pruning is over, which speaks to its non-random nature[4,18]. How neuronal activity determines the transition from multiple to single axon is still unclear. What is undisputed is that it is driven by competition between co-innervating inputs for synaptic territory occupancy at the post synapse[15,19]. In fact, the winner progressively takes over the synaptic territory and its axon calibre increases[20]. The loser, instead, progressively atrophies, loses attachment to the muscle fiber and withdraws precisely up until its first axonal branching point (Figure 2.2b), through a mechanisms that involves axosome shedding[21]. Indeed, excluding rare instances of reversal of fate, the percentage of territory oc-

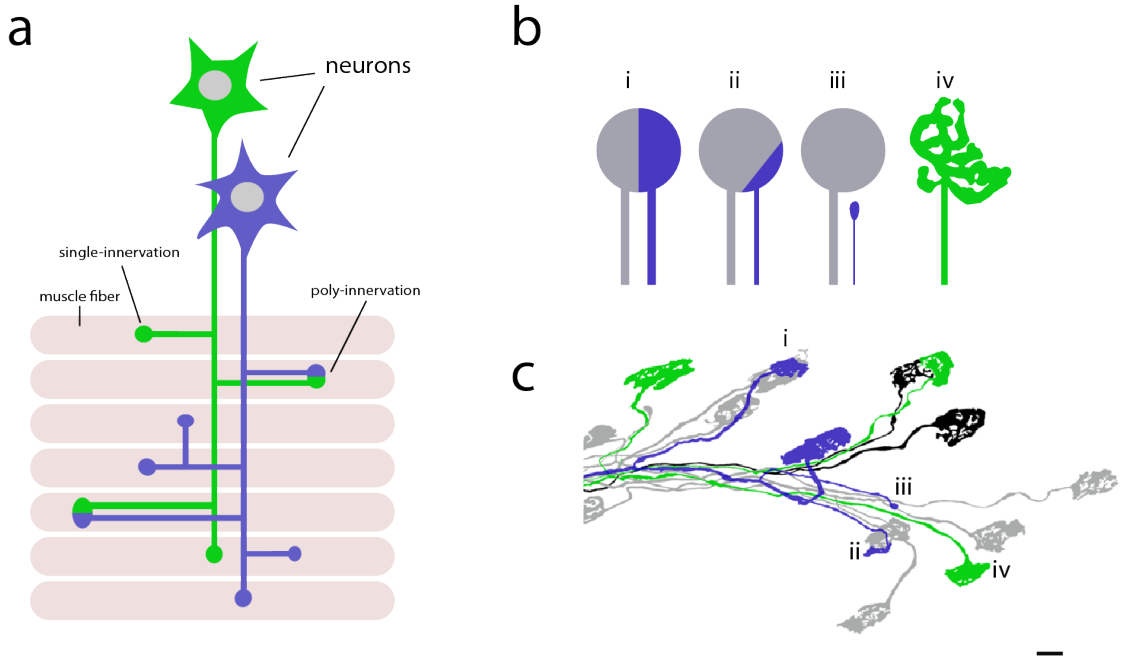

Figure 2.2: ***Synaptic competition at the mouse NMJ during pruning***. *a) Schematic representation of muscle fibers innervated two motor neurons. Two or more terminal branches innervating same muscle fiber is termed poly-innervation, otherwise a one-to-one connection of a synapse to a fiber is called single-innervation. Note how, as losing branches recede, axonal harbor, and thus motor unit, shrinks. b) Illustration of synaptic takeover between two competing synapses. As one input loses territory to its partner (i to iii), its axon caliber decreases and its contact to muscle fiber is lost. Eventually, one branch atrophies and recedes ("retraction bulb", iii), while the other consolidates and expands its territory and acquires a "pretzel" shape (iv). c) Confocal reconstruction of developing terminal motor axons branches. Synapses with same color belong to an individual motor neuron (i-iv: examples of progressive synaptic territory loss). Scale bar is 10µm. Modified from Wang et al. (2021); illustration in c) modified from Brill et al. (2016)*

cupation at the post synapse and axon calibre are predictive of competition outcome[20,22,23]. Territory occupancy is synergistic with synaptic strength, since the latter increases in the input taking over, and both positively regulate one-another[24].
A series of seminal studies have highlighted how it is the relative synaptic strength rather than the absolute amount of action potentials a motoneuron discharges that determines the "winner". Blocking the entire post-synapse through *in vivo* administration of α-bungarotoxin delays axonal retraction[19], but partial synaptic blockade, either pharmacological or genetic, dooms the inactivated synapse to lose and accelerates overall pruning speed[15,25].
How the synaptic strength of competing inputs is compared and decoded remains largely unresolved. Spike patterns have been shown to play a role in the removal of supernumerary axon branches. Postnatally, motoneurons, which first are electrically coupled, commence a divergence of spike timing. This allows the postsynapse to discriminate among inputs and ultimately strengthen only those inputs that contract in a concerted fashion with the muscle fiber[26]. Indeed, the postnatal switch from synchronized to asynchronized motor unit activity and motoneuron uncoupling, seems to coincide with a reduced expression of connexins which are components of gap junctions[27]. In accordance, genetic deletion of Cx40 lead to asynchronized motor neuron activity and faster synapse elimination[28]. In the next chapter I list a number of elucidated signalling pathways involved with pruning.

2.3 Molecular pathways involved in synapse elimination

2.3.1 The role of guidance cues

Molecules such as Semaphorins and Ephrins are mainly known for their contribution to axon guidance: the early developmental event where neurites project over long distances to connect to their specific targets while navigating complex environments. A process elegantly explained by the chemoaffinity theory, which postulates this to be possible thanks to precise

molecular matching between targets[29].
Recent studies have highlighted the guidance cues' versatility by implicating them in the regulation of axon pruning as well. The multi-faceted mode of action can be explained by the context dependent expression of their downstream effectors, activated precisely in time and space. The key to explaining their involvement in axon pruning relies on their repellent properties to induce local cytoskeletal collapse in the axon.
For example, in the CNS, a study of stereotyped pruning of the hippocampus by Riccomagno et al, shows that Sema3F leads to the activation of Npn-2, which triggers the downstream activation of β2Chn, a Rac-specific GAP. β2Chn, by inhibiting Rac-1 dependent effects on the cytoskeleton, induces axonal pruning of the infrapyramidal bundle[30].
Another recent study confirms the role of Sema3F in this location, mediated by activation of CRMP2, a member of the collapsin response mediator protein family. Indeed, deletion of the Crmp2 gene in mice lead to synapse pruning delay of the IPB. The presence of defects of the visual cortex and altered dendritic spine remodelling, indicates that the pathway might be used at several locations that undergo pruning. Interestingly however, no pruning delays occurred at the NMJ of CRMP2 null mice[31].
Involvement of Semaphorins in the axon pruning at some locations, but not others, might suggest that either the molecular pathways are not necessarily conserved for all the sites undergoing pruning or that specific isoforms have specialised to act at different locations. Hints for the latter hypothesis come from the potential role of Sema3A for pruning at the NMJ. Sema3A receptor, Nrp, has been shown to be expressed in pre-synaptic axon terminals[32]. Additionally, Sema3A secreted from Schwann cells participates in NMJ remodelling[33].

Similarly to Semaphorins, ephrins are another guidance cue family involved in the pruning of the CNS. In particular, Ephrin-B3–EphB2 reverse signalling has been shown to mediate stereotyped pruning of murine hippocampal mossy fiber axons through regulation of the actin dynamics[34]. At the NMJ, while the exact molecular cascade regulating motor axon pruning is yet to be elucidated, there is however some evidence for the involvement

of Ephrins guidance cues.

During the immediate postnatal period, myofibers innervated by a single motoneuron which initially are heterogeneous in their fiber type, start to progressively become homogeneous as the motor unit matures[35]. Prevailing models of muscle fiber type specification propose that a "matching" mechanism between muscle fibers and motor axons exists and the Eph/ephrin interaction could facilitate their recognition. Indeed, Ephrin-A3 ligand has been shown to be expressed specifically by type I (slow) twitch fibers. By providing a repulsive signal which inhibits the formation of stable synapses with fast motor neurons[36], they may actively help to determine which axon should be eliminated.

2.3.2 The role of neurotrophic factors and cell-death signaling

Target-derived factors need to be continuously supplied to maintain normal synapses. This is indicated by experiments in which the abolition of protein synthesis from muscle of live adult mice resulted in rapid disaggregation of the synaptic structures, loss of nerve contact with postsynaptic sites and axonal withdrawal, resembling of developmental NMJ pruning[37].
Neurotrophins are a main candidate for a role of trophic support, since not only are they essential for neuronal survival and differentiation[38–40] and can promote neurite outgrowth and strengthen synaptic transmission, but also have been involved in synapse elimination.
Members of neurotrophins include Brain derived neurotrophic factor (BDNF), Nerve growth factor (NGF), Neurotrophin (NT)-3, NT-4/5. Following maturation through proteolysis of the proneurotrophins, each mature neurotrophin is able to bind p75NTR, a death receptor family member, but exhibits more specific interactions with three Trk receptors to which they bind with different affinity to elicit a variety of downstream responses[41].
Of interest, BDNF and NGF expression and functional maturation are activity-dependent[42–45]. Additionally, NGF, BDNF, and NT-4 secretion can be enhanced by neuronal or synaptic activity[46–48]. Neurotrophins have been

shown to modulate the efficacy of synaptic transmission by both pre- and post- synaptic means. Indeed, at the developing neuromuscular synapses, BDNF application increased the frequency of miniature excitatory post-synaptic currents (mEPSCs), increased Acetylcholine synaptic release, and influenced paired-pulse facilitation[49–52]. Blocking the receptor with the anti-p75 antibody results in reduced endplate potentials (EPPs), suggesting that the potentiating mechanism is dependent on the BDNF-p75 axis[53].

The ability of neurotrophins released from postsynaptic cells to modify synaptic functions, combined with the fact that such modifications can be regulated by synaptic activity, hints at the possibility of their contribution to the activity-dependent refinement of synaptic connections.
Potentially, at the NMJ, the lack of neurotrophic factors can act as a punishment signal that induces local cytoskeletal disaggregation and axon pruning. The existence of such local effects by neurotrophins is backed up by the evidence at the developing nerve-muscle synapse: by using a nerve-muscle co-culture in which a single motor neuron innervates two myocytes, one of the two myocytes overexpressing NT-4 and the other not, Wang et al. showed that synaptically released neurotrophin NT-4 has an influence that is restricted to a spatial synaptic territory of less than 60 um[54].
Further evidence of the role of neurotrophins in axon pruning at the NMJ come from immunohistochemical stainings of rat tissue during the period of synapse elimination, which helped to determine the location of the components of this pathway. The receptor protein p75NTR is present in the nerve terminal, muscle cell and glial Schwann cell, whereas trkB mRNA and proteins and BDNF protein can be detected mainly in the pre- and postsynaptic elements[50,51]. ProBDNF protein is found in the muscle[45].

Intriguingly, the kind of BDNF has been revealed to be important for the fate of axons: proBDNF acts as a punishing signal promoting synapse elimination at the mouse NMJ, whereas, due to its synaptic strengthening properties, mature BDNF delayed synapse elimination[45]. These opposite outcomes derive from the mature BDNF binding to TrkB receptor, while pro-BDNF binds to P75 and the coreceptor sortilin[55–57].
In accordance with the hypothesis that pro-BDNF must bind concomitantly

to p75 and sortilin to mediate its "punishing signal" effects on pruning, in vivo experiments in which the NMJs were exposed to antibodies against p75NTR, which could also impair sortilin binding, delayed synapse elimination[45,53]. However, full KO of p75 did not affect synapse elimination.
Another unexpected result emerging from these studies was that blocking the BDNF-TrkB pathway, through inhibition of the receptor, accelerated elimination[45]. However, BDNF KO mice had no pruning defects. This lack of phenotype in the latter scenario may be explained by the notion that by removing both punishment (proBDNF) and reward (mBDNF) signals, synapse elimination occurs by default[45].
Additionally it appears that also receptor location has a different impact on synapse physiology. While muscle-derived p75NTR did not play a major role in postsynaptic organization, motor axon terminals lacking p75NTR resulted in a reduced number of synaptic vesicles and active zones[58]. This indicates that the BDNF from target muscle elicits its action through a retrograde signalling to activate presynaptically located p75NTR receptors.
Downstream, binding of BDNF to the receptor can activate the phosphokinase (PK) pathway. In particular, the pathway bifurcates to activate either PKA or PKC. Interestingly, PKA and PKC have been shown to have opposite effects on the outcome of synapse elimination in the NMJ of mammals. PKA acts at the pre- and postsynaptic sites to delay axonal elimination and nAChR cluster differentiation through a mechanism involving BDNF-TrkB receptors coupled to PLCγ[59,60]. On the other hand, PKC activity promotes axonal loss[44,61].
It is unclear how the choice between PKA or PKC activation is made. It can be envisioned that, while PKA could be activated by the BDNF-TrkB signaling to reinforce the synaptic connections of the "winner" axon, PKC could be activated by the pro-BDNF - P75/sortilin pathway in the weak axons which are to be eliminated (Figure 2.3).

Other neurotrophic factors might contribute to synapse elimination as well. For example, prolonged periods of synapse elimination has been shown both in absence of muscle-derived fibroblast growth factor binding protein 1

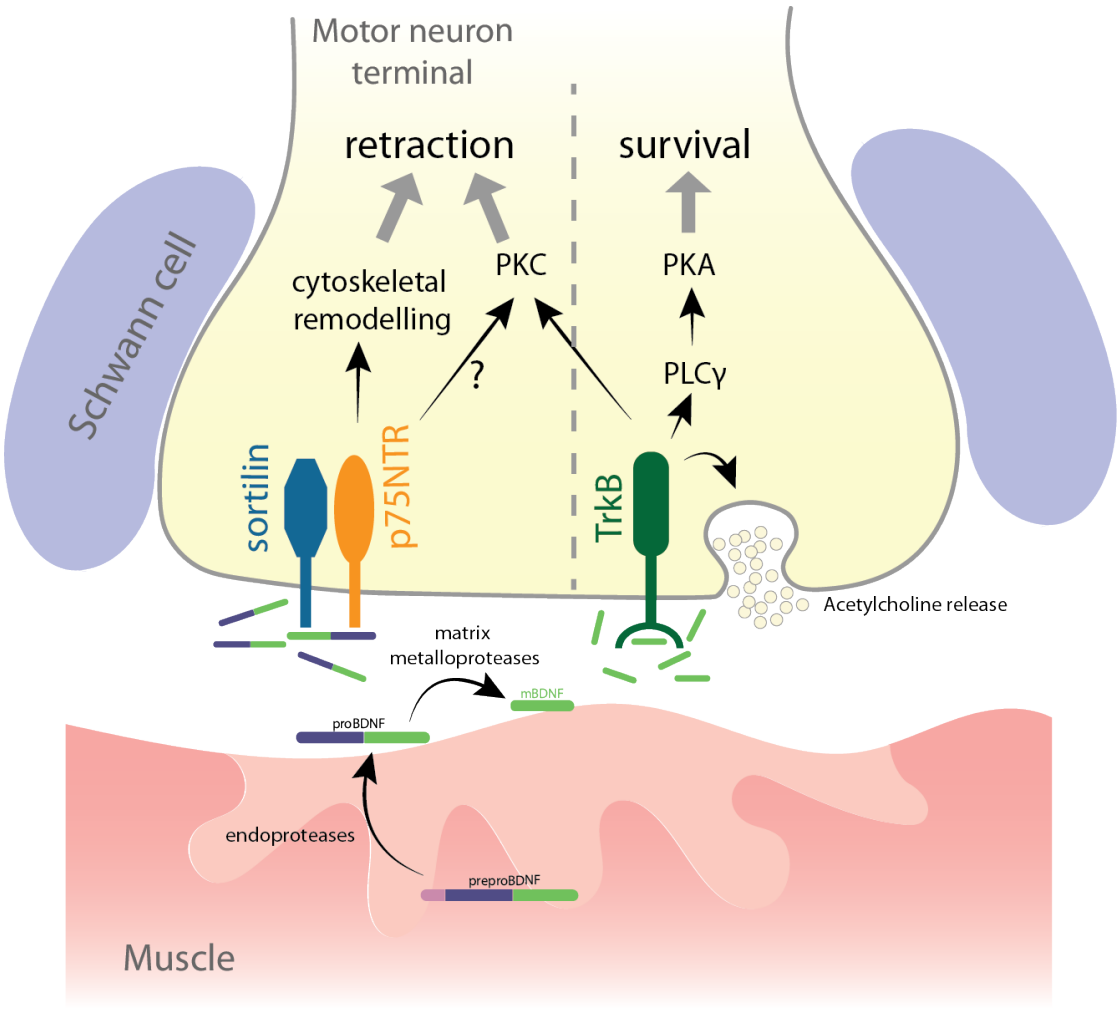

Figure 2.3: ***BDNF signaling cascades and pruning***. *BDNF pathways exerts opposite outcomes on neuronal pruning. Mature BDNF (mBDNF) has been shown to increase Acetylcholine synaptic release and enhance axonal and dendritic growth and survival. BDNF precursor proBDNF or mBDNF arises from a series of intra- or extracellular proteolytic cleaveages of preproBDNF through specific metalloproteases. mBDNF signals through TrkB to in a cascade that involves PLCγ and PKA activation. On the other hand, proBDNF binds presynaptically to p75NTR and sortilin to induce pruning through cytoskeletal remodelling, possibly by activating PKC. Illustration modified from Deinhardt et al. (2014)*

(FGFBP1)[62], or when GDNF was transgenically overexpressed in muscle, or delivered subcutaneously[20,63]. Although neurotrophins are thought to mediate their effect through an increase in neuronal survival or stabilization of synaptic connections, GDNF is likely to mediate its effects through induction of axonal branching. In fact, GDNF exposure produced expansion of motor units by increasing axon branching and enlarging postsynaptic AChR sites. This is evidenced by the fact that chronic GDNF exposure from birth forces even the mature NMJ to a constant state of dynamicity, where instances of retraction and regrowth were witnessed at the synapse. Interestingly, the effect of GDNF seems to be temporarily restricted, since when exposure was initiated from P10 instead of birth, no hyperinnervation occurred[20].

On the other hand, research on the role of NT-3 and NT-4 on axonal pruning is rather lacking. It has been shown that NT-3 increased the frequency of miniature excitatory postsynaptic currents (mEPSCs), indicative of an enhancement of neuromuscular transmission[49]. Moreover, postsynaptically, the overexpression of NT-4 in muscle increased the mean burst duration of Acetylcholine channels and neurotransmitter release[48]. Albeit the transgenic overexpression of NT-3 and NT-4 were ineffective in producing multiple innervation[63], full KO of NT-3 resulted in complete denervation of hindlimb muscles by P7. The extent to which this is directly caused by the lack of support to motoneurons or as a secondary effect, is not clear.

Aside from p75NTR receptors, another cell-death related signaling molecule involved in pruning is the proinflammatory cytokine tumor necrosis factor α (TNFα). TNFα has been found to be expressed in postsynaptic muscle cells and is involved in presynaptic axonal elimination at the NMJ. Indeed, genetic ablation of TNFα globally or specifically in skeletal muscle cells, but not in motoneurons or Schwann cells, delayed synaptic elimination in mice[64]. This indicates that retrograde signaling from the muscle side is triggering axonal pruning presynaptically. However, there is still a lack of understanding of the exact molecular components that cause presynaptic axon pruning.

Overall, several neurotrophins and cell-death related factors have shown to have an effect on axonal pruning to different extents. It is generally accepted

that neuronal growth factors are able to stabilize synapses by providing trophic support. On the other hand, neurotrophin deprivation could give rise to "punishing signal" that triggers axon pruning by activating the cell-death signaling cascades to eliminate weakened and inappropriate synapses. Another mechanism which could be paramount in promoting synapse loss is the one occurring as a consequence of signals that disrupt the adhesion of the nerve to the postsynaptic site, which I will discuss next.

2.3.3 The role of cell adhesion molecules

Cell adhesion molecules play critical roles in the development and maturation of the NMJ, and such adhesive interactions between prejunctional and postjunctional sites need to be disassembled during the process of axonal pruning. The neural cell adhesion molecule (NCAM), a homophilic binding glycoprotein, is a good candidate to consider at the NMJ for mediating a bond between pre and post-synaptic structures.
Indeed, it has been shown that denervated muscle fibers upregulate NCAM on their surface. This could confer a more permissive substrate for upcoming axons in order to favor re-innervation[65]. Therefore, the lack of NCAM could be essential to drive axon pruning. NMJ stability and size have been shown to depend on NCAM, since NMJs from NCAM null mice were smaller and postsynaptic junctional fold development was delayed[66,67]. Intriguingly, NCAM null mice displayed a delay in both the withdrawal of poly-innervation and in the selective accumulation of synaptic vesicle protein in the presynaptic terminal[67].
The effect of delay is quite counterintuitive if one considered only NCAM's adhesive role, but the absence of paired-pulse facilitation and the inability to maintain effective transmission with repetitive stimuli in NCAM null junctions - most likely due to defects in vesicle docking and release[67] - suggests that the impaired neurotransmitter release process might contribute to the innervation delay. It would be interesting to know if other molecules with a known structural support at the NMJ, such as laminins and collagens, have a role in axon pruning.

Another class of molecules affecting axon pruning is the Class 1 major histocompatibility complex (MHC1) which could serve as recognition tags for compatible synaptic partners. In the NMJ, MHC1 are expressed at the NMJ during the period of synapse elimination[68]. Although the exact identity of the cellular location and the isoform type has not been established yet, deleting MHCI delayed synapse elimination in mice, while overexpressing MHCI modestly accelerated developmental synapse elimination[69]. One proposed mechanism is that MHCI levels could render some inputs weaker and thus more susceptible to elimination, although clear mechanistic aspects are lacking and necessitate further investigation.

2.3.4 The role of the cytoskeleton

The highly accurate spatial and temporal specificity that occurs in the large scale reformation of synapses during synapse elimination, which is usually restricted to single neurite branches, demands likewise tightly controlled mechanisms able to trigger the process of disassembly, locally. Ultimately, for certain neurites to disappear, the molecular pathways guiding pruning need to converge on cytoskeleton dismantling.
The cytoskeleton is composed of microtubules (MT), actin, and neurofilaments which together contribute to the morphology and functionality of all cell types. There is increasing evidence for the central role of the cytoskeleton in the pruning process. For example, knocking out neurofilament light chain (NF-L) from motoneurons causes synapse elimination delay[70]. The reduction of NF-L levels and consequent axonal remodelling delays were also recapitulated as a result of the loss of glial isoform neurofascin (Nfasc155). This indicates that the molecular underpinnings of synapse elimination are driven by a combination of cell-autonomous and non-cell-autonomous means. Possibly, this is a result of external cues providing rewards (release of trophic factors from target muscle) and punishment (hostile environment driven by terminal Schwann cells or muscle), both of which could be activity-dependent.

There is evidence that also actin dynamics drives retraction and is modulated by specific semaphorins and ephrins[30,34], as previously discussed in Section 2.3.1. Interestingly both studies implicate Rac1, an actin regulator, in affecting the stereotyped pruning of murine IPB during postnatal development. How opposing activity of Rac1 (downregulation through Sema3F[30], or activation through Ephrin reverse signaling[34]) both lead to the same outcome of the IPB pruning, has yet to be clarified, but could be a consequence of the involvement of different downstream effectors. Alternatively both pathways might be needed, but at temporally restricted and non-overlapping instances.

Of the three cytoskeletal components, the role of MT breakdown seems to be central and conserved across various forms of pruning and different experimental models and species, from insects to mammals[71–74]. MT destabilization is an early event that precedes pruning and could act as local trigger to determine which neurite to eliminate[21,71,74]. Retreating axon branches have sparser MT density[21,74], and MT stabilization through pharmacological means protects against MT depolymerization and axon fragmentation[75] and delays pruning[74]. Although the molecular machinery that executes MT breakdown in pruning events is largely unknown, genetic evidence at the murine NMJ show that impairing MT severing through Spastin-KO delays the removal of redundant axons[74]. In addition there are indications in *Drosophila* that Katanin-like molecule, Kat60L, is involved in the pruning of dendrites, but not axons[76]. Future work should elucidate if Kat60L role is conserved in mammals as well.

MT could affect pruning purely through mechanical cytoskeletal stability means or by providing intracellular resources, such as synaptic vesicles, organelles (e.g. mitochondria), RNA, trophic factors and so forth[21]. In support of this, axonal transport is virtually absent in losing axons[74]. Due to the preponderant role of MTs, their structure and functions will be discussed in more detail.

2.4 MT cytoskeleton: structure and functions

Microtubules are mainly known for their role in neuronal transport. Indeed, motor-driven transport is almost entirely dependent on MTs, as demonstrated by early experiments using drugs that disrupt the MT cytoskeleton[77]. Apart from providing the tracks for intracellular cargo transport, the dynamic remodelling of MTs directs and reinforces cell shape, forms spindles in mitosis and meiosis, provides force generation, and in the polarized and excitable neuronal cells MTs contribute to the formation and maintenance of axons and dendrites, often in an activity-dependent manner[77–83].

2.4.1 MT structure

Structurally, microtubules (MT) are non-covalent polymers of globular α and β-tubulin assembled into a heterodimer into 1:1 stoichiometry (Figure 2.4a). These α -β heterodimers polimerize into a linear chain called "protofilament". The radial assembly of 13 protofilaments generates a 25nm diameter long hollow tube[84,85] (Figure 2.4b). The dimer is incorporated into the MT lattice from the α-tubulin in a head to tail fashion, a characteristics that endows the MT with an intrinsic polarity. After a delay, GTP hydrolysis occurs from the β-tubulin specifically. The lattice is thus composed of an inner of GDP-rich domain, and a stabilizing GTP-rich domain at the growing MT end. This inherent subdivision separates the lattice into a "stabile" and a "labile" domain (Figure 2.4c).
The MT ´minus´ end is intrinsically more stable/inert, and bound by capping proteins such as gamma tubulin and CAMSAPs which further stabilize the structure[78,86]. The ´plus´end, on the other hand, is more dynamic and undergoes frequent cycles of growth and shrinkage, a.k.a. "dynamic instability"[87–89]. Shrinking events, or "catastrophes", are frequent when the outer GTP "cap" is lost[90], which causes the protofilament to splay apart in a fountain-like structure[91–93] (Figure 2.5). On the other hand, growth events or "rescues" occur naturally in the presence of high abundance of free tubulin in the environment[91] . The stochastic exchanges between "catastrophe" and "rescues" enable MT to rapidly respond to environmental needs, as well

as explore the intracellular space[94,95], a fundamental characteristic during early morphogenic events.

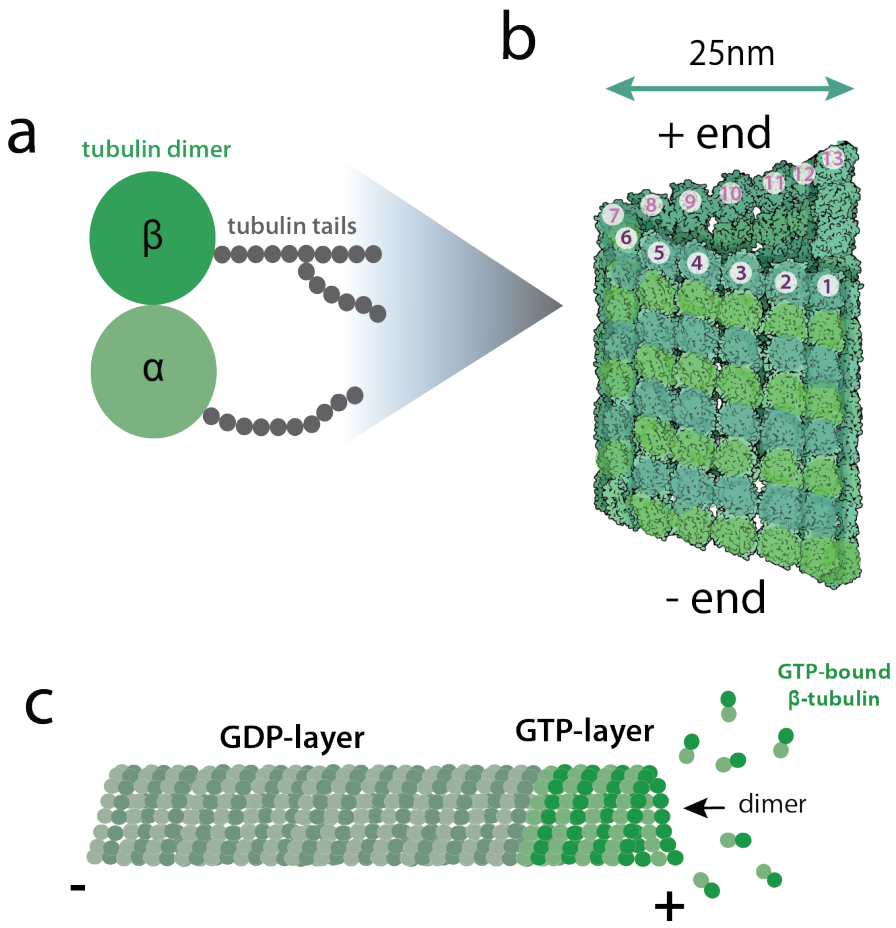

Figure 2.4: ***MT composition***. *a) Tubulin is a globular and highly conserved protein and has an unstructured C-terminal segment protruding from the surface, called "tubulin tail". MTs assemble dynamically from α and β tubulin heterodimers. b) The addition from the + end in a head-to-tail fashion of 13 dimers (pink-violet), forms a 25nm hollow tube, which conveys the MT an intrinsic polarity. c) The dimer is integrated into the lattice from the growing plus-end side. After some time, hydrolysis of GTP-bound β-tubulin to GDP occurs. Thus the MT has a stable, GDP-layer at the - end, and a more dynamic GTP-layer close to the + end. Adapted from David Goodsell (2014).*

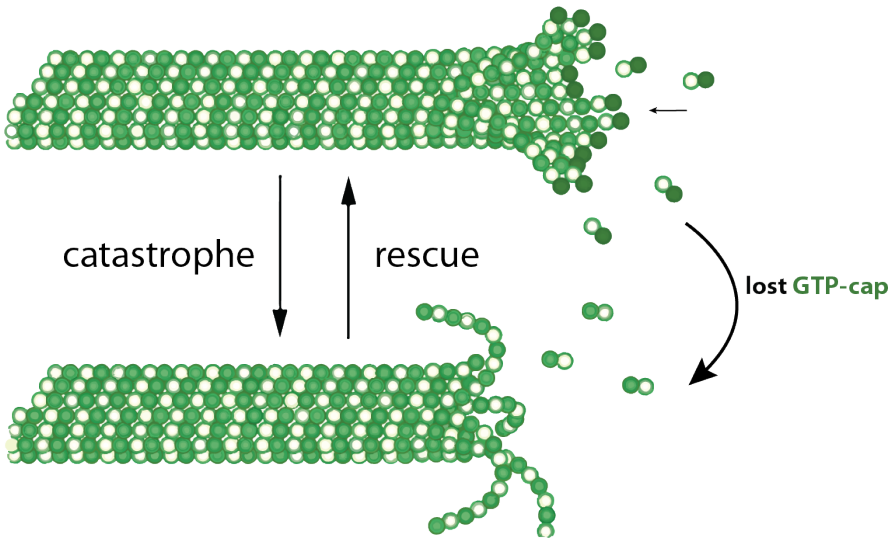

Figure 2.5: ***MT dynamic instability***. *MTs undergo rapid cycles of growth (rescue) and shrinkage (catastrophe). Catastrophe is frequent when the stabilizing "GTP-cap" is lost. This induces depolymerization and causes protofilaments to spay apart. Modified from Akhmanova and Steinmetz (2015).*

2.4.2 MT architecture in neurons

Among their other functions, MTs play a key role in establishing and maintaining neuronal polarity, which is the basis for the establishment of different compartments such as axons and dendrites. This polarized morphology underlays its ability to process, receive and transmit signals and to establish an asymmetric distribution of cargos through axonal transport.
Distinct from other cell types, following differentiation, neuronal MTs become acentrosomal, meaning they lose their contact to the centrosome: the major microtubule-organizing center (MTOC) and nucleation site[96–99]. MTs rely instead on gamma tubulin and on calmodulin-regulated spectrin-associated family (CAMSAP)/Patronin–mediated minus-end growth[100–102] for nucleation. One known mechanism of nucleation is the formation of a new MT from the lattice of a pre-existing branch[103–105].
As such, MTs exist as dense bundles that span the length of axons and

dendrites. They are not single continuous filaments, but rather individual fragments, spaced in a tiled fashion and cross-linked by MT associated proteins[93,106]. The amount of overlap is dependent on MT length and density, and has important repercussions in the overall efficiency of axonal transport. Intuitively, the longer and the more abundant the MT filaments, the more processive the transport. Indeed it was shown in *C. elegans*, that cargo pause time inversely correlates with MT abundance[107]: a consequence of the fact that at the end of the filament, cargos come to a stop and some time is needed to re-engage with the next MT filament. In silico simulation have also shown that cargo run length is proportional to MT length[108]. Closely spaced and parallel MTs enhance the processivity of motor proteins by allowing them to engage simultaneously with more MTs[109,110].

In vertebrate axons, the MT network is unipolar, meaning MT's plus-end tips faces toward the synapse and their minus-end toward the cell body (plus-tip-out orientation). In dendrites, MT present a mixed polarity, although the exact proportions change between organisms and throughout neuronal development[111]. MTs function as rail roads to transport cargos bidirectionally: from cell body to nerve terminals (anterograde axonal transport), and backwards from nerve terminals to cell body (retrograde axonal transport)[79,112]. It was well understood early that MTs' intrinsic polarity is necessary to establish the directionality of axonal transport, but it was debated whether structure alone would be sufficient to faithfully direct such intricate events. Indeed, MTs do not function alone; the effort to better understand how MT architecture and function could be controlled by the interplay between different 1) tubulin isoforms, 2) MT post-translational modifications (PTMs) and 3) MT associated proteins (MAPs) saw the emergence of the concept of the "tubulin code"[113,114].

In primis, tubulin isotypes, being the building blocks of MTs, impose specific properties that dictate the structure and function of the entire MT polymer. Eukaryotic cells have multiple tubulin genes. In particular, humans have nine α and nine β tubulin isotypes with varying expression across development and different brain regions[115–118]. Not only are tubulin isotypes highly conserved across species, but their amino acid sequence bears more than

95% identity among their members, with most variability located on the unstructured carboxy-terminal tail[119,120]. It is likely that the distinct functions of the isotypes likely originate from their subtle sequence variations. In this respect, the C-terminal tail which protrudes from MT backbones, remains highly accessible to MAPs and is subjected to a range of tubulin post translational modifications (PTMs) that regulate MT dynamics and MAP binding[121].
Seeing how the MT is a blend of isotypes of varying proportions[122], early studies assumed that the dimer pairs could assemble independently of isotype constraints. Recent studies are challenging this view in light of how some tubulin isotypes are not interchangeable and might require specific binding partners. For example, mutation in the human β1-tubulin (Tubb1) leads to disorganized MTs of blood platelets and congenital macrothrombocytopenia[123], even though six other β-tubulin isotypes are simultaneously abundant in the cells[124]. Similarly Tubb3 knock-out mice have neuronal migration defects that cannot be rescued by other isoforms[125].
This suggests that functionality differences could also be imparted through assembly of specific α and β pairs. Thus, the incorporation of specific tubulin isotypes into the MTs may regulate MT properties by controlling the accessibility to certain MAPs and may have different susceptibility to PTMs.

2.4.3 PTM of MTs

PTM of tubulin can occur at the C-terminal tail or on the lattice itself. A variety of modifications exists (Figure 2.6). How they are established, maintain and how they can affect MT properties and their ability to interact with MAPs is under continuous scrutiny[113,126]. Due to their prevalence in neuronal MTs, special attention will be given to acetylation, polyglutamylation and detyrosination.

Acetylation is found primarily in the axon initial segment and axon shaft, but it is rare in dynamic structures such as growth cones and synapses[127]. It is reversibly added to the MT lumen in position Lys40 by αTAT1[128] and removed by HDAC6 and SIRT2[129,130]. In light of the results that loss of

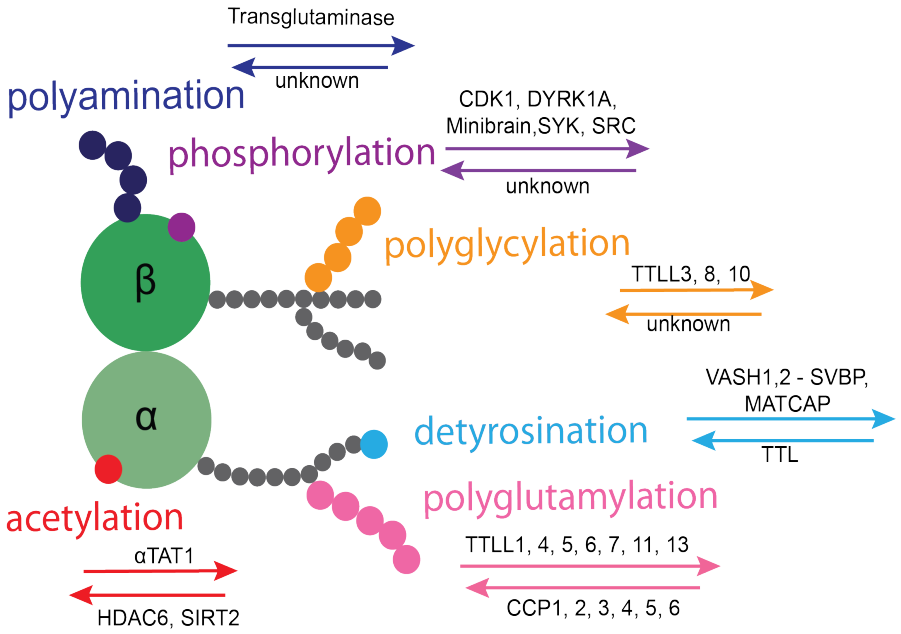

Figure 2.6: ***Tubulin post-translational-modifications***. *MT can undergo post-translational-modifications (PTM) at the tubulin body or at the tubulin tails (in gray). These modifications are reversibly catalysed by a range of enzyme families, as indicated. Abbreviations: TTL, tubulin-tyrosine ligase family; TTLL, tubulin–tyrosine ligase-like family; CCP, cytosolic carboxypeptidase protein; αTAT1, α-tubulin N-acetyltransferase 1; HDAC6, histone deacetylase; SIRT, sirtuin; SVBP, small vasohibin binding protein; VASHs, vasohibins; MATCAP,microtubule-associated tyrosine carboxypeptidase; Modified from Janke and Magiera (2020)*

α-tubulin acetylation led to MT instability in axons[131], this modification is classified as a MT stabiliser. This stabilization is achieved by weakening intra-protofilament interactions, which enhance MT flexibility and prevent breakages through repeated mechanical stress[132,133].

Another modification affecting MT stability is tyrosination. It is an α-tubulin C-terminal tail specific event, catalysed by tubulin tyrosine ligase[134,135] and removed through detyrosination[136] by vasohibins bound to SVBP cofactor[137,138] and the recently identified, the atypical metalloprotease MATCAP[139]. Detyrosination is found in long lived MTs and is generally more abundant in the axon shaft, contrary to tyrosination which is mainly found in distal axon regions and in MT labile domain. The presence of detyrosination spares MT from nocodazole-mediated disassembly[140], as such is considered a marker for MT stability[120,141].

First discovered in 1990[142], polyglutamylation is a very abundant axonal modification and consists of a two-step enzymatic addition of glutamate residues onto the tubulin tails. The first step consists in the addition of a single glutamate molecule or "seed"; the second step consists in the elongation of this seed into a chain[143].

Glutamylation is catalysed by the family of enzymes of tubulin tyrosine ligase like (TTLL). Excluding TTLL3, TTLL8 and TTLL10 which are glycylases, and TTLL12 whose specific function is yet unknown but predicted to be inactive for glutamylation, there are as many as 9 functional glutamylases in mammals[135,144–149]. Albeit both α and β tubulin heterodimers can be modified by this enzymatic family, each TTLL enzyme has a preference for either β or α-tubulin substrate and has acquired a specialized function to promote either monoglutamylation or polyglutamylation[150,151]. Enzymatic removal of glutamates to reverse TTLL effects is achieved by cytosolic carboxypeptidases (CCP 1 to 6)[152,153]. Of the six mammalian enzymes, which catalyse both deglutamylation and generation of Δ2-tubulin[154,155], CCP1 and CCP6 are the two highest expressed in neuronal tissue[156]. Polyglutamylation coats the MTs with a negative electrostatic charge, which could in part enhance the interactions between the MT lattice and the positively charged protein domains, thus favouring the recruitment of MAPs. Both

Katanin and Spastin bind preferentially polyE MTs[157], and Spastin activity is modulated by the length of polyE chain[158].
The polyE chain can reach lengths of up to 13 glutamates in vitro, as well as form complex "branched" structures, when enzymatic activity of the glutamylases goes un-obstructed[159]. How physiological these settings are is under debate. PolyE could directly and indirectly affect transport by altering MT architecture through severing enzymes[160], or by affecting motor proteins such as kinesin-1 and kinesin-3[120,145,161].

2.4.4 MT Associated Proteins

Increasingly higher levels of precision and sophistication are achieved through interaction between *cis* and *trans* elements. While PTMs and tubulin isoforms are "cis" factors and provide a code and instructions, Microtubule-Associated- Proteins (MAPs) represent the "trans" factors, which can interact with MT by binding MT tips, soluble, non-polymerized tubulin subunits or the entire MT lattice[92].
They affect MT stability by promoting growth, depolymerisation, influence interaction with motor proteins or providing structural support[162–164]. One class of MAPs is the family of plus-end-interacting-proteins (+TIPs): an evolutionary conserved structural element which has the ability to localize to the growing plus tip of MTs. Among them, the end-binding (EB) protein family is composed of three members in mammals (EB1-3). While EB1 and EB2 appear to be expressed ubiquitously, EB3 is strongly expressed in muscle and brain tissue[165,166]. EBs are known for modulating MT dynamics and for scaffolding other +TIPs and to regulate the local protein composition at growing MT tips, by recognizing specific motifs found in interacting partners, specifically the SxIP (which binds to the homology domain of EB - EBH) and CAP-Gly domains (which binds to EEY/F motifs of EB)[92,167]. EBs belong to the "autonoumous tip trackers" category of +TIPs, since their CH (Calponin homology domain) and linker protein domain region are sufficient to independently recognize the GTP-cap structure at growing MT ends[91,168,169] (Figure 2.7). A total of couple hundred of EB molecules bind to

MT ends and display a comet-like appearance in fluorescence microscopy[116]. EB3's property to bind to growing MTs has been used to develop genetic tools that enable real time *in vivo* tracking of MTs, for example through fusion of EB3 to fluorescent proteins such as YFP[11,74,85,170]. Imaging them provides critical information on MT dynamics, and an indirect measure of MT length[74].

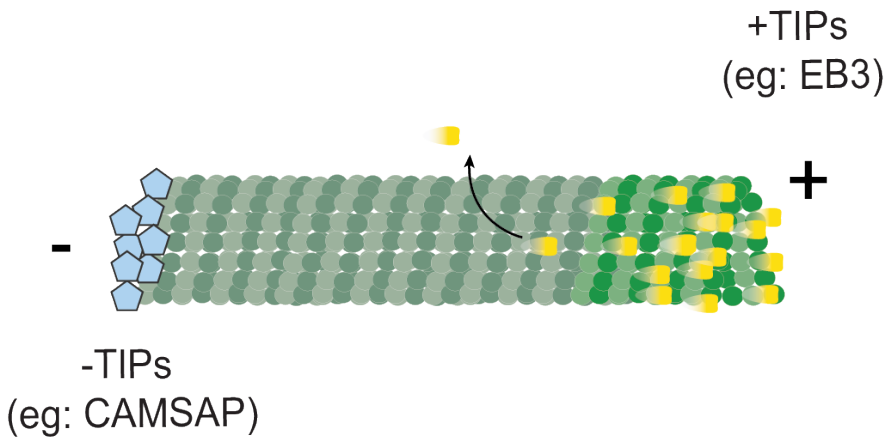

Figure 2.7: ***Plus-end MT tracking proteins.*** *Plus-end-tracking proteins (+TIPs) recognize conformational changes at the growing plus-end of MTs, and are thus removed from the GDP-rich lattice. They include proteins such as EB1, EB3 and CLIP-170. Conversely Minus-end-tracking proteins (- TIPs), recognize minus-end of MT and through binding stabilize the lattice and prevent its disassembly. Modified from Akhmanova and Steinmetz (2015).*

Severing enzymes

Another class of MAPs are the severing enzymes. Severing of MTs is an ATP-dependent event carried out by a family of AAA-ATPases, which include the enzymes Spastin, Katanin and Fidgetin[171,172] (Figure 2.8). These severases elicit their effect by producing nicks along the MT lattice, causing breakage into shorter fragments[173]. These cuts can either serve as new nucle-

ation sites, promoting a burst in MT mass and number[174,175], or conversely induce destabilization and depolymerisation of the original filament, causing opposite effects on the cytoskeleton[176–178]. This ambivalent response to severing has been reported in several animal models and diverse experimental conditions[79,179,180]. The net effect depends, among other factors, on the position of the cut along the lattice in the labile or stable structure[181,182], on the concentration of free tubulin and/or local MAPs availability to stabilize new emerging structures such as CLASPs or tau[180,183–185]. For example, it was observed that catastrophe events induced by the nanoscale damages inflicted by Spastin can be evaded by spontaneous incorporation of GTP-bound tubulin into the lattice, as long as the formation of these "GTP-islands" outpaces Spastin-induced depolymerisation[184]. Notably, these lattice defects arise also by other means, such as through mechanical stress[183], through molecular motor movement[186,187] or even spontaneously[188]. The exposed lattice acts as a recruitment signal for the MAP Sjorgen's syndrom nuclear autoantigen-1 (SSNA1/NA14), which coats the MT and protects the MT from Spastin activity[189]. This MT "repair" process is thought to rejuvenate the MT lattice[184].

The biological function of Spastin

Given that Spastin activity is critical during neuronal development, as it mediates axon branch loss during NMJ elimination[74], and as its catalytic activity is dependent on polyglutamylation[157,190,191], special interest will be given to this particular severing enzyme.

Molecularly, Spastin assembles into a hexamer around the MT filament and creates nicks by pulling single tubulin subunits by the C-terminal tail in an ATP dependent manner[171,192]. Oligomerization through the AAA domain is triggered by the vicinity to the MT substrate, which confers spatially regulated and controlled severing. The recruitment occurs by interaction of the positively charged ring of the severase to the negative charge of the MT tails, reinforced by the negative charge of polyglutamylation[157,190,191].

To avoid severing off-target effects it is paramount that Spastin activity is tighly regulated. This is achieved in a number of ways. At the transcription

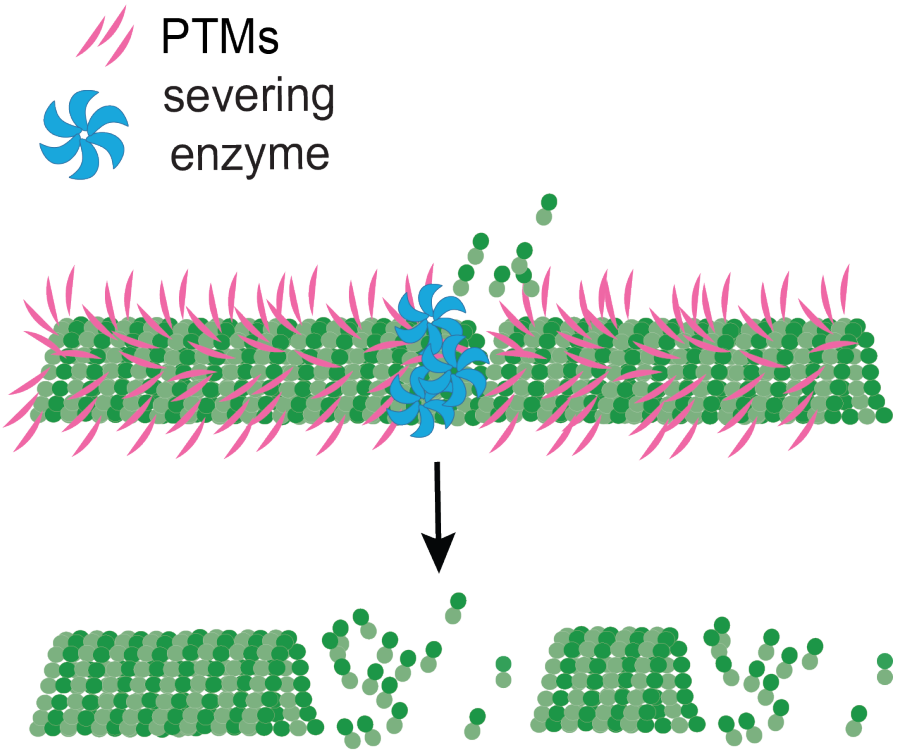

Figure 2.8: ***MT severing enzymes.*** *Spastin, Katanin and Fidgetin are a class of severases that cut MT by creating nicks into the lattice. Recruitment occurs through binding to specific decorations of tubulin tails. Spastin recruitment and activity, for example, is triggered by polyglutamylation. Proximity to the MT lattice causes assembly of the Spastin hexamer, which by pulling onto the tubulin C-terminal tail, generates lattice defects and leads to MT breakage. Adapted from Kuo and Howard (2021)*

level, Spastin expression is modulated positively by transcription factors such as NRF1, Sox1 or negatively by Elk1[193], or by miRNAs such as miR-192, miR-30, miR-33 and miR-96[194–196].
Post-transcriptionally, SUMOlation alters Spastin severing activity[197], while Spastin phosphorylation at Ser268 mediated by HIPK2 regulates its proteasome-mediated degradation[198]. At the protein-protein level, interaction with other MAPs such as Tau or SSNA1/NA14 can also affect net outcome of Spastin activity. Tau overexpression protects MTs from severing[180,199] possibly by forming condensates or "tau islands" from which Spastin or Katanin are excluded[200], conversely loss of Tau increases Spastin activity[201].
Another regulation is through alternative splicing, which give rise to four Spastin isoforms. Of the four, the two least abundant have no clear biological function reported as of now[202]. Of the remaining two, m1 gives rise to the full length protein, while m87 is the shorter isoform which lacks the N-terminal domain, responsible for hydrophobic interaction with membranes and lipids[203]. Albeit both isoforms conserve the capacity to oligomerize, interact and sever MT thanks to AAA and MTDB[192], as well as participate in endosomal trafficking thanks to the MIT domain[204], m1 has a more preponderant role in membrane remodelling and ER shaping by directly interacting with the ER proteins REEP1 and atlastin[205–208]. It also serves functions in lipid droplet metabolism and endosomal fission[209–212]. On the other hand, m87 has a higher solubility, is ubiquitously expressed and more abundant than m1 in the CNS[174,213] and might play important roles in endosomes and axonal transport[211,214].
Spastin role exceeds the developmental period, and indeed it was originally discovered in the context of hereditary spastic paraplegia (HSP), a neurodegenerative disease of the upper motor neurons for which Spastin mutations account for 50% in autosomal dominant familial and 20% of sporadic cases[215,216]. Mechanistically, the disease could evolve as a combination of loss of function and gain of function modalities[217], impairing axonal transport and axonal growth and affecting organelle distribution[218,219]. Furthermore, mutation specifically of the m1 isoform seem to be neurotoxic, possibly due to the non-soluble nature of the mutated gene product, which causes

its accumulation in CNS motor neurons or due to dysfunctional spastin-ER interactions[220]. Core pathological findings report dying-back degeneration of long axonal tracks (lateral corticospinal tracts and sensory neurons of ascending dorsal columns)[202]. This raises interesting parallels between disease and physiological axon pruning where axons retract in a "dying-back"-like fashion. The nerve-muscle explant is a valuable resource for the understanding the modalities of Spastin regulation and its effect on cytoskeleton and overall cell physiology to shed light on the disassembly of axons and synapses.

2.4.5 Molecular motors and transport

Axonal transport is essential for regulating axon composition, neuronal development, maintenance and survival[93,180]. Understanding transport allows to comprehend the cellular dynamics of neuronal functioning.
Historically, it was thought that almost all the macromolecular synthesis occurred in the cell body. In this view, the functional significance of anterograde transport is to supply the terminals with organelles, membrane components and other biomolecules, while the retrograde transport is a means to return worn out materials from nerve terminals to the cell body for degradation[221–225]. Although as a general mechanism these concepts still stand, it is rather simplistic especially in light of evidences of local translation and synthesis in axons[226]. This implies an increased complexity of the biological system, of transport regulation and of its biological significance. In this light, an alternative function of the retrograde motion is to transfer information about the axonal status and of the terminal environment to the cell body in order to coordinate cell responses to external stimuli.
For example, a widespread phenomenon in the developing nervous system is the retrograde transport of trophic factors, such as the nerve growth factor, derived either from target cells or from the environment in which the axons lay. In the context of axonal pruning, neuregulin transport is synchronised between Schwann Cells and neurons to coordinate myelination[227]. As transport is heavily reliant on the cytoskeleton, it is of value to understand how

MT dynamics and architecture is regulated through PTMs and MAPs and how these in turn affect transport.
Classically, axonal transport is divided into "fast" and "slow", depending on the speed reached by the cargoes; vesicles and mitochondria for example move by fast axonal transport at speeds of $\sim$1 μm/s, whereas cytoskeletal components move in slow axonal transport at speeds of $<$0.1 μm/s[228,229]. In the past it was thought that these two forms of transport were completely unrelated and structurally distinct. However, it is now clear that both fast and slow axonal transport are mediated by the same "fast" ATP-dependent molecular motors: kinesin and dynein. The slower rate is simply due to prolonged pauses between movements[230,231]. Kinesins mediate the transport in the anterograde direction while dynein moves cargoes in the retrograde direction[221]. The kinesin superfamily comprises 45 genes in the human genome, 38 of which are expressed in the brain[232]. In particular, kinesin-1, kinesin-2, and kinesin-3 families all contribute to axonal transport. Kinesin-1 family members are heterotetramers composed of two heavy chains (KIF5A–C), which comprise the motor domain and the ATP and MT binding motifs, and two light chains (KLC1/2), which interact with the tails of the KIFs and regulate cargo binding and motor activity[233,234].
Although kinesin-1 motors are more likely to detach from the MT track upon encountering obstacles[162,163], they are highly processive, taking 8 nm steps in a straight path along a single protofilament[235]. They are responsible for the transport of several vesicles, organelles, proteins, and RNA particles and the slow axonal transport of cytoskeletal proteins. In particular, mitochondria are transported by KIF5 and KIF1Bα[236].
Members of the kinesin-2 family (KIF3A/KIF3B/KAP3) mediate the fast transport of late endosomes and lysosomes[237,238] while kinesin-3 motors (KIF1A and KIF1Bb) carry dense core vesicles and synaptic vesicle precursors[239–241].
The dynein motor is encoded by a single gene[242] and it is composed of two heavy chains and additional intermediate, light intermediate and light chains. As for kinesins, the heavy chain contains ATP and MT-binding motifs, while its amino terminus interacts with the additional chains to form

the cargo-binding domain. It is a fast motor, with velocities from 0.5 to 1 μm/s, although unlike kinesins, single dynein motors take frequent back and side steps during movement along the MT[243,244]. This characteristic is thought to be important in allowing the motor to navigate around obstacles along its path[162,245]. Moreover, when the activity of multiple dynein motors is coordinated, dynein transport shifts to unidirectional and highly processive[246,247]. Most dynein functions in the cell require the dynein activator, dynactin[248,249].

Cargos are bound simultaneously by different motor types and scaffolding proteins. Both motors are assisted by adapter proteins, which link them to their cargoes and regulate their activity and determine which motor will be used[238]. Apart from the biophysical properties of individual motors, it is also the combination of motor type, adaptors, and scaffolding proteins, and MT properties which lead to distinct patterns of motility and localization along the axon[221,250,251]. For this reason, it is important to consider their competitive or cooperative interaction.

It is evident that axonal transport is crucial for the proper maintenance and function of a neuron. Its importance is underscored by the findings that impairment of the axonal transport machinery is causative, or is a common factor, in several neurodegenerative disorders, including Alzheimer's, Parkinson's, Huntington's and Upper and Lower motor neuron diseases[252–256].

Beyond disease, transport organization during synapse elimination could be one prominent factor in tipping the balance in winning and losing axons by providing an asymmetrical distribution of resources. In this respect, more arborized motoneurons have been shown to be at a disadvantage when competing against motoneurons with more modest arborization, indicating that availability of resources may be a contributing factor in the competition outcome[257]. This explains the continuous scientific effort into decoding the interaction among motors, MT orientations, stability and modifications. By acting as "road signals", PTMs represent an elegant way to direct and coordinate axonal traffic. Additionally, motor proteins have been shown to have specific preference for PTMs. For example, Kinesin-1 favours movement on stable, detyrosinated and acetylated MTs[182,258–262] while Kinesin-2 and

Dynein are recruited to dynamic tyrosinated MTs[262–265]. Molecular motors have also been shown to recognize distinct MT properties, including MT polarity and MT stability. A clue into how these properties are integrated to regulate transport came from a seminal work by Tas et al. who showed that MTs with similar orientations and modifications segregate into bundles within the MT cytoskeleton. For example, in dendrites of cultured rat hippocampal neurons stable and acetylated MTs are mostly oriented minus-end out, while dynamic and tyrosinated MTs are oriented in the opposite direction. This induces a bias in transport, as exemplified by Kinesin-1 which, due to its molecular properties, moves in a plus-end direction and selectively interacts with acetylated MTs. Such organization guides this motor out of dendrites (mixed polarity) and into axons (plus-end-out polarity) and explains why kinesins mediate anterograde trafficking[262].

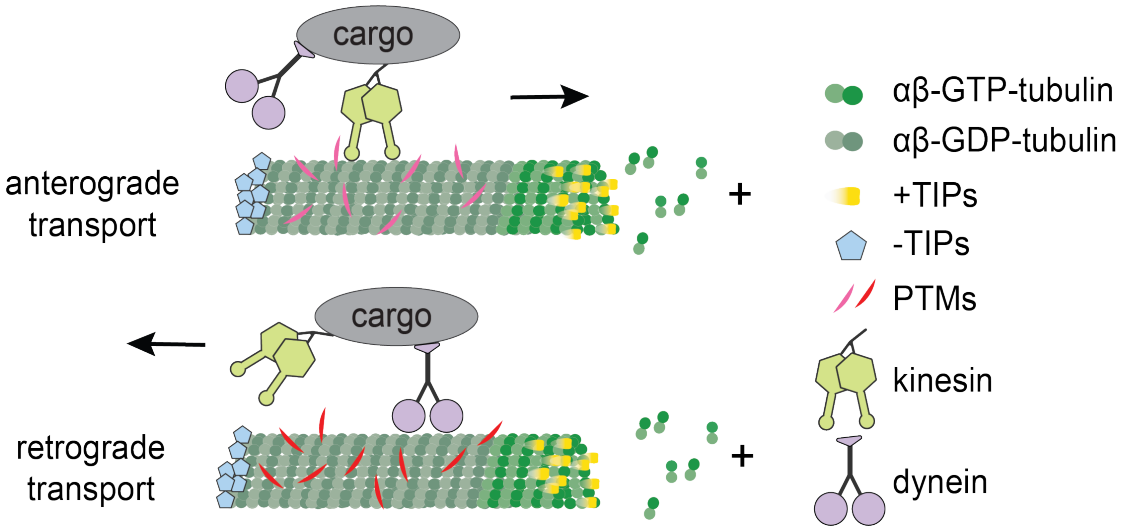

Figure 2.9: ***MTs drive axonal transport*** *MT motor proteins, kinesin and dynein, transport organelles, vesicles, RNA granules, and proteins along the axon. Kinesins drive anterograde transport while dyneins drive retrograde transport. The density and dynamics of the MT cytoskeleton have direct repercussions on axonal transport. A composition of PTMs, MAPs and scaffolding proteins sustain efficient axonal transport and affect molecular motors. Modified from Kapitein and Hoogenraad (2015)*

It is still unclear whether the same architectural principles of separating PTM decorations in district MT subsets to affect specific motors and MAPs are a generalized mechanism to achieve polarized sorting. It is however worth investigating, particularly for Polyglutamylation, the highest expressed PTM in neurons, which has been shown to affect motor proteins such as kinesin-1 and kinesin-3 in single molecule assays and in cultured neurons[120,145,161,266,267]. However, it remains largely unexplored whether similar results are recapitulated in animal models or how this code translates into shaping cell- or tissue-level events.

2.5 Aims and experimental strategy

Several processes contributing to synapse elimination have now been outlined, including neuronal activity, neurotrophic or "punitive" factors, gap junctions, glial or cytoskeletal components. Nevertheless, a comprehensive understanding of how all the involved pathways are tied to each other and in which measure they contribute to the mammalian pruning is still lacking. It is clear, however, that the changing activity patterns and the resulting molecular signalling events need to converge on intracellular remodelling processes that allow dismantling of specific presynaptic terminals.
Intuitively, due to the regressive nature of this physiological morphogenic event, ultimately these signals and pathways must converge into localized and branch-specific MT cytoskeletal dismantling. Given the required specificity, the 'tubulin code' provides a good framework for enabling such localized regression. Hence, in this study, I explore the role of the 'tubulin code' in guiding synapse elimination in mammals, with a focus on PTMs of MTs and the enzymes that mediate these modifications. The murine NMJ is a comparably large and accessible synapse and offers several advantages to tackle this question, thanks to the possibility of carrying out advanced imaging, labeling and next generation sequencing. These characteristics make the study of synapse elimination approachable at the subcellular and molecular level.

Thus, for my PhD project I focused on the following aims:

- Establish a cell specific RNA sequencing approach to generate a motor neuron translatome and mine the dataset to discover genes involved in mammalian pruning, both within and beyond the tubulin code-related proteins affecting the MT cytoskeleton.

- Genetically manipulate the tubulin code editors and erasers to observe changes to MT PTMs, MT mass and dynamics, axonal transport and whether they ultimately affect synapse elimination.

- Manipulate neurotransmission to elucidate if the activity of glutamylation modifying enzymes is under the control of neuronal activity.

3 Results

In this chapter, content stated with 'I' reflects my own opinion and work, while statements with 'We' reflect the collaborative work product of myself and our collaborators.

3.1 Motoneuron transcriptome of mice undergoing axonal pruning

Axonal pruning is progressively resolved by the first two postnatal weeks in mice[3,21,268]. Neuronal activity plays a crucial role in the process and some molecular players have been elucidated, including the MT severase, Spastin, which has been shown to delay pruning when genetically deleted due to an increase in the MT mass which stabilizes MT cytoskeleton[74,227]. However, despite decades of studying the NMJ system, clear mechanistic pathways are still lacking of both the general pruning process and of how Spastin contributes to pruning. Ribotag[269,270] has been successfully utilized *in vivo* and *in vitro* to characterize the actively translated mRNA from polysomes[270–274]. Hence this experimental tool was chosen in an effort to identify the molecular players in an unbiased and unsupervised fashion.

To achieve motor neuron specific mRNA isolation, *ChaT*-Cre mice, which express the Cre recombinase in cholinergic neurons, were crossbred with RiboTag knock-in mice[270], in which the 60S ribosomal subunit is tagged with hemagglutinin (HA). Motor-neuron mRNA bound to polysomes were isolated through immunoprecipitation with an HA antibody according to the protocol described in the Method section (5.7, Figure 3.1a). We have chosen 5 timepoints (Postnatal (P) day 5, 7, 9, 11, 14) of wildtype (WT) samples

3.1 Motoneuron transcriptome of mice undergoing axonal pruning

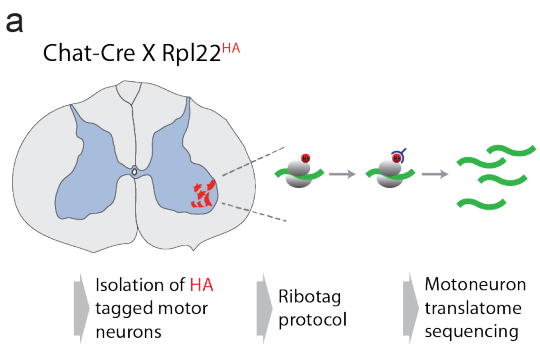

b

timepoints

Motor neuron	Spinal cord	Spastin^{mnKO}
P5	P5	P5
P7		
P9	P9	P9
P11		
P14		P14*

Figure 3.1: ***Strategy to isolate and sequence motoneuron specific mRNA.*** ***a)*** *Schematic of Ribotag technique illustrating the main steps of the protocol. Motoneuron cells are labelled with HA through the breeding scheme of ChaT-Cre X Rpl22-HA. Spinal cord is dissected, followed by Ribotag immunoprecipitation protocol and sequencing of resulting mRNA derived from active translating polysomes of motoneurons.* ***b)*** *Summary table of timepoints used in each category of samples: WT motoneurons isolated with Ribotag, whole signal cord and motoneuron Spastin^{KO} isolated with Ribotag; each timepoints consists of biological triplicates except for when marked with *, which consists of 1 sample.*

that span the window of intra branch NMJ competition, where pruning is naturally resolved by day 14. Additionally 3 timepoints (P5, P9 and P14) of Spastin^{KO} samples, where pruning is delayed compared to wildtype, and two total spinal cord samples which serve as control and comparison for the other samples (P5 and P9) (Figure 3.1b).

We sequenced the ribosome-bound mRNA from the soma of the motor neurons and obtained the resulting translatome in collaboration with the Core Facility Next-Generation-Sequencing (Elisabeth Graf, Institute of Human Genetics, Helmolz Zentrum Munchen). Prior to sequencing, I immunostained the spinal cord sections for HA and the cholinergic neuron marker Choline Acetyl transferase (ChaT). The broad extent of colocalization of ChaT and HA confirm the faithful HA-expression solely in motor neurons (Figure 3.2a). Only samples with mRNA content higher than 100ng and with a RIN (RNA integrity number) higher than 8.5, indicating negligible RNA degradation during the immunoprecipitation and RNA isolation, were further considered for sequencing. Following sequencing, reads passed

a primary quality control process of fast-Q files. Through PCA analysis of transcripts, two distinct groups clearly emerged: the motor neurons and the whole spinal cord samples. Age was a second component for segregation, with P5 samples segregating furthest from P14 (Figure 3.2b). These result highlight the molecular difference between the total RNA from spinal cord and the efficiency of the immunoprecipitation of motor neuron mRNA. I further confirmed the specificity of RNA pull-down from motor neurons by gene ontology analysis and by measuring the relative expression levels of motor neuron enriched genes in Ribotag pull-down compared to whole spinal cord RNA.

Indeed, the analysis of enrichment of motor neurons versus spinal cord indicated a negative fold change for markers of oligodendrocytes (Sox10, Olig2, Cspg4) and astrocytes (Gfap, Slc1a3, Aldh1l1, Olig2, Cspg4). A positive fold change was measured instead for motor neuron specific markers (Isl1, ChaT, Mnx1), which became more evident at the P9 stage compared to P5. This is indicative of continued maturation towards motor neuron identity (Figure 3.2c).

I corroborated the sequencing results with RT-qPCR, a standard technique used to validate sequencing data. The canonical neuron marker Chat was ∼20 times more expressed in the ribotagged samples compared to the spinal cord (Figure 3.2d). On the other hand, Gfap was ∼80 times more expressed in spinal cord compared to the ribotagged motor neuron (Figure 3.2d).

Many categories in accordance with motor neuron development terms also emerge through Gene ontology (GO) analyses, such as **'axon development'**, **'neuron development'**, in the category "Biological Process" when considering the top 500 differentially expressed genes in motor neurons compared to spinal cord (Table 3.3a). By further increasing the stringency of the search to the top 150 differentially expressed genes in motor neurons compared to spinal cord, neuronal cell component terms emerge in the GO field "Cellular Component", such as **"synapse", "axon", "cell body"** (Table 3.3b). The neuronal identity of the transcripts is also evident from GO of pathway analysis of the 5316 differentially expressed genes in motor neurons when comparing transcriptional changes from P5 to P14, particularly

in the downregulated group of genes (Figure 3.2e and f). The upregulation of pathways involved in calcium mediated events and downregulation of "developmental biology" and "axon guidance" pathways, is in accordance with the maturation of motor neurons from P5 to P14.
Taken together these data indicate that the sequenced mRNA is of high purity and specifically immunoprecipitated from motor neurons, hence the translatomic data were subsequently utilized to mine information regarding the pruning process.

3.2 Expression of glutamylase enzymes during developmental pruning

Destabilizing the cytoskeleton is a prerequisite to achieve axonal pruning. It was previously shown by Brill et al. that the absence of the MT severing enzyme, Spastin delays axonal pruning in mice[74]. Together with the fact that Spastin activity can be regulated by PolyE of MTs[157,158], I explored, how the enzymes that mediate PolyE were translationally regulated during the time period that coincides with axonal pruning. The polyglutamylation of MTs is catalyzed by glutamylases: a set of tubulin-modyfing enzymes shown to have non-redundant roles and differential tubulin substrate specificity in the adult brain[135,144,146–149,151,275]. Insofar, the available expression data of Glutamylases is derived from RT-qPCR analyses of adult brain extracts. Thus, several aspects of the glutamylases' activity and regulation are still unclear. In particular, the extent to which their expression pattern and their isoform specific functions are conserved across different cell types, and how they contribute to Spastin-mediated axonal pruning during development still needs to be thoroughly investigated.
Using our translatome dataset I investigated the expression profile of "seeding" and "elongating" glutamylases in motor neurons during the postnatal synapse elimination period, at different time points: postnatal (P) day 5, 7, 9, 11, 14. "Seeder" glutamylases are enzymes able to add the first glutamate to tubulin tails (i.e. monoglutamylation), whereas "elongators" are able to

3.2 Expression of glutamylase enzymes during developmental pruning

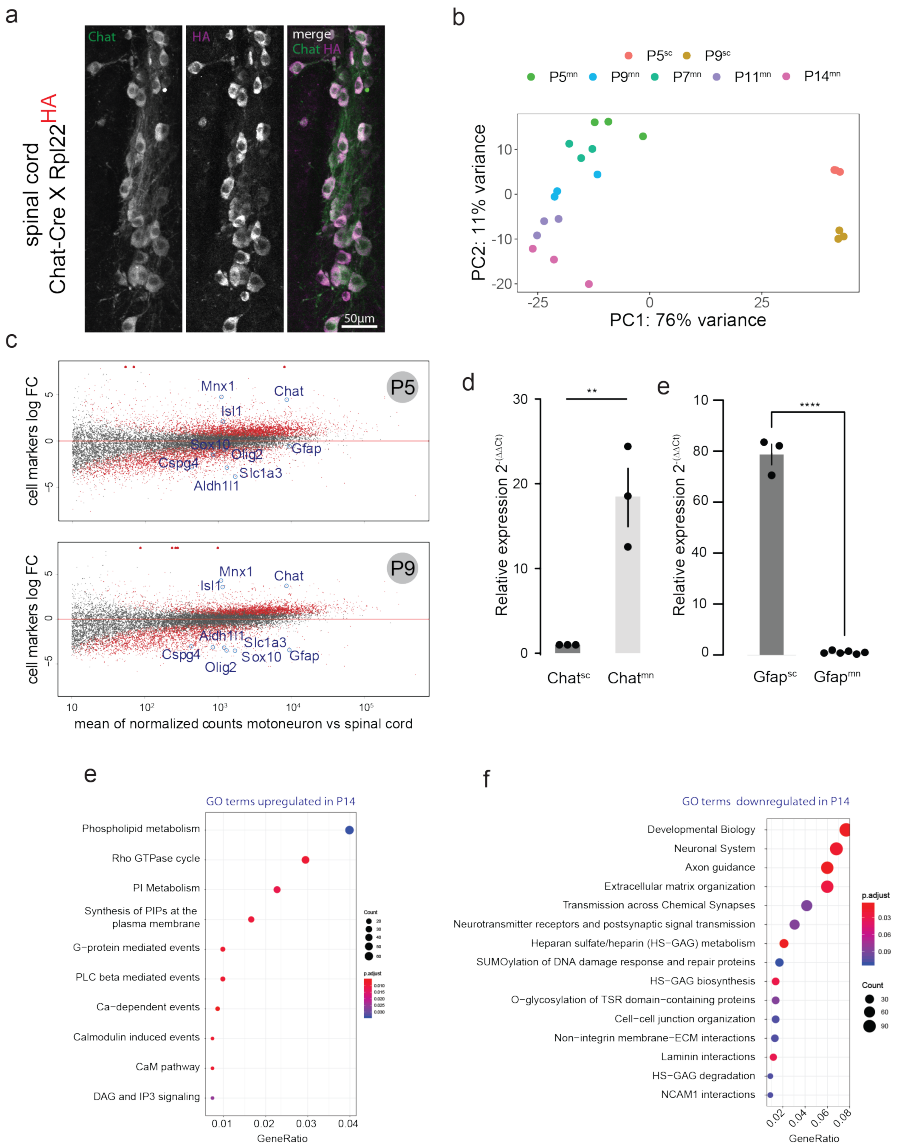

Figure 3.2: ***Ribotag effectively enables cell-type specific translatome from young motoneurons***. *a) Spinal Cord sections stained for Choline acetyltransferase (ChaT, green) and Hemagglutinin (HA, magenta) colocalize in $Rpl22_{HA+}$ mice. No spurious HA expression is noticeable outside of somatic $ChaT_+$ motor neurons cells lying in ventral horn.* ***b)*** *PCA plot of mRNA samples from spinal cord (sc) and mRNA from IP from motor neurons (mn). Individual dots represents a single animal, color coded by age. Cell type identity accounts for the highest degree of variance among samples, with motor neurons segregating furthest from spinal cord samples.* ***c)*** *MA plot at P5 and P9 highlights enrichment of motor neuron specific cell markers in $Rpl22_{HA+}$ motor neuron translatome samples, compared to total spinal cord. Genes above cutoff threshold of FDR $\leq$ 0.05 and a $\mid Log_2\ FC \mid \geq$ 1.5 are depicted in red. Genes above the red horizontal line are enriched in pull-down group, and include motor neurons markers (Mnx1, ChaT, Isl1).* *(continues on page 41)*

3.2 Expression of glutamylase enzymes during developmental pruning

(a) GO "Biological Process" in Motor neuron vs Spinal Cord at P9

GO term	Description	Bonferroni
GO:0000902	cell morphogenesis	6.25e-11
GO:0006812	cation transport	2.03e-10
GO:0035295	tube development	1.73e-9
GO:0030198	extracellular matrix organization	3.97e-9
GO:0048666	neuron development	4.03e-9
GO:0031175	neuron projection development	4.13e-9
GO:0061564	axon development	1.97e-8

(b) GO "Cellular Component" in Motor neuron vs Spinal Cord at P9

GO term	Description	Bonferroni
GO:0045202	synapse	9.21e-6
GO:0043209	myelin sheath	1.73e-5
GO:0030424	axon	3.39e-4
GO:0098793	presynapse	7.26e-4
GO:0044297	cell body	2.12e-3
GO:0015630	MT cytoskeleton	2.64e-3
GO:0150034	distal axon	6.82e-3
GO:0031252	cell leading edge	1.63e-2

Table 3.3: ***Gene Ontology Analysis of motor neuron vs spinal cord at P9***. *a) GO category "Biological Processes" generated using top 500 most differentially expressed genes by comparing motor neuron against spinal cord at P9 using a cutoff of padj $\leq$ 1,e-7 and $|\ Log_2\ FC > 2$. b) GO category "Cellular Component", generated by using top 150 most expressed genes.*

Figure 3.2 *(continues from previous page)*: *Conversely astrocytic (Gfap, Slc1a3, Aldh1l1) and oligodendrocitic markers (Sox10, Olig2, Cspg4) are de-riched.* ***d)*** *RT-qPCR on spinal cord and $Rpl22_{HA+}$ IP samples is used to validate sequencing results. Results were calculated according to $2^{-\Delta\Delta Ct}$ method, using primers of a tested efficiency $\geq$ 90%. ChaT is $\sim$ 20 times more expressed in IP mRNA from motor neurons than spinal cord (**p $\leq$ 0.01, two-tailed t-test); conversely Gfap is $\sim$ 80 times more expressed in spinal cord than motor neuron samples (****P $\leq$ 0.0001, two-tailed t-test). The amplification threshold cycle (Ct), was the average of 2 or 3 technical replicates from each biological sample. A total of 3 animals per group were used for statistical testing; error bars are mean $\pm$s.e.m.* ***e and f)*** *Gene ontology (GO) enrichment analysis of motoneuron transcripts at P14 over P5, separated into upregulated and downregulated. Categories with more representation have higher gene ratios (x-axis). The count reflects the number of genes within the GO term, and significance is denoted with color scale.*

add sequential glutamates onto previously monoglutamylated tubulin tails. I first quantified the expression profiles of the mammalian glutamylases in order to assess if and which glutamylase is responsible for Spastin-mediated pruning.

Among the 5316 differentially expressed neurons, across the 5 tested time points, TTLL1 (Tubulin Tyrosine Ligase Like 1) was the most expressed elongator enzyme of the glutamylases family (Figure 3.3a), while TTLL7 was the most expressed motor neuron initiator glutamylase (Figure 3.3b), also confirmed by RT-qPCR (Figure 3.3c).

To test whether glutamylation has a role in the regulation of MT mass and synapse elimination *in vivo*, we generated two mouse models: a) the first to deplete polyglutamylation on α-tubulin ($TTLL1^{mnKO}$, *ChaT*-Cre x TTLL1 conditional knockout); b) the second to deplete monoglutamylation on β-tubulin ($TTLL7^{mnKO}$).

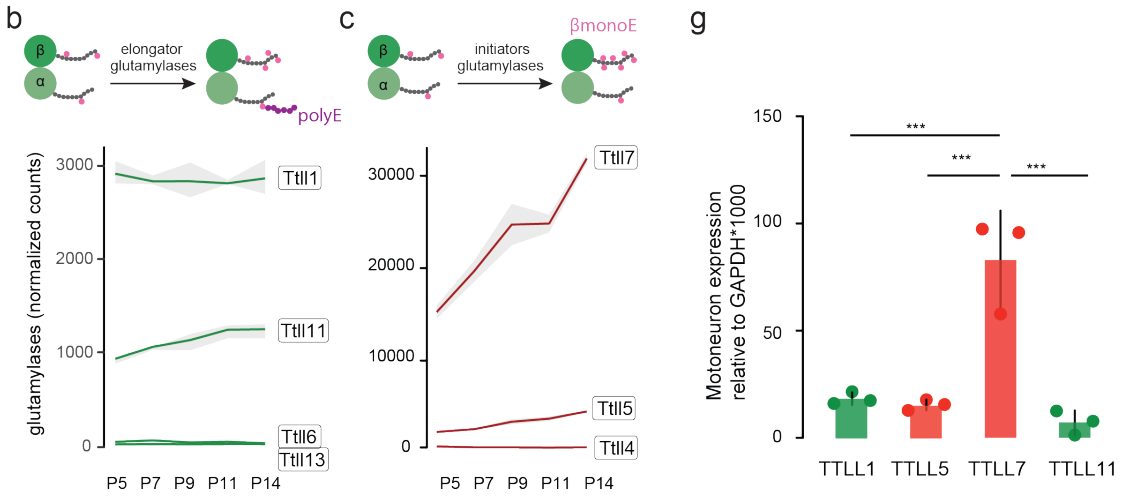

Figure 3.3: ***Expression of glutamylases in motor neurons.*** ***a)*** *Normalized read counts of elongator glutamylases in motoneurons at 5 time points of development.* ***b)*** *Normalized read counts of initiator glutamylases in motoneurons at 5 time points of development. Data are expressed as mean and s.e.m.*

3.3 TTLL7 genetic ablation in motor neurons does not affect axonal pruning

Using the motorneuron specific knock-out mouse lines we generated from floxed lines generously gifted by Carsten Janke's Lab (Institut Curie, PSL Research University, France), I first investigated if TTLL7 (TTLL7$^{\text{mnKO}}$), the highest expressed "seeder" of single glutamates on β-tubulin, can instruct axonal pruning. The polyglutamylation pattern was unchanged in the TTLL7$^{\text{mnKO}}$ compared to controls (Figure 3.4 a & b), while βmonoE immunofluorescence intensity was significantly decreased in terminal axons of TTLL7$^{\text{mnKO}}$ compared to TTLL7$^{\text{mnWT}}$ at P9 (Figure 3.4 d & e). Hence, TTLL7 can add the first branch point glutamate onto the tail of the β-tubulin isoform, but it cannot perform the sequential addition of glutamates into a chain. This corroborates the hypothesis of a divergence of the glutamylases enzymes to be either a "seeder" or "elongator"[150,266]. Quantification of tubulin intensities in TTLL7$^{\text{mnKO}}$ vs TTLL7$^{\text{mnWT}}$, showed that the reduction of βmonoE did not lead to changes in the MT content (Fig-

ure 3.4c). Consequently, pruning speed of motor axons was unchanged in TTLL7^{mnKO} compared to control at all three time points analyzed (Figure 3.4f).

MT dynamics were not affected upon genetic deletion of TTLL7, as evinced from analysis of Thy1-EB3-YFP comets in nerve-muscles explants[11]. In fact, similar EB3 comet density, comet length and EB3 particle velocity were seen in TTLL7^{mnKO} and littermate controls (Figure 3.5 a & b). Additionally, the analysis of comet orientation, which can reveal if the direction of growth of MTs is altered, (canonically in mammals, MTs grow towards synapse, referred as 'plus tip out'[111]), was unchanged between the two genotypes (Figure 3.5 d).

With these results I show that the glutamate "seed" on β tubulin (βmonoE), alone does not have a strong enough negative charge to electrostatically recruit Spastin to MTs[157,190]. To summarize, TTLL7 is the highest expressed "initiator" in motor neurons and while TTLL7 promotes monoglutamylation of MTs, it does not affect pruning or cytoskeletal mass.

3.3 TTLL7 genetic ablation in motor neurons does not affect axonal pruning

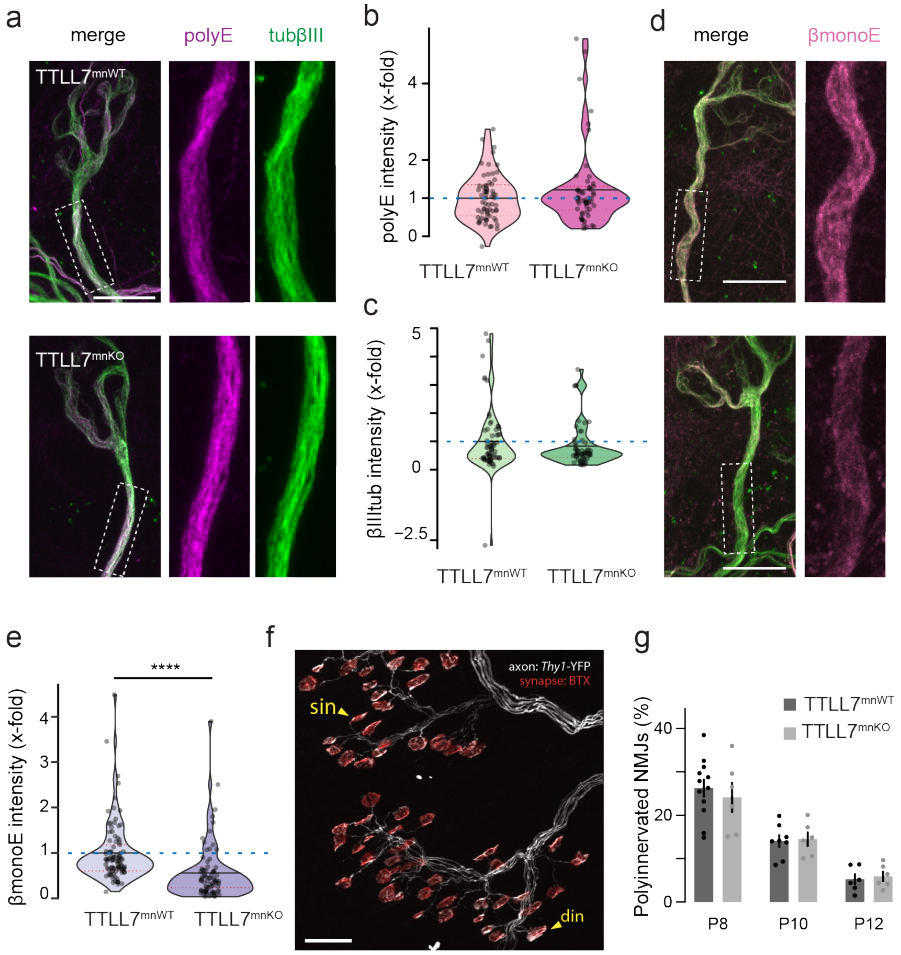

Figure 3.4: ***Deleting TTLL7 in motor neurons does not affect axonal pruning***. ***a)*** *and* ***d)*** *Immunostaining for MT PTMs in axons of triangularis sterni muscle fixed at P9. TTLL7^{mnKO} mouse were compared to WT littermates for the following modifications: polyE (magenta), β-monoE (pink) and βIII-tubulin (green). Inset shows enlarged axonal area.* ***b)***, ***c)*** *and* ***e)*** *Quantification of immunostaining intensities of TTLL7^{mnKO} versus WT littermates.* ***b)*** *Polyglutamylation levels are normalized to βIII-tubulin, p = 0.59 (two tailed Mann-Whitney, n = 65 / 55 axons from 9 animals) and* ***c)*** *βIII-tubulin intensity are normalized to neurofilament staining, p = 0.26 (two tailed Mann-Whitney, n= 65/55 axons from 9 animals)* ***e)*** *intensity levels of β-monoE normalized to βIII-tubulin, ****$p \leq$ 6.8e-11 *(two tailed Mann-Whitney, n = 94/76 from 9 animals). Data are expressed as mean and IQR. Confocal image of a synaptic field in a fixed triangularis sterni muscle at P9 (Thy1-YFP-16, white; α-bungarotoxin, red; scale bar 50 μm). Yellow arrowhead points to singly innervatd NMJ (sin) and doubly innervated NMJ (din).* ***g)****Percentage of polyinnervated synapses of TTLL1^{mnKO} versus WT littermates, evaluated on Thy1-YFP-16 transgene. Statistics calculated independently in each age group, p $\geq$ 0.05 (two-tailed unpaired t-test). Each dot represents a single animal. Scale bars 10μm.*

3.3 TTLL7 genetic ablation in motor neurons does not affect axonal pruning

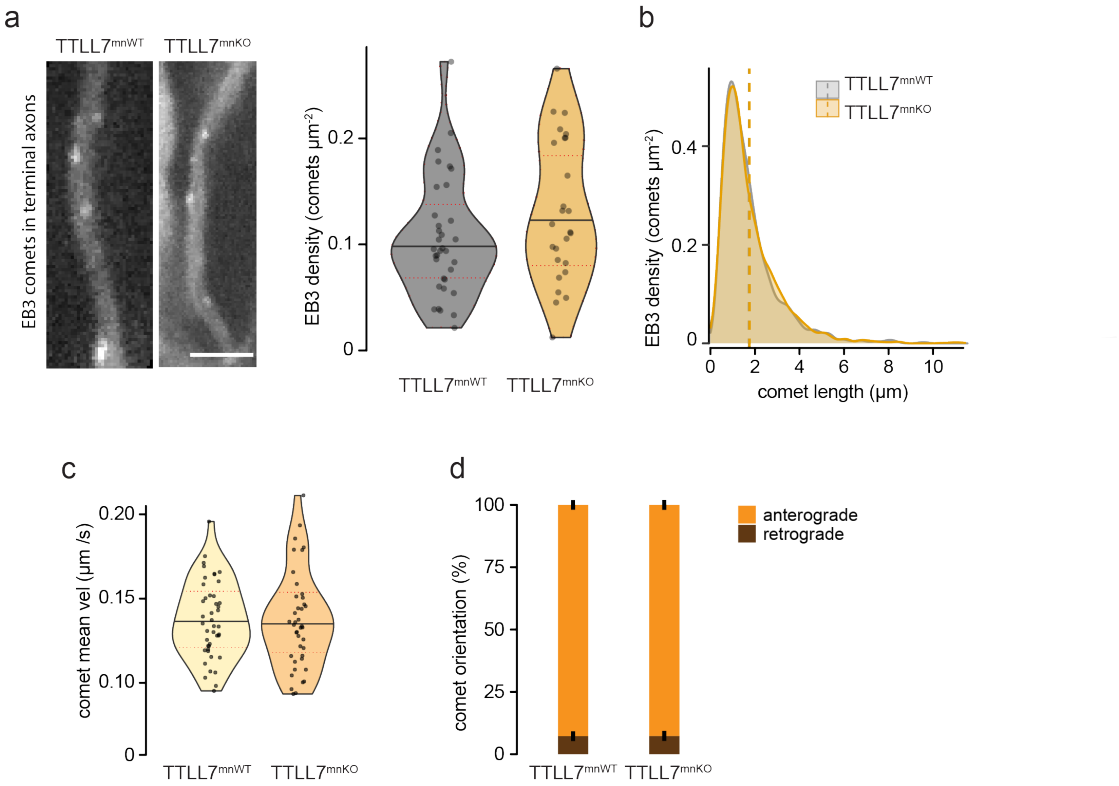

Figure 3.5: ***Deleting TTLL7 in motor neurons does not affect cytoskeletal dynamics of pruning axons.*** *No difference was seen in several paramenters of MT dynamics that were quantified in TTLL7^{mnKO} and compared to TTLL7^{mnKO} control littermates (a total of 6 animals were used in all experiments).* ***a)*** *Single frame from a time-lapse recording (20s) in a P11 Thy1-EB3-YFP explant showing a singly innervated NMJ in TTLL7^{mnWT} and TTLL7^{mnKO} animals (scale bar 2.5 µm) and their associated Eb3 comet density quantification, which is unchanged between two groups, p= 0.11 (Mann-Whitney unpaired test, n = 34/26 axons).* ***b)*** *Comet length distribution in the two genotypes was unchanged, p = 0.46 (two-sample Kolmogorov-Smirnov test, n =2184/2312 respectively from 34/26 axons, vertical dashed lines consists of mean value).* ***c)*** *Comet mean velocity p = 0.88 (two-tailed unpaired t-test, n = 44/41 axons).* ***d)*** *Comet orientation p = 0.78 (Mann-Whitney unpaired test, n = 44/41 axons). Data are expressed as mean and s.e.m.*

3.4 TTLL1 genetic ablation delays pruning

The diversification of enzymatic functions of glutamylases but the lack of involvement of TTLL7 in axonal pruning, prompted me to explore if the highest expressed "elongator" glutamylase TTLL1 has instead a role. Toward this end, I performed quantitative immunostainings for polyglutamylation on P9 as before in TTLL1$^{\mathrm{mnKO}}$ and the TTLL1$^{\mathrm{mnWT}}$ littermate controls. I found a drastic reduction of polyE in TTLL1$^{\mathrm{mnKO}}$ mice, as expected from its putative function (Figure 3.6d-e).

Polyglutamylation has been shown *in vitro* to act as a docking signal for the MT severing enzyme Spastin[157, 190]. Consistent with this, the depletion of the elongator glutamylase TTLL1 in motor neurons led to an increase in MT mass at P9 (Figure 3.6g). Immunostainings of triangularis sterni muscles with antibodies against single glutamate seeds on the β-tubulin tails (βmonoE), showed unchanged levels of β-tubulin monoglutamylation in the TTLL1$^{\mathrm{mnKO}}$ (Figure 3.6b and e). This confirms the specificity of the mouse model to solely deplete the long polyE tails[266]. The fluorescence intensity of acetylated tubulin, a PTM associated with stable and long-lived MTs, was significantly decreased in the TTLL1$^{\mathrm{mnKO}}$ compared to control (Figure 3.6c and f). This can be explained by the reduced severing activity of Spastin in TTLL1$^{\mathrm{mnKO}}$, which gives rise to a surplus of MTs. This younger MT population did not have sufficient time to accumulate the acetylation, resulting in the decreased ratio of this PTM over the whole MT mass.
Therefore, the absence of TTLL1 in motor neurons decreases the overall tubulin polyglutamylation, leading to an increased MT mass and changes the post-translational profile as a consequence of impaired Spastin recruitment.

3.4.1 Impairing polyglutamylation of α-Tubulin-4A affects axonal pruning

TTLL1 might not efficiently add the first glutamate onto the tubulin tail. The unaffected tubulin mass in absence of TTLL7 shown in 3.3 indicates that this monoglutamylase is not responsible for priming the tubulin with

3.4 TTLL1 genetic ablation delays pruning

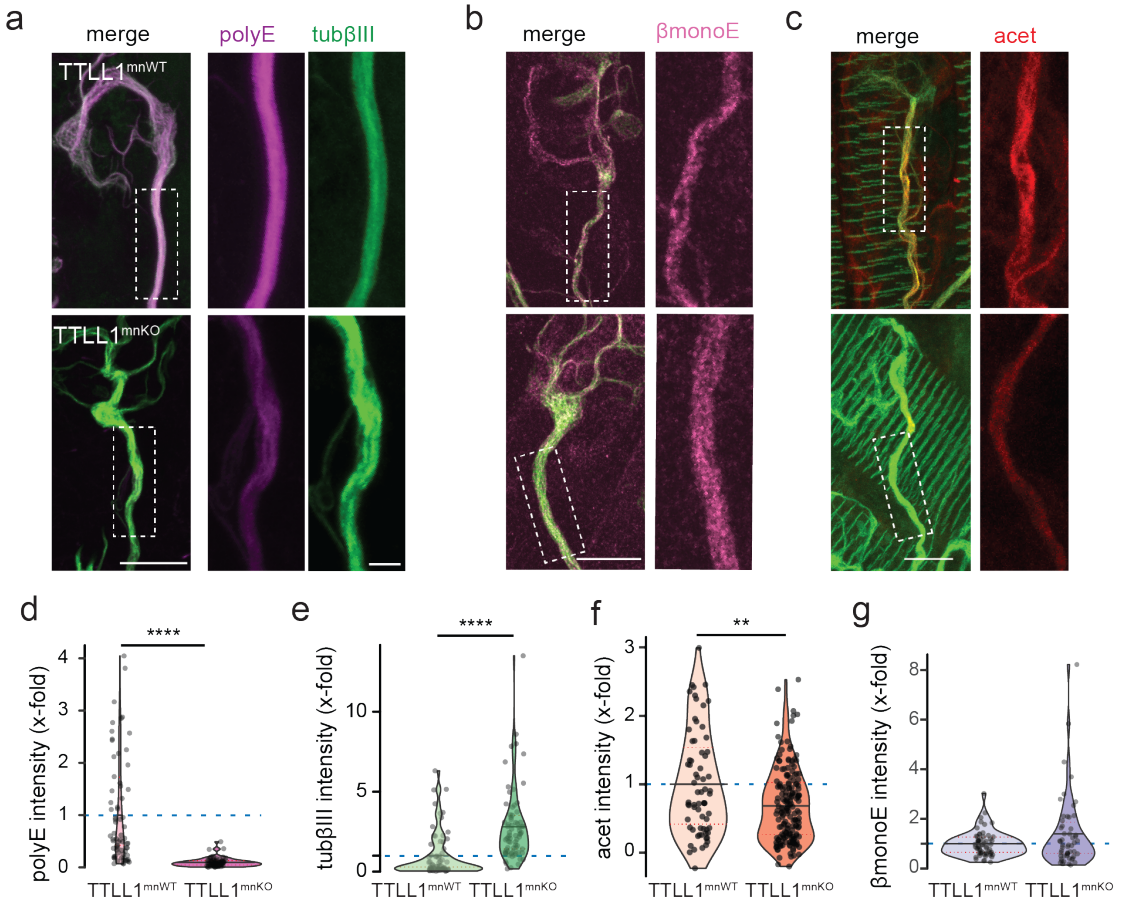

Figure 3.6: ***Deleting TTLL1 in motor neurons delays axonal pruning***. ***a)*** *through* ***c)*** *Immunostaining for post-translational modifications of MTs in axons of triangularis sterni muscle fixed at P9. TTLL1^{mnKO} mouse were compared to WT littermates for the following modifications:* ***a)*** *polyE (magenta) and βIII-tubulin (green),* ***b)*** *β-monoE (pink), and* ***c)*** *acetylation (red). Inset shows enlarged axonal area.* ***d)*** *to* ***g)*** *Quantification of immunostaining intensities of TTLL1^{mnKO} versus WT littermates; scale bars 10µm (insets 5µm).* ***d)*** *Polyglutamylation levels are normalized to βIII-tubulin, ****p ≤ 2.2e-16 (Mann-Whitney U unpaired two tailed test, n = 70/72 axons from 6 animals)* ***e)*** *intensity levels of β-monoE normalized to βIII-tubulin, p = 0.71 (Mann-Whitney unparied test, n=58/54 from 6 animals) and* ***g)****intensity levels of acetylation normalized to βIII-tubulin, **p≤ 0.005 (Mann-Whitney unparied test, n = 88 /177 from 13 animals).* ***g)*** *βIII-tubulin intensity are normalized to neurofilament staining , ****p ≤ 1.1e-11 (Mann-Whitney U unpaired two tailed test, n = 70/72 axons from 6 animals) Data from immunostainings are expressed as mean and IQR.*

the glutamate "seed" for TTLL1. By plotting translatome glutamylases expression as fold change in motorneurons over spinal cord at P5, it emerges that TTLL1, TTLL7, TTLL5, TTLL11 or TTLL2 are enriched in motor neurons compared to spinal cord (Figure 3.7). Of these, only TTLL5 is a known monoglutamylase[143] and thus a promising candidate for acting upstream of TTLL1, which should be interesting to investigate in the future.

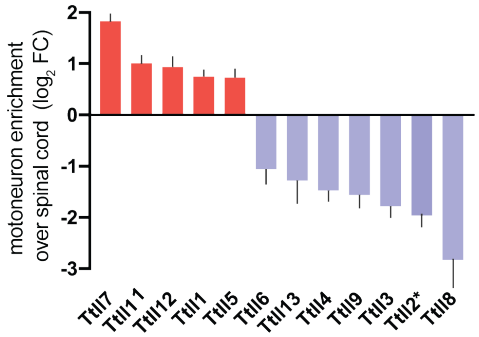

Figure 3.7: ***Fold change enrichment of glutamylases in motor neurons over spinal cord at P5.*** *The monoglutamylase, TTLL5 is 1.6 times more expressed in motor neurons than spinal cord tissue, p-adj ≤ 1.5e-8. Data are expressed as Log_2 fold change values from DESeq2 expression analysis. Estimated standard error was done using three biological replicates in both the spinal cord group and motor neuron group at P5. Asterisc indicates genes did not pass differential expression cut-off of adjusted p-value Benjamini-Hochberg, p-adj ≤ 0.05.*

Additionally, my data and previous literature suggest that TTLL7 uses β-tubulin as a substrate, while TTLL1 uses α-tubulin[151], which could explain the lack of effects of TTLL7. The motor neuron translatome indicate that several α-tubulin isoforms are expressed during the pruning period (Figure 3.8a) and their expression changes substantially from P5 to P14. Interestingly, although Tuba4a expression is the lowest in motor neurons (2.3% at P5 and 4.4% at P14 Figure 3.8a), it is the tubulin isoform with the highest net increase in the two ages (a 63% increase in P14 compared to P5, Figure 3.8b), followed only by Tuba1b with a moderate overall increase of 9% from P5. Furthermore, Tuba4a expression steadily increases over time, while the

other α isoforms present a drop in expression around P9 (Figure 3.8c). To verify if Tuba4a is the substrate of TTLL1 and thus its polyglutamylation can also instruct axon remodelling, we utilized Tuba4a knock-in mice, which carry a mutation in α-Tubulin tail that hampers its glutamylation[117]. Immunostaining intensity for polyE normalized on βIII-tubulin were decreased in terminal motor axons at P11 as expected (Figure 3.8e &f). Concomitantly, βIII-tubulin intensity normalized on neurofilament increased (Figure 3.8g), reminiscent of the TTLL1$^{\text{mnKO}}$ phenotype (Figure 3.6e). Likewise, pruning speed was delayed in Tuba4a$^{\text{KI}}$ compared to control littermates (Figure 3.6g). Thus we show that hindering polyglutamylation of Tuba4a tails delays motor axon remodelling by affecting tubulin levels, and this α-tubulin isoform is a substrate of TTLL1.

3.4.2 The surplus of MTs in young TTLL1$^{\text{mnKO}}$ is abolished in adults

Next I investigated the effects on MTs when TTLL1 deletion is protracted into adulthood. Quite strikingly, reduced polyglutamylation became more persistent and evident in the adult compared to the young TTLL1$^{\text{mnKO}}$ vs TTLL1$^{\text{mnWT}}$ mice, suggesting that absence of this enzyme does not get compensated by the other 7 isoforms present in the system. Of interest, the surplus of MT mass seen during development was abolished (Figure 3.9 a & c). The unchanged mass between adult KO and WT was also seen in adult Spast$^{\text{mnKO}}$ (Figure 3.9 d). The commonalities between these mouse lines strengthens the notion of these two enzymes acting in concert in the same molecular pathway. It points to potential homeostatic mechanisms in axons that reduce the surplus of MTs during young ages, and to a steady-state in the adult.

3.4 TTLL1 genetic ablation delays pruning

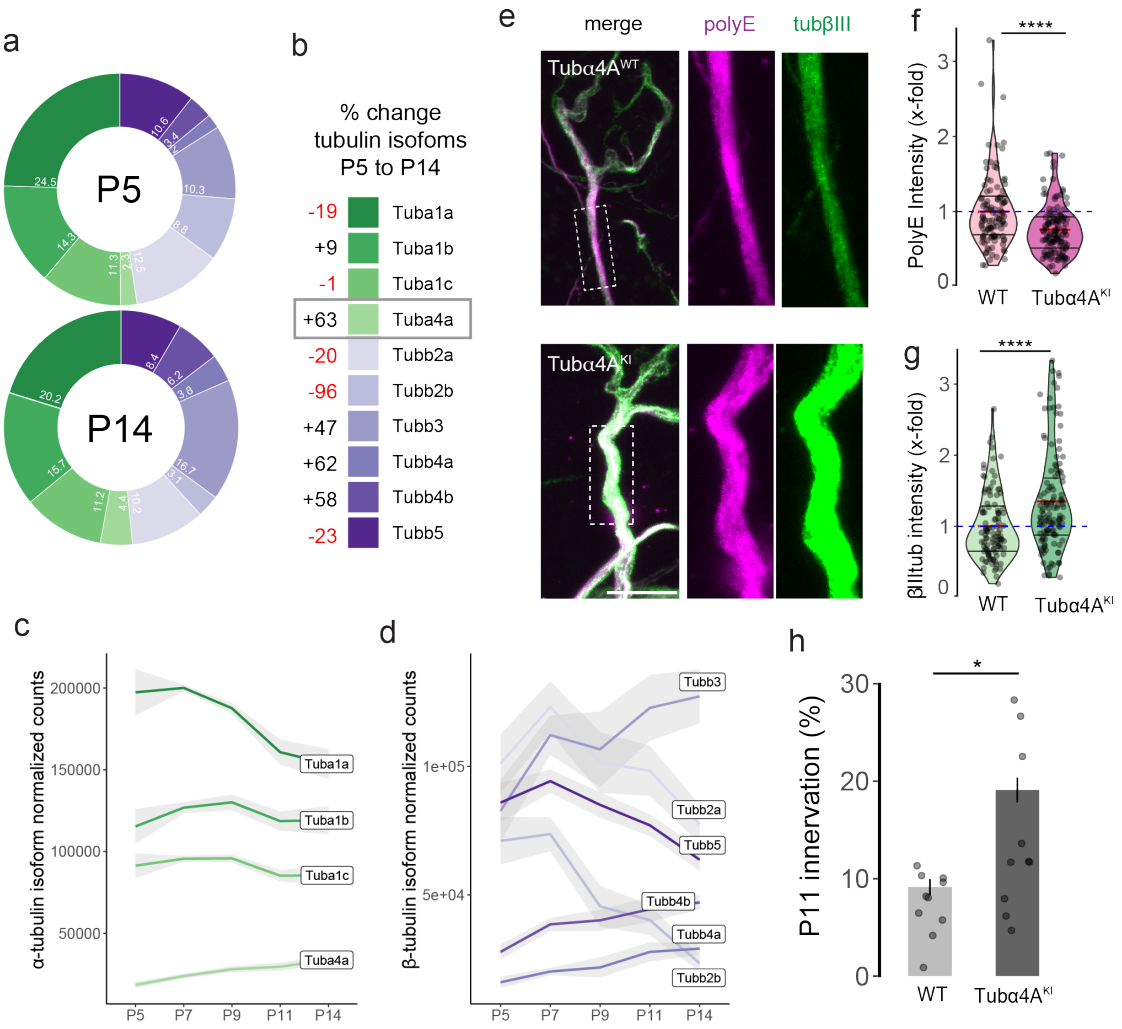

Figure 3.8: ***Preventing polyglutamylation of Tuba4a delays axonal pruning.*** *a) Percentage of tubulin isoform expression at age P5 and P14 in motor neurons from translatome data; β-tubulin color coded in violets, α-tubulin color coded in greens.* ***b)*** *Relative change of expression of tubulin isoforms at P14 compared to P5.* ***c)*** *Translatome derived normalized read counts of α-tubulin and* ***d)*** *β-tubulin isoforms across 5 developmental time points in motoneurons.* ***e)*** *Axonal immunostaining of triangularis sterni muscle for polyE (magenta) and βIII-tubulin (green) in $Tuba4^{KI}$ and $Tuba4^{WT}$ at P9. Dashed area corresponds to enlarged region; scale bar is 10µm.* ***f)*** *polyE normalized to total βIII-tubulin mass was significantly decreased in $Tuba4^{KI}$ compared to controls and* ***g)*** *βIII-tubulin normalized on neurofilament was significantly increased in $Tuba4^{KI}$ compared to controls, ****$p \leq 0.00001$ (both tests, Mann Whitney, n = 109/127 axons from a total of 11 animals).* ***h)*** *Polyinnervation of synapses at NMJs is increased at P11 in $Tuba4^{KI}$ compared to $Tuba4^{WT}$, *$p = 0.02$ (Wilcoxon rank sum exact test, n= 3/6 mice). Data in violin plots are mean and IQR, bar plots are mean and s.e.m.. Figures e) to g) were generated in collaboration with A.Z.*

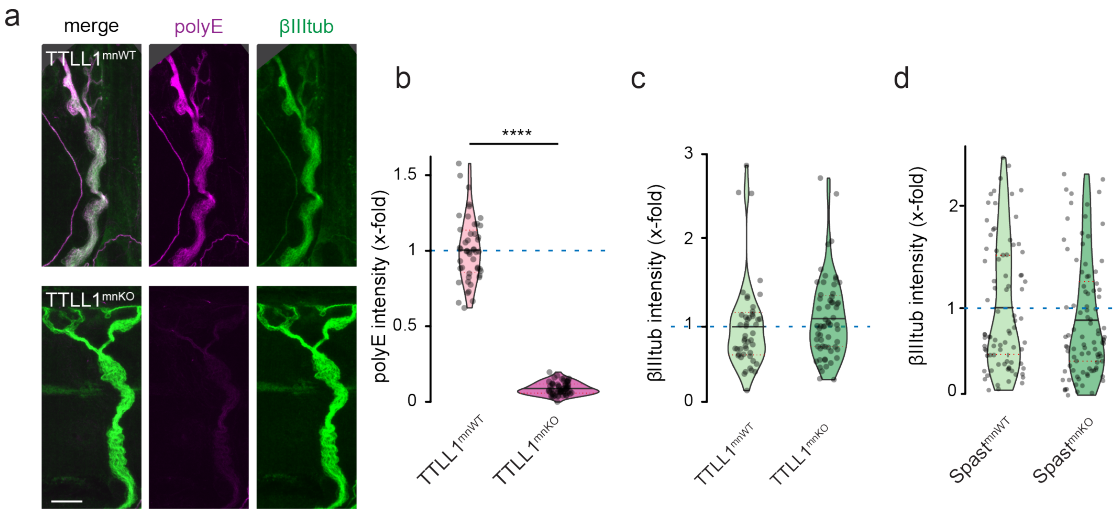

Figure 3.9: ***MT cytoskeleton of TTLL1^{mnKO} adjusts to steady-state in adult mice.*** ***a)****Immunostaining of MTs for polyE (magenta) and βIII-tubulin (green) in axons of triangularis sterni muscle fixed at 1 month.* ***b)*** *Quantified polyE fluorescence intensities were normalized to βIII-tubulin, ****p<0.0001(two-tailed Mann-Whitney test, n=48/61 axons).* ***c)*** *&* ***d)*** *βIII-tubulin fluorescence intensities were normalized to neurofilament and were unchanged in adult TTLL1^{mnKO} vs TTLL1^{mnWT}, p=0.15 (two-tailed Mann-Whitney test, n=48/61 axons) and adult Spastin^{mnKO} vs TTLL^{mnWT}, p=0.21 (two-tailed Mann-Whitney test, n=83/93 axons). Each knock-out mouse was compared to its control littermate. Statistical testing was performed based on axons for the comparison amongst genotypes from a total of 6 animals; data are expressed as mean and IQR. Scale bar is 10µm.*

3.4.3 TTLL1 genetic ablation in motor neurons delays axonal pruning

Due to the substantial effect on MT cytoskeleton caused by TTLL1 deletion in motor neurons, I next investigated how MT dynamics were affected in this knock-out mouse. Although TTLL1 deletion did not affect some parameters of the dynamics of the MT cytoskeleton of pruning axons, such as EB3-YFP comet density, velocity and orientation (Figure 3.10 a-c), the distribution of EB3 comet lengths (Figure 3.10d) was significantly, although slightly, increased in TTLL1^{mnKO} compared to TTLL1^{mnWT}. This indicates that the MT lattice is assembled more persistently in the absence of

TTLL1. Indeed, there is a lower density of MTs of around 1μm of length in the TTLL1^{mnKO} and higher density of MTs spanning 3-4 μm of length compared to TTLL1^{mnWT}. Here "length" is intended as the overall length that a single EB3 comets is consecutively tracked in a given movie, i.e. the MT filament´s persistence of growth. If we consider also the increased MT mass seen in TTLL1^{mnKO} (Figure 3.6a & d), we can deduce that MTs are more abundant and longer in this knock-out. This is in line with the failure to efficiently recruit or activate Spastin and sever MTs. In fact, due to the increased and less prone to be severed MT content, a higher percentage of neuromuscular synapses persisted in a competitive state in TTLL1^{mnKO} compared to TTLL1^{mnWT} littermates throughout the pruning period (Figure 3.10e & f). It was to the same extent as what seen in Spast^{mnKO} animals (ref Brill 2016). These data indicate that TTLL1 cell-autonomously orchestrates axonal pruning of motor axons during development by affecting MT mass.

3.4.4 TTLL1 genetic ablation delays axonal and dendritic pruning in the CNS

Having established that polyglutamylation of MTs drives motor axon pruning, in collaboration with Michaela Rusková from the Balastik Lab (Department of Molecular Neurobiology, Institute of Physiology of the Czech Academy of Sciences, Prague, Czech Republic), we investigated if glutamylation of MTs is a generalized mechanism of action that mediates synapse elimination also in the central nervous system.
For this, we used a mouse line where TTLL1 is neuronally deleted (TTLL1^{KO}, Nestin-Cre x TTLL1$^{fl/fl}$) which, similarly to what found in motoneurons, also induces hypoglutamylation in the CNS[266]. We focused on the hippocampal area, a brain region known to undergo both dendritic pruning in the granule cell layer[31], and axonal pruning of the infrapyramidal bundle (IPB) of mossy fibers of the dentate gyrus[276,277].
We proceeded to quantify spine density of hippocampal granule cells before

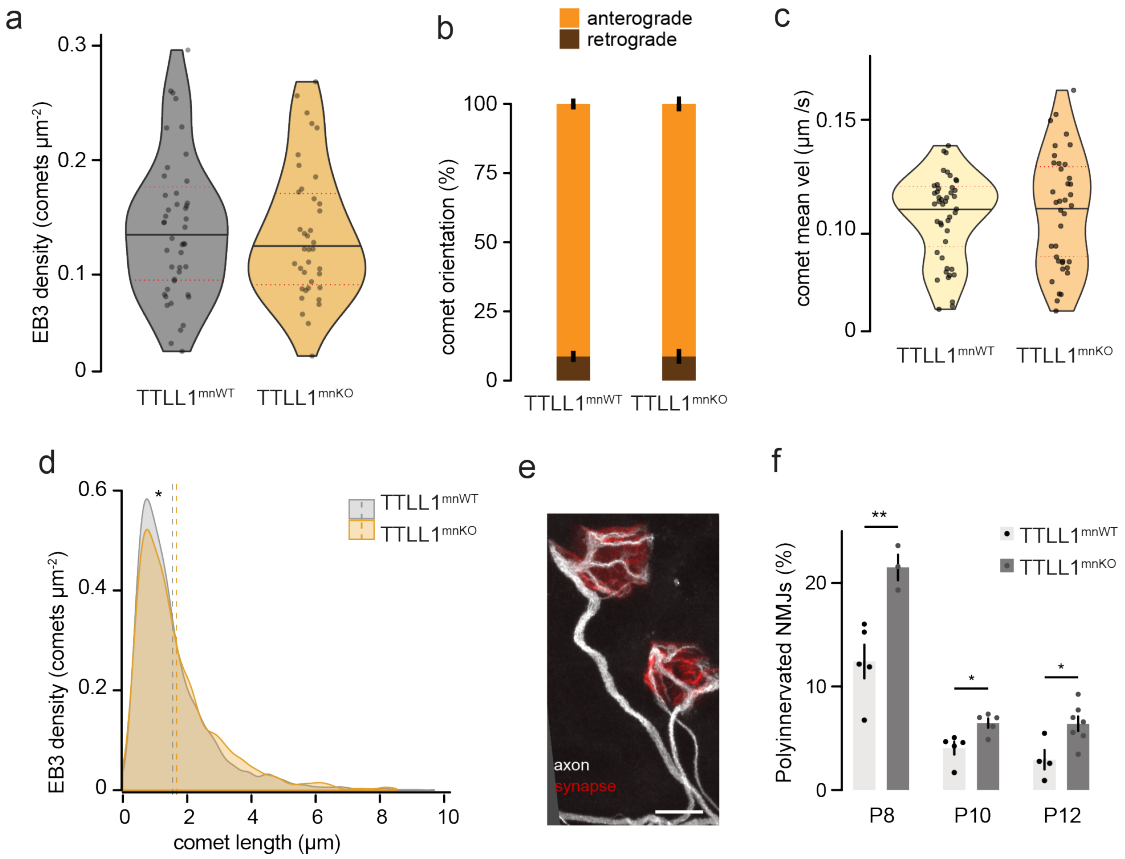

Figure 3.10: ***MTs in motor neurons devoid of TTLL1 grow more persistently than controls.*** *Several parameters of MT dynamics were unaltered in TTLL1^{mnKO} and compared to TTLL1^{mnWT}, including* ***a)*** *Eb3 comet density, p= 0.77 (two-tailed unpaired test t-test),* ***b)*** *Comet orientation, p = 0.36 (Mann-Whitney unpaired test),* ***c)*** *Comet mean velocity p = 0.61 (two-tailed unpaired Mann-Whitney test).* ***d)*** *Distribution of EB3 comet lengths was significantly different in TTLL1^{mnKO} compared to TTLL1^{mnWT}, *p $\leq$ 0.01 (two-sample Kolmogorov-Smirnov test, n =2287/1752 EB3 particle tracks were considered respectively from 45/38 axons; vertical dashed lines consists of mean value). A total of n = 45/38 axons were considered for comparison amongst genotypes from 6 animals.* ***e)*** *Singly and doubly innervated synapse. Axon (white) is labelled by βIII-tubulin. Synapse (red) is labelled by α-bungarotoxin (10µm scale bar).* ***f)*** *Percentage of polyinnervated synapses of TTLL1^{mnKO} versus WT littermates, evaluated on Thy1-YFP-16 background. Each dot represents a single animal. Data are mean and s.e.m..*

(3 weeks of age, P21) and after the pruning phase (8 weeks). While initial density was similar in TTLL1^{KO}vs TTLL1^{WT} (Figure 3.11 a&c), pruning did not occur at 8 weeks of age in TTLL1^{KO}(Figure 3.11 b&c). To confirm that the lack of TTLL1 affects also axon pruning in the CNS, we quantified the IPB length of 3 weeks old TTLL1^{KO} and WT mice (Figure 3.11 d). Calbindin immunostaining of coronal section of the hippocampus show an increase in the IPB/CA3 length ratio in TTLL1^{KO} compared to controls (Figure 3.11 e &f), suggestive of a delayed pruning in the knock-out animals.

Taken together, these data suggest that polyglutamylation of MTs mediates remodelling, not only in the peripheral nervous system, but also in the central nervous system. As such, it might be a generalized mechanism of action, able to have an effect on different cell types as well as different cell compartments, such as PNS and CNS, dendrites and axons.

3.4.5 TTLL1 genetic ablation does not affect axonal transport

Next, I investigated the effects of reduced α-tubulin polyglutamylation to axonal transport in terminal motor axon branches of TTLL1^{mnKO} and controls at P11. Previous reports have shown that mitochondrial transport is affected in cultured hippocampal neurons of TTLL^{KO} mice[151], and Spastin mutations induce lysosomal dysfunctions[278]. This could point to a common feature in TTLL1 and Spastin deletion. We have used the keima reporter[279], to examine mitochondrial and lysosomal organelles. A pH drop in the organelles, resulting from the fusion of mitochondria to lysosomes when these are targeted for degradation, induces a measurable excitation shift in the keima reporter (Figure 3.12a). I labeled the motor axons through intraventricular injection of AAV9-mito-keima at P3, then measured the transport in the intercostal nerve at P11 (Figure 3.12b). Neither anterograde nor retrograde flux of mitochondria (Figure 3.12c) and mitolysosomes was changed in TTLL1^{mnKO} compared to controls (Figure 3.12d). A possible interpretation is that at P11, while the TTLL1 deletion increases cytoskeletal mass,

3.4 TTLL1 genetic ablation delays pruning

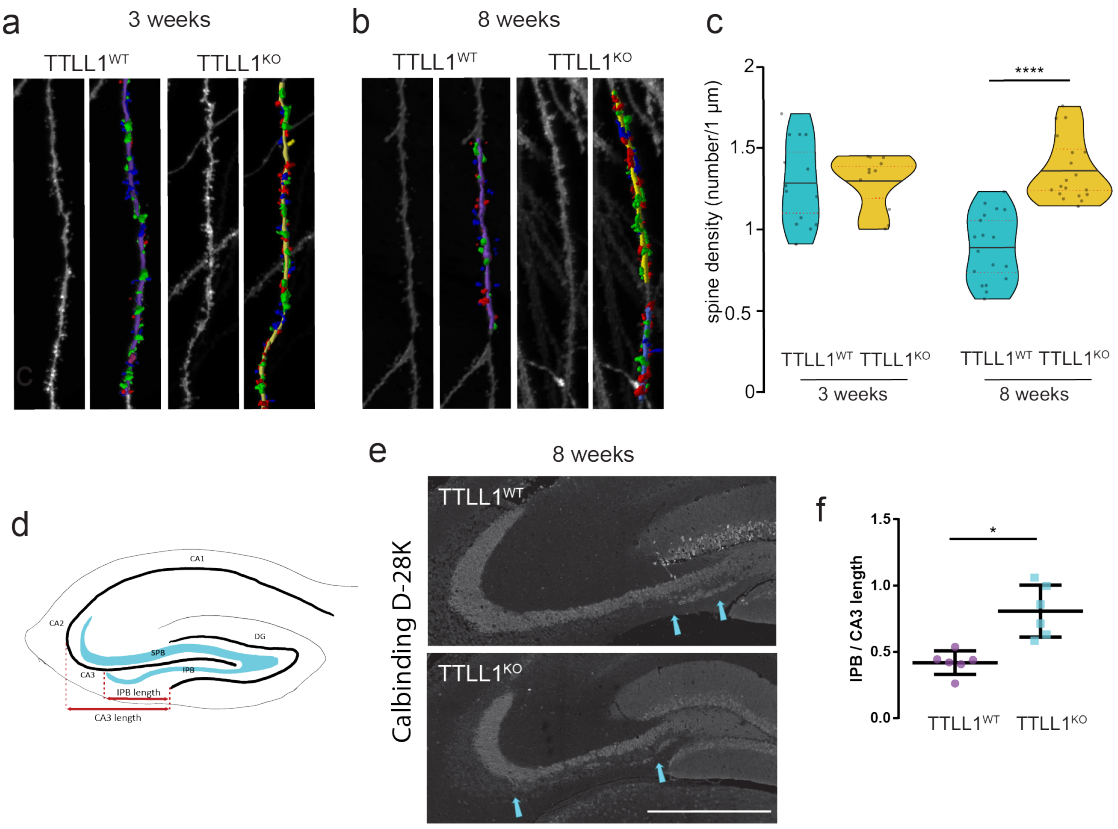

Figure 3.11: ***Deleting TTLL1 delays pruning in the CNS.*** *Dendritic spine density of hippocampal granule cells was calculated at* ***a)*** *3 weeks and* ***b)*** *8 weeks in* $TTLL1^{WT}$ *and* $TTLL1^{KO}$ *(by crossing Nestin-Cre x TTLL1 conditional knockout). Left side panel is an illustrative high resolution confocal image from brain slice, right side is an example of spine reconstruction.* ***c)*** *The quantification of spine density was not significantly different among* $TTLL1^{WT}$ *and* $TTLL1^{KO}$ *at 3 weeks,* $p<0.89$*(two-tailed Mann-Whitney test, n=14/11 dendrites from 6 animals), but was significantly increased in* $TTLL1^{KO}$ *at 8 weeks compared to littermate controls,* $****p \leq 0.0001$*(two-tailed Mann-Whitney test, n=18/19 dendrites from 8 animals).* ***d) to f)*** *The axonal length of the Infrapyramidal bundle (IBP) of the hippocampal mossy fibers is higher in* $TTLL1^{KO}$ *compared to* $TTLL1^{WT}$ *at 8 weeks. IPB and CA3 lengths were calculated according to the schematic in* ***d)*** *and were generated from* ***e)*** $TTLL1^{WT}$ *and* $TTLL1^{WT}$ *coronal brain sections immunostained with Anti-Calbindin D-28k. Blue arrows point to infrapyramidal bundle. Scale bars correspond to 250 µm.* ***f)*** *Quantification of IPB length normalized to CA3 was significantly increased in* $TTLL1^{KO}$ *at 8 weeks compared to littermate controls,* $**p = 0.002$ *(two-tailed Mann-Whitney test, n=6/6 brain slices from individual animals). Data are generated in collaboration with M.R. and expressed as individual points and mean and IQR for the calculation of spine densities, and individual points and mean and s.e.m for IPB lengths.*

the axonal transport might already be at maximum capacity and therefore the surplus of MTs does not induce an additional increase of transport. Hyperglutamylation has detrimental effects on cells, and data from primary hippocampal cultures and single molecule assays has shown that it affects transport[145,151,267]. My data highlight the difference in physiology between adult and young stages.

On the other hand, MT dynamics and MT transport were unaffected, indicating that pruning defects in the KO were a consequence of cytoskeletal stability. It is possible that homeostatic mechanisms arise in adult motor axons to bring the tubulin levels to a steady state level once the pruning process is over.

3.4.6 TTLL1 genetic ablation might alter the organization of organelles

The lack of effect on axonal tranport of mitochondria and mitolysosomes in TTLL1$^{\text{mnKO}}$, but the striking phenotypic effects both in the PNS and CNS, motivated me to investigate further the cause for the outcome of these results. Recent literature has shown that the positioning of organelles and severases such as Spastin and ER have impactful effects on energy availability, distribution of nutrients and local compartmentalization[205,205–208,211]. It is intriguing that Spastin has two main isoforms: a longer isoform (m87) that severs MT, and a truncated version (m1) that interacts with and localizes to ER[192,202,203]. Using my translatome data I first verified if these isoforms are expressed in motor neurons during axonal pruning. From these it emerges that m1 is more expressed than m87 in both motor neuron and spinal cord tissues (Figure 3.13a). Intrigued by the possible ER-mediated effects of Spastin, in collaboration with Martina Schaeffer (DZNE, Munich, Germany), we carried out EM of TTLL1$^{\text{mnWT}}$ and TTLL1$^{\text{mnKO}}$ of the intercostal nerve axons of triangularis sterni muscle of P9 mice. Density analysis of different organelles such as mitochondria, lysosomes, and ER were comparable in TTLL1$^{\text{mnKO}}$ and TTLL1$^{\text{mnWT}}$ (Figure 3.13). However, the preliminary analysis might point to a different distributions of such organelles

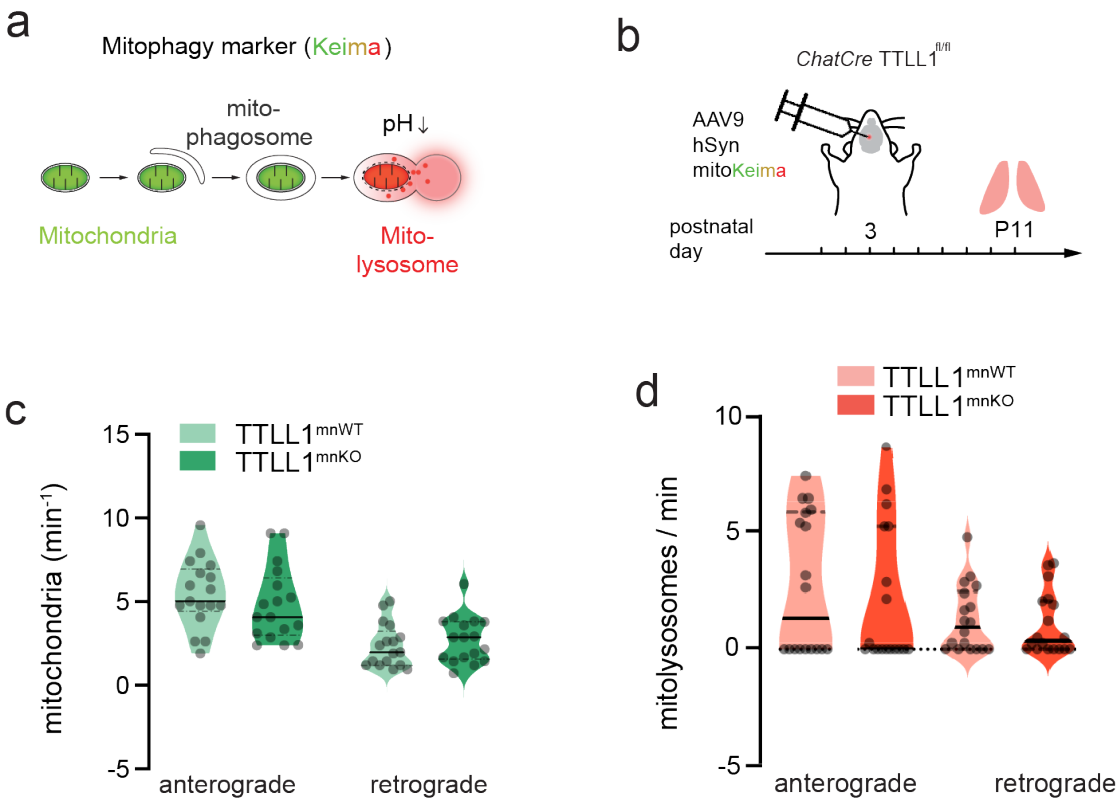

Figure 3.12: ***Deleting TTLL1 does not affect neuronal transport at P11.*** *Neuronal transport of mitochondria (green) and mitolysosomes (red) was carried out by injecting the* ***a)*** *mitokeima reporter* ***b)*** *intraventricularly at P3, as described in the M&M section 5.6, and imaging intercostal nerves in triangularis nerve-muscle explants at P11.* ***c)*** *mitochondrial flux was unchanged in $TTLL1^{mnWT}$ and $TTLL1^{mnKO}$, in both anterograde and retrograde direction, $p \geq 0.5$ (Ordinary one-way ANOVA with Holm-Šídák multiple correction post-hoc test, $n = 17/17$ axons from a total of 6 animals).* ***d)*** *Mitolysosome flux was unchanged in $TTLL1^{mnWT}$ and $TTLL1^{mnKO}$, in both anterograde and retrograde direction, $p \geq 0.9$ (Kruskal-walliss with Dunn's multiple correction test, $n = 17/17$ axons from a total of 6 animals). Data are mean and s.e.m. AVV injections were performed in collaboration with N.M.*

in the TTLL1^{mnKO} compared to controls (Figure 3.13).
In the future, efforts will be placed to confirm these results and verify if Spastin^{KO} induces similar outcomes as TTLL1^{KO} in terms of organelle organization.

3.5 Deleting CCP1 and CCP6 accelerates axonal pruning

CCPs, cytosolic carboxy-peptidases, are deglutamylases which carry out the opposite function of glutamylases (TTLLs), i.e. removing glutamates from tubulin tails (Figure 3.14a)[152,153,156]. We tested if the deletion of deglutamylases reverses the effects indicated above, in order to see if the enzymatic activities of the glutamylases/ deglutamylases families act in a rheostatic balance to adjust the function of Spastin. As shown in the motoneuron translatome data, CCP1 is the highest expressed deglutamylase at all the postnatal ages tested (Figure 3.14b), followed by CCP6 (Figure 3.14c). All the other CCPs (CCP2, 3, 4, 5) are also detectable, but at overall lower levels (Figure 3.14c), as also indicated in previously published data from adult mice brain lysates[156].

CCP6 can partially rescue the loss of CCP1, as indicated in an analysis of adult time points in the mouse brain[266]. To avoid this compensatory effect, we generated mutant mice with a deletion of CCP1 and CCP6 specifically in motor neurons. We crossbred *ChaT*-Cre to CCP1 and CCP6 conditional knockout mice (CCP1/6^{mnKO}). Unexpectedly, immunostaining quantifications of polyglutamylation (polyE) normalized to βIII-tubulin, indicated a significant decrease in CCP1/6^{mnKO} compared to controls (Figure 3.15 a & c). The overall MT mass measured by βIII-tubulin fluorescence was drastically reduced compared to littermate controls at P9 (Figure 3.15 e). Opposite to the results in TTLL1^{mnKO}, I observed an increase in the fraction of acetylated MTs in CCP1/6^{mnKO} (Figure 3.15 b & d). The increased ratio of a stabilized MT population but an overall lower MT mass suggests that Spastin could be rapidly depleting the pool of polyE-positive

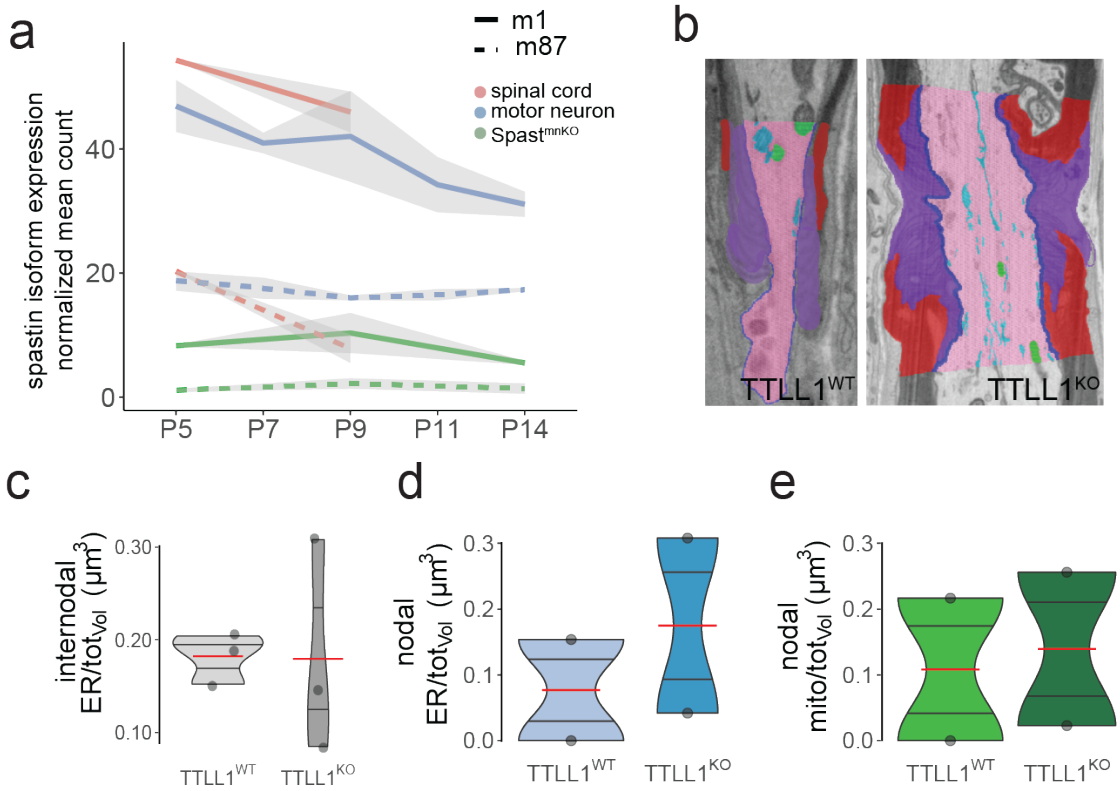

Figure 3.13: ***TTLL1 genetic deletion might affect organelle distribution at nodes or Ranvier.*** ***a)****Normalized read counts of Spastin isoforms in motoneurons at 5 time points of development. Data are expressed as mean and s.e.m..* ***b)*** *Ultrastuctural analysis of node of Ranvier in $TTLL1^{KO}$ and $TTLL1^{WT}$. Single electron micrograph are pseudo-colored as follows: paranodal regions in red, nodal regions in violet; ER in blue; mitochondria in green.* ***c)*** *Volumetric quantification of ER over the total internodal axoplasmic region in $TTLL1^{KO}$ compared to $TTLL1^{WT}$, $p = 1$ (Mann Whitney unpaired test from n= 3/3 individual axons).* ***d)*** *Volumetric quantification of ER over the total nodal axoplasmic region in $TTLL1^{KO}$ compared to $TTLL1^{WT}$.* ***e)*** *Volumetric quantification of mitochondria over the total nodal axoplasmic region in $TTLL1^{KO}$ compared to $TTLL1^{WT}$. Single data points in b), c) and d) correspond to quantification values from individual axons, each reconstructed from 20 single micrograph slices. Data are expressed as mean (red) and IQR. EM reconstruction was done in collaboration with M.S.*

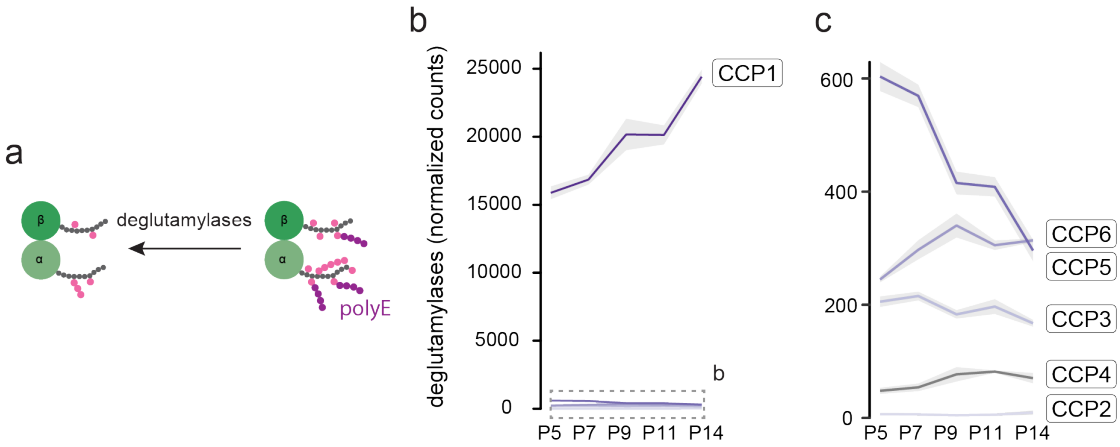

Figure 3.14: ***Expression of deglutamylases in motor neurons.*** ***a)*** *Schematic of enzymatic removal of glutamates from tubulin tails by deglutamylases.* ***b)*** *Normalized read counts of deglutamylases in motoneurons at 5 time points of mouse development (mean ± s.e.m) and dashed region,* ***c)*** *close up on expression of remaining CCPs.*

MTs. In accordance with an increased efficiency of Spastin severing in the CCP1/6^{mnKO}, the terminal axon branches pruned faster, as I found a lower fraction of polyinnervated neuromuscular synapses in the double knock-out (Figure 3.15 f). These data agree with a higher Spastin recruitment to MTs as a result of CCP1 and CCP6 absence and highlight how glutamylases and deglutamylases work in concert to regulate rheostatically the glutamylation of tubulin tails.

3.5.1 Deleting CCP1 and CCP6 affects MT dynamics

MT dynamics was substantially altered in the CCP1/6^{mnKO} compared to controls, unlike TTLL1^{mnKO} or TTLL7^{mnKO}. There was in fact a significant drop in EB3 comet density in the CCP1/6^{mnKO} versus control (Figure 3.16a & b). Interestingly, this drop in the double knock-out was also evident when the data were sub setted by age (Figure 3.16c). Furthermore, similarly to what previously reported in Kleele et al[11], the EB3 density in controls did not change across time within the controls, indicating that the proportion of MTs in the growth phase is relatively stable across developmental times

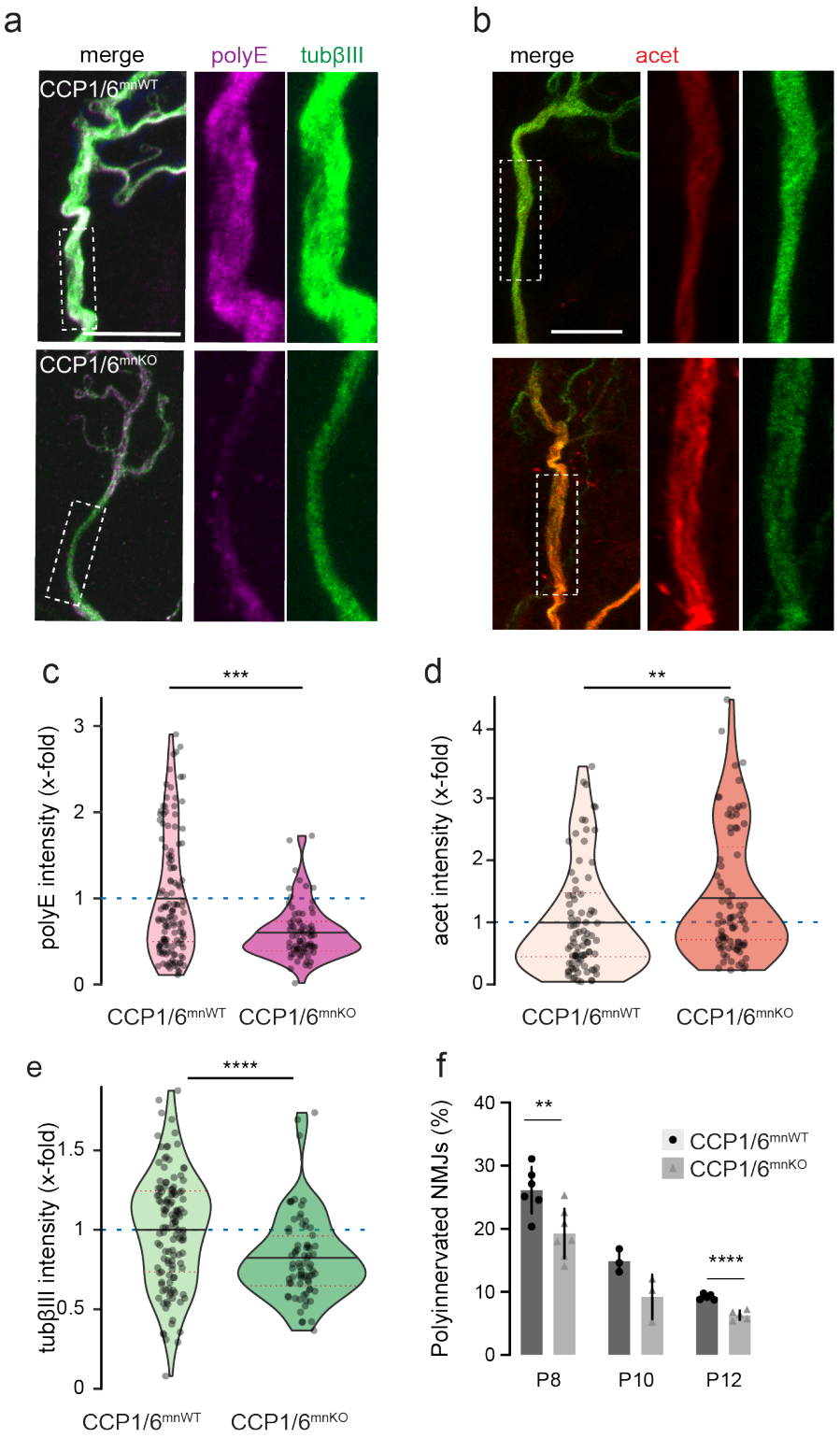

Figure 3.15: ***Deleting CCP1/6 accelerates axonal pruning***. ***a)*** *and* ***b)*** *Immunostaining for post-translational modifications of MTs in axons of triangularis sterni muscle fixed at P9. CCP1/6^{mnKO} mouse were compared to WT littermates for the following modifications:* ***a)*** *polyE (magenta) and βIII-tubulin (green),* ***b)*** *acetylation (red).*

Figure 3.15 *(continues from previous page)*: *Inset shows enlarged axonal area.* ***c)***, ***d)*** *and* ***e)*** *Quantification of immunostaining intensities of CCP1/6^{mnKO} versus WT littermates.* ***c)*** *Polyglutamylation levels are normalized to βIII-tubulin, *** p≤ = 0.0003 (two tailed Mann-Whitney, n = 130 / 76 axons from 6 animals),* ***d)*** *intensity levels of acetylated MTs normalized to βIII-tubulin, **p ≤ 0.0025 (two tailed Mann-Whitney, n = 86/80 from 8 animals).* ***e)*** *βIII-tubulin intensity are normalized to neurofilament staining, ****p = 0.00013 (two tailed Mann-Whitney, n= 130/77 axons from 6 animals). Immunostaining data are expressed as mean and IQR.* ***f)*** *Percentage of polyinnervated synapses of CCP1/6^{mnKO} versus WT littermates, evaluated on Thy1-YFP-16 transgene. Statistics calculated independently in each age group, P8 **p≤0.015, P10 p ≥0.06, P12 ****p ≤ 0.0002 (two-tailed unpaired t-test with Holm-Šídák multiple comparison correction). Each dot represents a single animal.*

(Figure 3.16c).
EB3 comet speed, i.e. how fast the MT lattice is assembled, was increased in the CCP1/6$^{\mathrm{mnKO}}$ compared to CCP1/6$^{\mathrm{mnWT}}$ (Figure 3.16d). In mammals, MT filaments are predominantly found in the "plus-tip-out" orientation (i.e. towards synapse)[111].
I found an unaltered comet orientation, meaning that the directionality of growth of the MT lattice in the double knock out had an anterograde orientation (Figure 3.16e). This suggests that the overall structural organization of MTs was intact in the CCP1/6$^{\mathrm{mnKO}}$. Similarly, the length of the EB3 comet, which is a surrogate measure of persistence of growth of the MT lattice, was also unchanged between the two groups (Figure 3.16f). Given the many alterations in the MT parameters, in order to get a clear picture of the MT status in the CCP1/6$^{\mathrm{mnKO}}$ I carried out a correlative analysis by combining live imaging data of EB3 dynamics with confocal data of overall MT mass through immunostaning. By constructing a map of the triangularis sterni muscle with sequentially higher magnification during the live imaging acquisitions, I was able to trace back the same axon (among more than 600) at the confocal. Analysis of correlation of EB3 comet density, normalized to immunostaining intensity of β-III tubulin, did not show a change in the

CCP1/6^{mnKO} compared to control (Figure 3.16f, g &e). This indicates that the double KO does not affect the overall ability of EB3 to be recruited to MTs, since similar proportions of EB3 comets to tubulin mass were found in CCP1/6^{mnKO} and CCP1/6^{mnWT}.

Taken together, these data suggest that the absence of deglutamylases does not significantly modify the ability of MTs to grow persistently, or to affect the overall structural organization of MTs. However, the higher MT growth rate but lower overall tubulin mass in the CCP1/6^{mnKO}, might point out that the MTs (or a subpopulation) are subjected to fast cycles of assembly and disassembly in the CCP1/6^{mnKO}, with a net effect of higher disassembly. This altered MT dynamics of the double KO mutant mice could have arisen as a consequence of transient hyperglutamylation due to the lack of deglutamylases (CCP1 and CCP6) and higher Spastin recruitment. I next tested this hypothesis by concomitantly deleting CCP1 and Spastin in motor neurons.

3.5.2 Spastin prevents accumulation of polyglutamylation in CCP1/6^{mnKO} at P9

CCP1 deletion induces hyperglutamylation in the Purkije cells of adult mice[266], but not in young P9 CCP1/6^{mnKO} mice motor neurons, as shown in the previous chapter (section 3.5). A possible explanation is that decreased glutamylation levels in young CCP1/6^{mnKO} motor axons could be due to Spastin activity itself. Indeed, translatome analysis of motor neurons indicated that the expression of Spastin is highest at P5 and then gradually decreases over time (Figure 3.17a). This is in agreement with previous reports for remodeling axons[218]. Therefore, I expected that an acute deletion of Spastin and CCP1 would lead to hyperglutamylation.
I injected AAV vectors encoding *Cre* under the human Synapsin promoter (*AAV9-hSynCre*) into a conditional knockout for CCP1 and Spastin, at P3, crossbred to TdTomato reporter mice (CCP1$^{fl/fl}$ x Spast$^{fl/fl}$ x TdTomato). At P9, I conducted immunostaining analysis (Figure 3.17b). I subdivided ax-

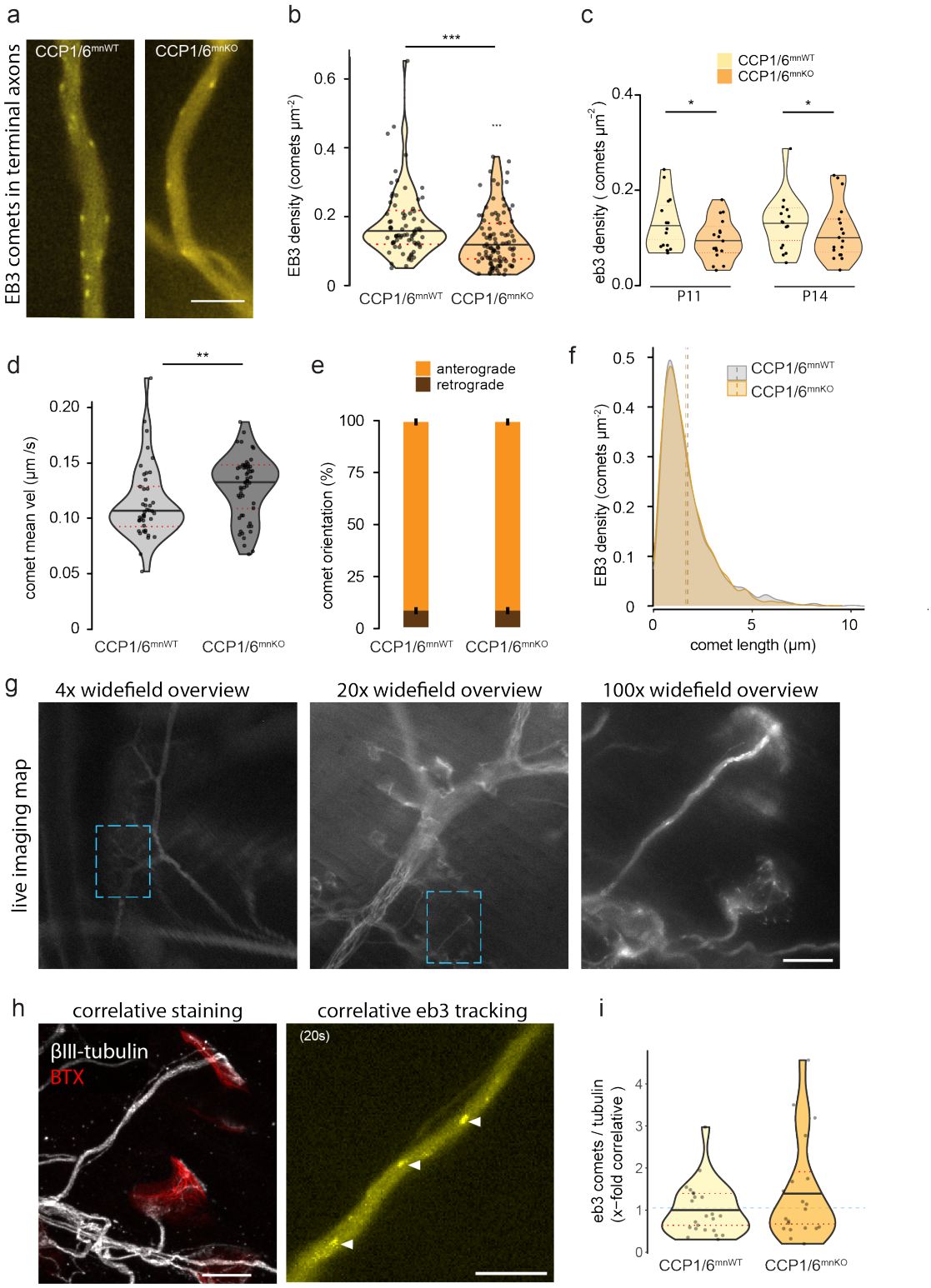

Figure 3.16: ***Cytoskeletal dynamics of are significantly altered in absence of CCP1/6 in motor axons.*** *(continues on next page)*

Figure 3.16 *(continues from previous page)*: ***a)*** *Single optical slice from a time-lapse sequence (20s) of a P9 Thy1-EB3-YFP explant showing a singly innervated NMJ in CCP1/6 ^{mnWT} and KO mice (scale 5µm). Parameters of MT dynamics quantified in CCP1/6^{mnKO} and CCP1/6^{mnWT} included:* ***b)*** *EB3 comet density, ***p≤ 0.0006 (two-tailed unpaired test t-test, n= 74/94 axons from 26 animals), and* ***c)*** *EB3 comet density subdivided into ages, p ≤ 0.04 (unparied one-tailed t-test. n = 16/17, 6 animals).* ***d)*** *Comet mean velocity **p ≤ 0.008 (two-tailed unpaired Mann-Whitney test, n= 43/55 axons from 18 animals).* ***e)*** *Comet orientation, p = 0.24 (Mann-Whitney unpaired test, 68/55 from 22 animals),* ***f)*** *Comet length distribution of EB3 in CCP1/6^{mnKO} was not significantly different compared to CCP1/6^{mnWT} distribution, p = 0.64 (two-sample Kolmogorov-Smirnov test, n =1913/1780 EB3 particle tracks were considered respectively from 55/63 axons from 20 animals; vertical dashed lines consists of mean value).* ***g)*** *Increasingly higher magnifications of widefield microscopy in order to map the location of single synapses, enabling a correlative analysis of tubulin mass and EB3 comet density (scale bar 10µm).* ***h)*** *(left) Confocal image of terminal NMJ traced back from live imaging. Fixed and immunostained for βIII-tubulin (white) and α-bungarotoxin (red) Scale bars 10µm. (right) Single frame from time-lapse recording (20s) of the same terminal axon captured in confocal; white arrowheads point to Eb3 comets (scale 5µm).* ***i)*** *Quantification of correlative analysis of EB3 comets density over βIII-tubulin mass, p = 0.48 (two-tailed unpaired Mann-Whitney test, n= 23/24 axons).*

ons' TdTomato fluorescence intensities into quartiles, and used the 3rd quartile of the data as a proxy for successful *Cre*-mediated excision (*Spast/CCP1^{cKO}*; iCre+, CCP1$^{fl/fl}$ x Spast$^{fl/fl}$ x TdTomato). The 1st quartile was instead considered as not recombined and therefore defined as control axons (*cWT*; iCre-, CCP1$^{fl/fl}$ x Spast$^{fl/fl}$ x TdTomato). As expected from the acute ablation of Spastin and CCP1, the quantitative immunostainings showed increased polyglutamylation levels, as well as a significant increase in the MT mass in the Spast/CCP1^{cKO}axons compared to the subset of non-recombined branches (Figure 3.17c, d &e).

It is unlikely that the lack of hyperglutamylation in CCP1/6^{mnKO} is a consequence of hindered antibody recognition by excessive branches of polyglu-

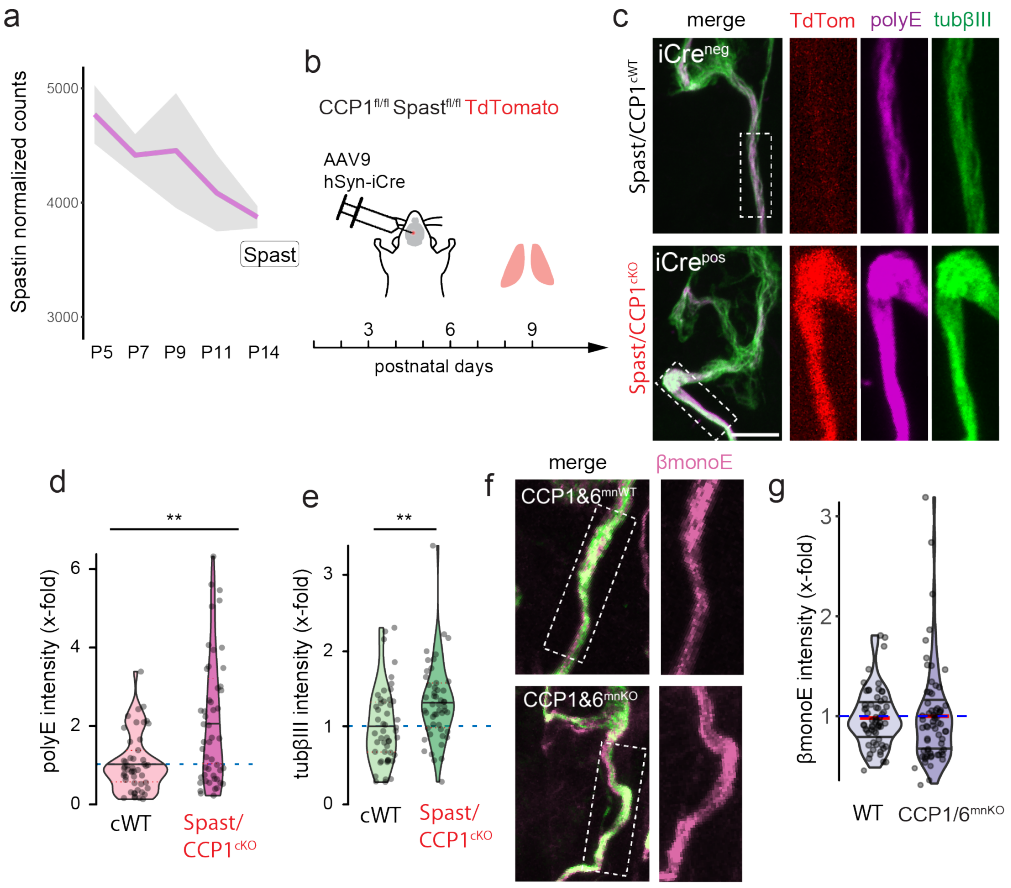

Figure 3.17: ***MTs are hyperglutamylated in motor axons devoid of CCP1 and Spastin.*** ***a)*** *Normalized read counts from translatome data shows that Spastin gene decreases over time in motoneurons at 5 time points of mouse development (mean ± s.e.m).* ***b)*** *CCP1 and Spastin are deleted in a subset of cholinergic motor neurons by injecting AAV9-hSyn-Cre vector intraventricularly at P3 into a CAG-tdTomato reporter mouse crossed to $CCP1^{fl/fl}$ and $Spastin^{fl/fl}$ (as described in M&M section 5.6). Terminal axons of triangularis nerve-muscle explants are then immunostained and imaged at P9. TdTomato fluorescence expression induced by hSyn-Cre mediated excision of STOP cassette of reporter was used as proxy for succesful CCP1 and Spastin deletion in a subset of motor neurons. Axons with tdTomato intensities falling in the upper quantile range ($3^{r}d$ quantile) were categorized as $iCre^{+}$, those falling in the lower quantile range ($1^{s}t$ quantile) were considered $iCre^{-}$.* ***c)*** *Singly innervated NMJ (boxed axon region is enlarged in the adjacent image) showing endogenous fluorescence of tdTomato (red) and fluorescence from immunostaining for polyE (magenta) and βIII-tubulin (green) and relative fluorescence quantification (d-f) in a subset of axons which are either controls (negative for tdTomato fluorescence; cWT) or knock-out for CCP1 and Spastin (positive for tdtTomato fluorescence; Spast/CCP1cKO).* *(continues on next page)*

Figure 3.17 *(continues from previous page)*: ***d)****Polyglutamylation levels are normalized to βIII-tubulin, ** p≤ = 0.0011 (two tailed Mann-Whitney, n = 50 / 50 axons from 8 animals).* ***e)*** *βIII-tubulin intensity are expressed as x-fold of mean fluorescence of iCre⁻, **p = 0.0014 (two tailed Mann-Whitney, n= 50/50 axons from 8 animals). Immunostaining data are expressed as mean and IQR.* ***f)*** *and g) βmonoE immunofluorescence in CCP1/6^{m}nKO and control axons was used to recognize branching glutamates on tubulin tails. Intensities are normalized to βIII-tubulin and expressed as x-fold of mean value of CCP1/6^{m}nWT, p= 0.35 (two tailed Mann-Whitney, n= 61/63 axons from 6 animals).*

tamylated chains, which could arise by the unrestrained TTLL1 activity in the absence of CCP1[159]. Both quantification of GT335-immunoreactivity to detect branching glutamates (data not shown)[280,281] and quantification of βmonoE to detect glutamate seeds, were unchanged in CCP1/6$^{\mathrm{mnKO}}$ mice compared to control (Figure 3.17f &g). Thus, it can be assumed that the number of branching points in CCP1/6$^{\mathrm{mnKO}}$ and control are comparable. These results, taken together, indicate that the deglutamylases act upstream of Spastin and induce hyperglutamylation and severing of MTs.

3.5.3 Adult CCP1/6$^{\mathrm{mnKO}}$ have disrupted axonal transport and show signs of degeneration

A decrease of Spastin expression over time has important biological consequences. A low Spastin expression and activity in adult axons is sufficient at homeostasis, but could lead to the accumulation of polyglutamylation and, in combination with the loss of CCP1 and CCP6, ultimately to neurodegeneration[266]. Recent studies have shown that Spastin is not able to rescue the degeneration induced by the lack of CCP1 in the adult cerebellum[266].
Immunostainings of polyE and βIII-tubulin showed that in adult motor axons of CCP1/6$^{\mathrm{mnKO}}$ mice there is a drastic increase of polyglutamylation in CCP1/6$^{\mathrm{mnKO}}$ compared to controls (Figure 3.18a &b), consistent with lower Spasting severing in the adult. Moreover, also the MT mass was considerably reduced in the CCP1/6$^{\mathrm{mnKO}}$ motor axons compared to control (Figure

3.18a &c).

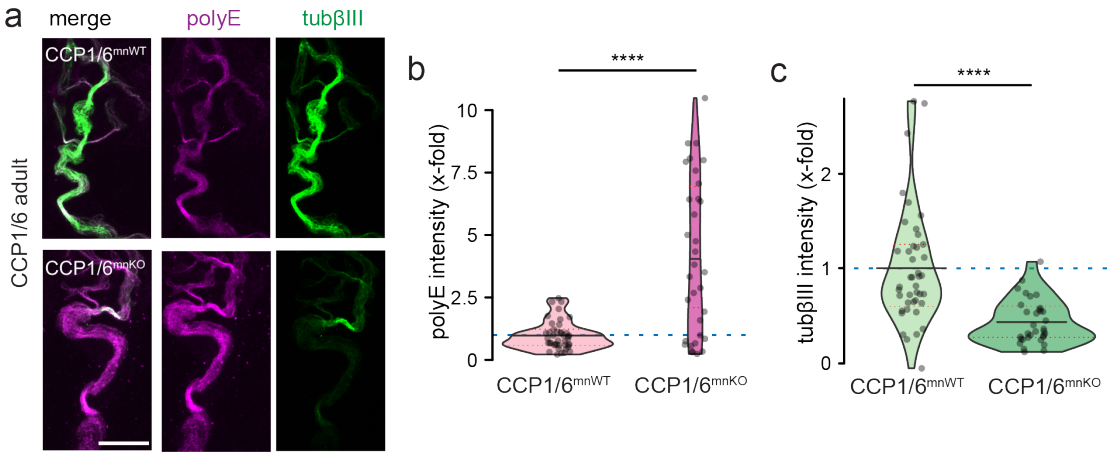

Figure 3.18: ***Adult cytoskeletal mass is decreased and hyperglutamylated in CCP1/6^{mnKO} compared to control.*** ***a)****Immunostaining of MTs for polyE (magenta) and βIII-tubulin (green) in axons of triangularis sterni muscle fixed at 1 month (scale bar 10µm).* ***b)*** *Quantified polyE fluorescence intensities were normalized to βIII-tubulin, **** p<0.0001(two-tailed Mann-Whitney test).* ***c)*** *βIII-tubulin fluorescence intensities are expressed as x-fold of mean fluorescence of CCP1/6^{mnWT}, **** p<0.0001 (two-tailed Mann-Whitney test). Statistical testing was performed based on axons (n= 42/33) for the comparison amongst genotypes from a total of 6 animals; data are expressed as mean and IQR.*

I investigated the functional consequences of the destabilization of the MT cytoskeleton in CCP1/6$^{\text{mnKO}}$ motor axons. I observed morphological differences in the adult motor neurons of CCP1/6$^{\text{mnKO}}$. In particular, denervation phenotypes were evident, as evinced from the presence of swellings at 3 months of age (Figure 3.19a). Moreover, CCP1/6$^{\text{mnKO}}$ at month 6 displayed impaired locomotor function (data not shown), indicating a cell-autonomous driven effect.

I explored the extent that these effects are due to impaired axonal transport. I quantified the transport of mitochondria and mito-lysosome using the mito-keima reporter, as described before 5.10. The keima reporter

has been injected in P3 mice intraventricularly, and then analyzed in adult nerve-muscle explants in vivo (Figure 3.19b &c). I observed an increased anterograde mitochondrial flux in the intercostal nerve in the CCP1/6^{mnKO} compared to control. Retrograde mitochondrial flux was unaltered (Figure 3.19 d &e). However, the overall flux of mito-lysosomes was lower in both anterograde and retrograde directions in the CCP1/6^{mnKO} compared to CCP1/6^{mnWT}, with a net of roughly 3 mito-lysomes less moving toward the soma each minute (Figure 3.19f). These data indicate that trafficking is impaired in the double KO and point to a distal accumulation of mito-lysosome.

The increase of anterograde trafficking in the KO might be a compensatory mechanism to boost the delivery of healthy mitochondria, in order to counteract the increase of dysfunctional ones. To confirm if organelle accumulation occurs in synapses, I measured the mitophagy-index at the NMJ, consisting in the ratio of keima-red fluorescence over the total fluorescence (Figure 3.19 g &h). There was a wider extent of mito-lysosome accumulation in CCP1/6^{mnKO} compared to CCP1/6^{mnWT} controls (Figure 3.19i), which was exacerbated with age. Hence, disrupting deglutamylase activity not only affects axonal transport in adult, but also leads to imbalances in the axonal homeostasis which could in turn affect neurotransmission.

Further analysis of transport parameters of mitolysosomes show that average speed, run speed and run length are lower in CCP1/6^{mnKO}, while pause rate is higher. The shorter run lengths correlate with shorter MTs, while higher pause rates are and indication of the sparsity of MT bundles. These results are in agreement and corroborate overall the lower MT mass in CCP1/6^{mnKO} in adult, and further show that apart from being less abundant, the MTs are overall shorter. However, it is unlikely that the the effect on organelle transport is solely a consequence of MT architecture. Polyglutamylation, for example, has been shown to reduce overall mitochondria motility in certain experimental conditions[151]. The extent of the contributions and the mechanism need to be elucidated further.

3.5 Deleting CCP1 and CCP6 accelerates axonal pruning

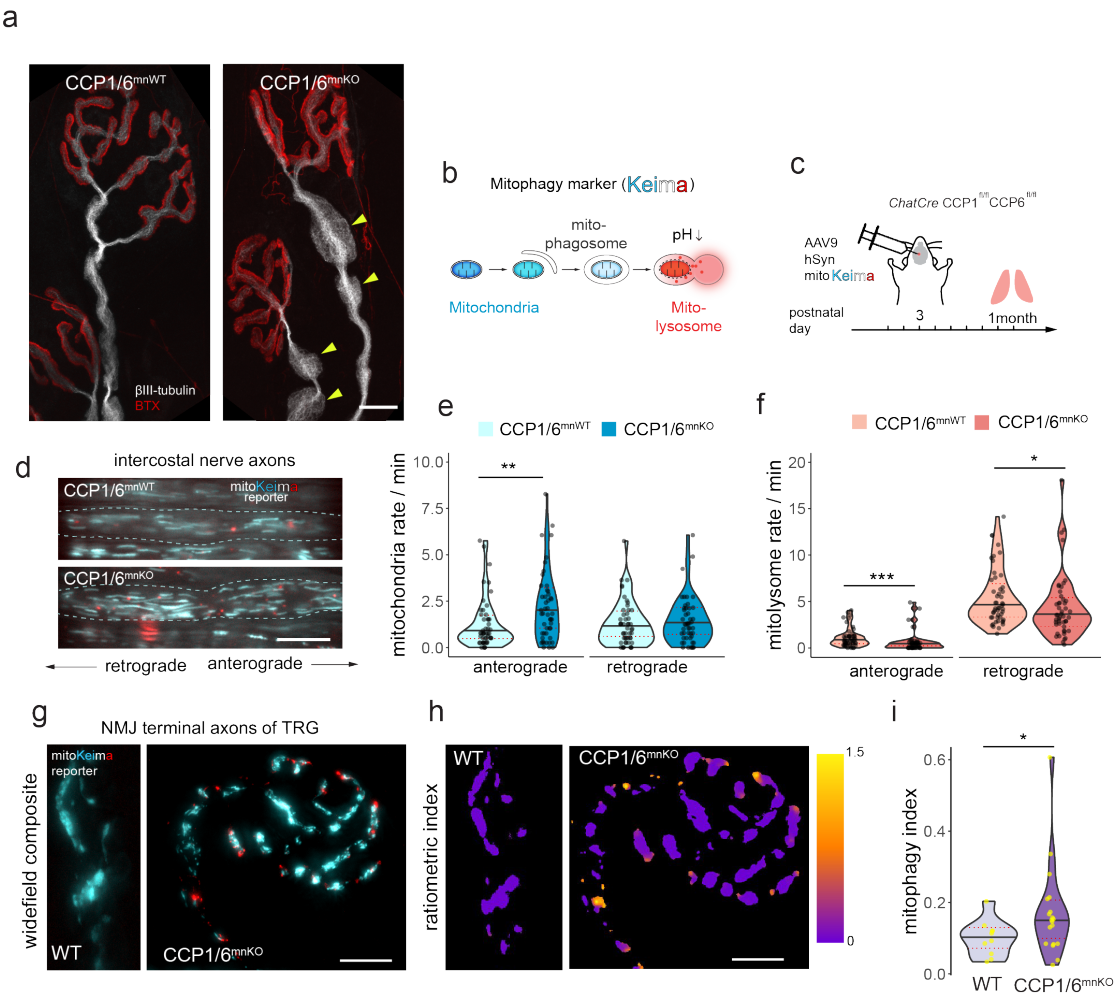

Figure 3.19: ***Neuronal transport is altered in adult CCP1/6^{mnKO} compared to controls.*** ***a)*** *The presence of axonal swellings (yellow arrowheads) in 1 month old CCP1/6^{mnKO} but not CCP1/6^{mnWT}, points to a severe cytoskeletal misorganization in the knock-out and is a sign of neurodegeneration (axons in white, βIII-tubulin immunostaining; synapse in red, α-bungarotoxin).* ***b)*** *Cytosolic acidification of mitochondria (cyan) from fusion to lysosomes (red) causes a switch in the spectral fluorescence emission of the mito-keima reporter, allowing for simultaneous imaging of both organelles.* ***c)*** *A mito-keima construct is delivered intraventricularly in mice at P3 through AAV9 adeno associated viral vectors and expressed neuronally through hSyn promoter (AAV9-hSyn-Cre mitoKeima). Triangularis sterni is dissected and imaged from 1 month old animals.* ***d)*** *Single optical slice from time-lapse recording (20s) of triangularis sterni muscle-nerve explant at the intercostal nerve (icn) of mitochondria (cyan) mitolysosomes (red) of 1 month old in CCP1/6^{mnKO} and CCP1/6^{mnWT} mice. Scale bar 10 μm.* ***e)*** *and* ***f)*** *Anterograde and retrograde organelle flux of 1 month old CCP1/6^{mnKO} and CCP1/6^{mnWT} mice is substantially altered in both mitochondria (cyan) and mitolysosome (red) organelles.*

Figure 3.19 *(continues from previous page)*: ***e)*** *Anterogradely moving mitochondria were increased in CCP1/6^{mnKO} compared to CCP1/6^{mnWT}, **p ≤ 0.005 (Mann Whitney, n= 50/48 axons), while retrograde mitochondria rates were similar in the two groups, p = 0.49 (Mann Whitney, n = 50/48 axons 8 animals).* ***f)*** *Anterogradely moving mitolysosomes were lower in CCP1/6^{mnKO} compared to CCP1/6^{mnWT}, ***p ≤ 0.0006 (Mann Whitney, n= 50/48 axons), and so were retrograde mitolysosome rates, *p = 0.025 (Mann Whitney, n = 50/48 axons 8 animals).* ***g)*** *Maximum intensity projection of NMJ from widefield of CCP1/6^{mnKO} and CCP1/6^{mnWT} depicting mitokeima reporter (cyan is mitochondria, red is mitolysosomes). Scale bar 10 µm.* ***h)*** *NMJ of CCP1/6^{mnKO} and CCP1/6^{mnWT} are pseudocolored ratiometrically according to the mitophagy index, calculated as described in 5.11.* ***i)*** *Mitophagy index quantification at NMJ was significantly increased in CCP1/6^{mnKO} compared to CCP1/6^{mnWT} at 1 month, *p ≤ 0.05 (One-tailed Mann Whitney U test, n = 10/19 axons). Data are expressed as median and IQR.*

3.6 Neurotransmission is an upstream regulator of glutamylase activity

Neuronal activity is one of the main drivers of axonal pruning. Blocking neurotransmission has the effect of depleting the presynaptic MT cytoskeleton[227]. To verify that neuronal activity is an upstream regulator of polyglutamylation, we blocked post-synaptic activity with α-bungarotoxin (BTX) and quantified the pre-synaptic axons. We injected BTX unilaterally in the thorax at P7 and quantified polyglutamylation and tubulin at P9 (Figure 3.21a).

Treatment with BTX has previously shown to reduce the overall tubulin mass compared to control untreated animals[227]. Here we show a significant reduction in polyglutamylation in the BTX-injected muscle compared to the un-injected control (WT^- *vs* WT^+; Figure 3.21c), suggesting that the lack of neurotransmission is able to modulate polyglutamylation. This reduction is reminiscent of what happens in the $CCP1/6^{mnKO}$ mice, where Spastin depletes polyglutamylation from MTs faster than it accumulates. To distin-

3.6 Neurotransmission is an upstream regulator of glutamylase activity

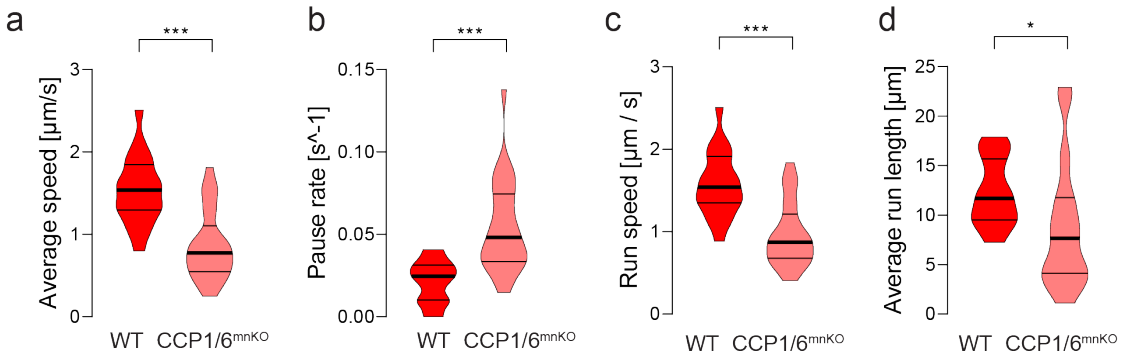

Figure 3.20: ***Transport parameters are altered in adult CCP1/6^{mnKO} compared to controls in intercostal nerve axons.*** ***a)*** *Average run speed, calculated including pauses, was decreased significantly in the double knock-out compared to controls (mean and s.e.m of mitolysosomes/min 1.53 ±0.10 vs 0.89±0.08), ***p ≤ 0.0001 unpaired t-test.* ***b)*** *Pause rate was increased significantly in the double knock-out compared to controls (mean and s.e.m of mitolysosomes/min 0.021 ±0.003 vs 0.054 ±0.005). ***p ≤ 0.0001,Mann Whitney test.* ***c)*** *Run speed, calculated excluding pauses, was decreased significantly in the double knock-out compared to controls (mean and s.e.m of mitolysosomes/min 1.57 ±0.09 vs 0.97 ±0.08), ***p ≤ 0.0001, unpaired t-test.* ***d)*** *Average run length was decreased significantly in the double knock-out compared to controls (mean and s.e.m of mitolysosomes/min 12.31 ±0.78 vs 8.82 ±1.2) *p = 0.035, unpaired t-test. Statistical testing was performed based on axons (n= 19/26) for the comparison among genotypes from a total of 6 animals; data are expressed as mean and s.e.m. Tracking parameters quantified in collaboration with N. M.*

guish between concerted Spastin-glutamylase activity and glutamylases directly, we injected BTX at P7 into mice that lack Spastin ($Spast^{KO}$). Corroborating previous reports[74], higher polyglutamylation was found in $Spast^{KO}$ compared to control mice (WT^{-} *vs* $Spast^{KO-}$;Figure 3.21c). Further, mRNA expression from Ribotagged motor neurons in Spastin conditional knockout (*ChaT*Cre X $Rpl22^{fl/fl}$ X $Spast^{fl/fl}$) did not point to compensatory upregulation of other severing enzyme RNAs, although as expected, Spastin levels were efficiently depleted in $Spast^{KO}$ transcriptome samples (Figure 3.21d). Treatment with BTX in $Spast^{KO}$ was able to rescue polyglutamylation to the levels of the un-injected control ($Spast^{KO+}$ *vs* WT^{-}; Figure 3.21c). This is a strong indication that the hypoglutamylation seen in the wildtype injected by BTX (WT^{+}) was driven by Spastin.

Notably, polyE immunofluorescence intensity significantly dropped when neurotransmission was blocked in $Spast^{KO}$ compared to when it was not ($Spast^{KO-}$ *vs* $Spastin^{KO+}$; Figure 3.21c). This indicates that neuronal activity controls 'elongating' glutamylases. An increased polyE intensity in BTX-injected motor axon devoid of Spastin compared to BTX-injected WT mice, corroborates the interplay of Spastin and glutamylases in neuronal remodeling ($Spast^{KO+}$ *vs* WT^{+}; Figure 3.21b &c) . These data indicate that the lack of post-synaptic transmission caused by BTX is evaluated as a punishment signal by presynaptic axons, which activate glutamylases to dismantle the cytoskeleton. In the absence of the downstream effector - Spastin -, the punishing signal can still activate glutamylases, which add polyglutamylation to MTs; Spastin however is absent, leading to hyperglutamylation.

Thus, we uncovered a fine-grained regulation of glutamylases via neurotransmission that control the pruning of motor axons, possibly via potential release of punishment factors by the postsynaptic muscle fiber.

3.6 Neurotransmission is an upstream regulator of glutamylase activity

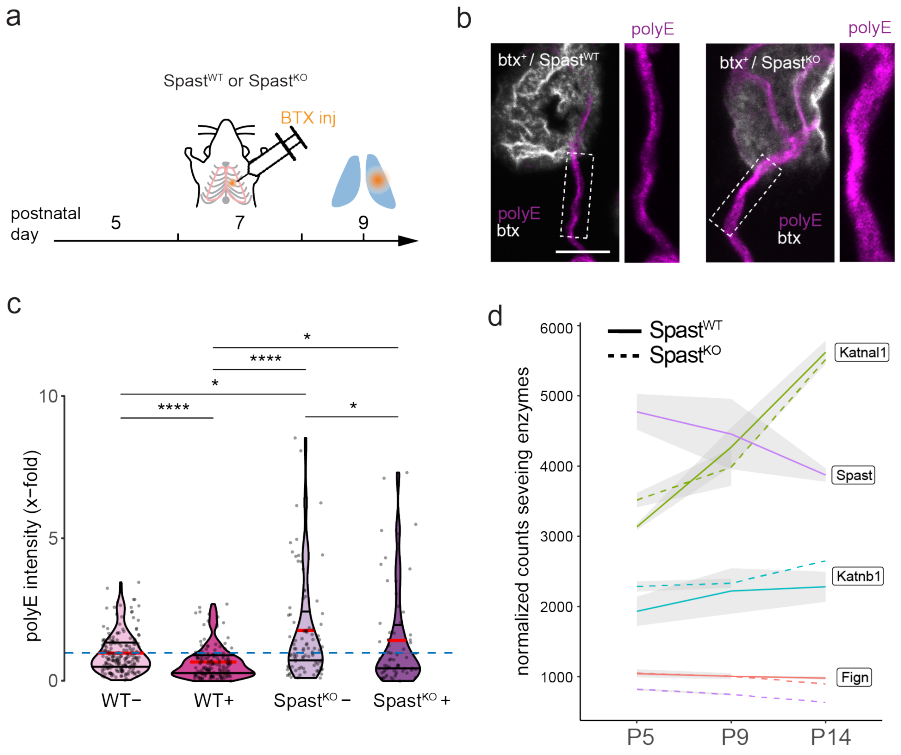

Figure 3.21: ***Neurotransmission modulates polyglutamylation of MTs. a)*** *α-bungarotoxin (BTX) is injected unilaterally in the thorax at P7 to block the post-synaptic transmission of Spastin^{WT} or Spastin^{KO} mice. The triangularis sterni muscle is isolated and immunostained at P9.* ***b)*** *MTs are stained for polyE (magenta) in axons of Spastin^{WT} or Spastin^{KO} mice, injected with α-bungarotoxin (BTX+). The dashed box shows enlarged axon area. Scale bar is 10µm.* ***c)*** *Quantified polyE fluorescence intensities were normalized to βIII-tubulin and several pair wise comparisons (p<0.0001 Kruskal-wallis general test) were conducted with Dunn's test and post-hoc Bonferroni correction, as follows: WT- vs WT+, ****$p \leq 0.0001$ $(n = 183/140$ axons); WT- vs Spas KO-, *$p \leq 0.05$ $(n = 183/91)$; WT- vs Spas KO+, $p = 0.53$ $(n = 183/65)$; WT+ vs Spas KO-, ****$p \leq 0.0001$ $(n = 140/91)$; WT+ vs Spas KO+ , *$p \leq 0.02$ $(n = 140/65)$; Spas KO- vs Spas KO+ ,* $p \leq 0.05$ $(n=91/65)$. Statistical testing was performed based on axons for the comparison amongst genotypes from a total of 15 animals; data are expressed as mean and IQR. The experiment was an equal effort between this author, G.W and A.Z.* ***d)*** *Normalized read counts from translatome analysis of severing enzymes in motoneurons of Spastin^{WT} or Spastin^{KO} mice at 3 time points of mouse development (mean ± s.e.m).*

3.7 Molecular pathways involved in mammalian axon pruning

3.7.1 Motor neuron deletion of p75 does not affect cytoskeletal mass or polyglutamylation

The next goal was to uncover the molecular mechanisms that are established downstream of neuronal activity. They ultimately converge into glutamylase/deglutamylase activation and cytoskeletal removal through polyE-Spastin. The first candidate was the BDNF pathway, well known for its crucial role in supporting neuronal survival. This neurotrophic factor is released by the muscle in the form of proBDNF. Following peptidic cleavage, mature BDNF binds post-synaptically to Trk receptors on neurons.
Specifically at the NMJ, the response to receptor binding depends whether mature or immature BDNF signals to motor neurons, as well as the type of Trk receptor found on the post-synaptic neurons. BDNF preferentially binds to TrkB receptors and this coupling promotes winning of competition in bound axons, while blocking TrkB accelerates pruning. Conversely, proBDNF acts as a punishment signal when bound to p75/Ngfr and sortilin on axons[45,282].
Given the differential responses due to the different receptors present at a given time during synapse elimination,I first assessed the expression pattern of these receptors using the translatome data.
As evinced from the expression data, BDNF mRNA was absent in motor neurons, since it is released from the muscle. On the other hand, the various BDNF receptors were expressed at different levels, the highest being TrkB/Ntrk2, follows TrkC/Ntrk2 while TrkA/Ntrk1 is barely detectable between P5 and P14 (Figure 3.22a). Both the co-receptor sortilin (Sort1), and p75/Ngfr are expressed in motor neurons. Of note, the mRNA abundance of p75 has a sharp decrease at around P9 (Figure 3.22a), the stage at which around 50% of synapses have terminated competition.
Given the compelling expression pattern and the availability of existing mouse model, I probed for changes in overall tubulin mass or polyglutamy-

lation pattern in mice lacking p75 in motor neurons (*ChaT*-Cre X $p75^{fl/fl}$). No changes were present in singly innervated synapses (Figure 3.22b to d) in neither tubuling mass (Figure 3.22b &c) nor polyglutamylation levels (Figure 3.22b &d).
However, BDNF might exert its function prior the resolution of competition, by giving a selective advantage to one of the competing branches. To assess this scenario, I analysed competing synapses at the doubly innervated stage, subdividing one of the axons pairs as either "winner" or "loser", according to the total amount of tubulin mass (Figure 3.22e & f). PolyE over tubulin ratio was not different in "winner" axons compared to "loser" axons (Figure 3.22g) and the deletion of p75 did not affect the polyglutamylation ratio compared to controls (Figure 3.22f).
The lack of phenotype in the $p75^{mnKO}$ could be due to the necessity of the sortilin co-receptor to be deleted as well, for the pro-BDNF to exert its "punitive" effects on the cytoskeleton. Indeed, NMJ exposed in vivo to antibodies against p75 that impair sortilin binding shows delayed synapse elimination. However, the full genetic KO of p75 in the presence of sortilin did not affect synapse elimination[45]. A mouse model which concomitantly lacks p75 and sortilin would answer this question, but was lacking at the time of investigation.

3.7.2 TNFα KO increases mass but has no effect on the glutamylation of MTs

Another promising pathway involved in synapse elimination which I tested at the NMJ is the Tumor necrosis factor alpha (TNFα). It has been shown that muscle, but not motorneuron derived TNFα, affects axonal pruning[64]. Transcriptionally active genes associate with the TNFα pathway in motor neurons spanning the period of axonal pruning are shown in (Figure 3.23a). Notably, the highest expressed receptor is TNfrsf21/DR6, followed by Tnfrsf1a and Tnfrsf1b. This pathway is known to signal through caspase activation. In motor neurons, I found Caspase 3 to be more expressed than Caspase 6 which might suggest that it is the preferred isoform downstream

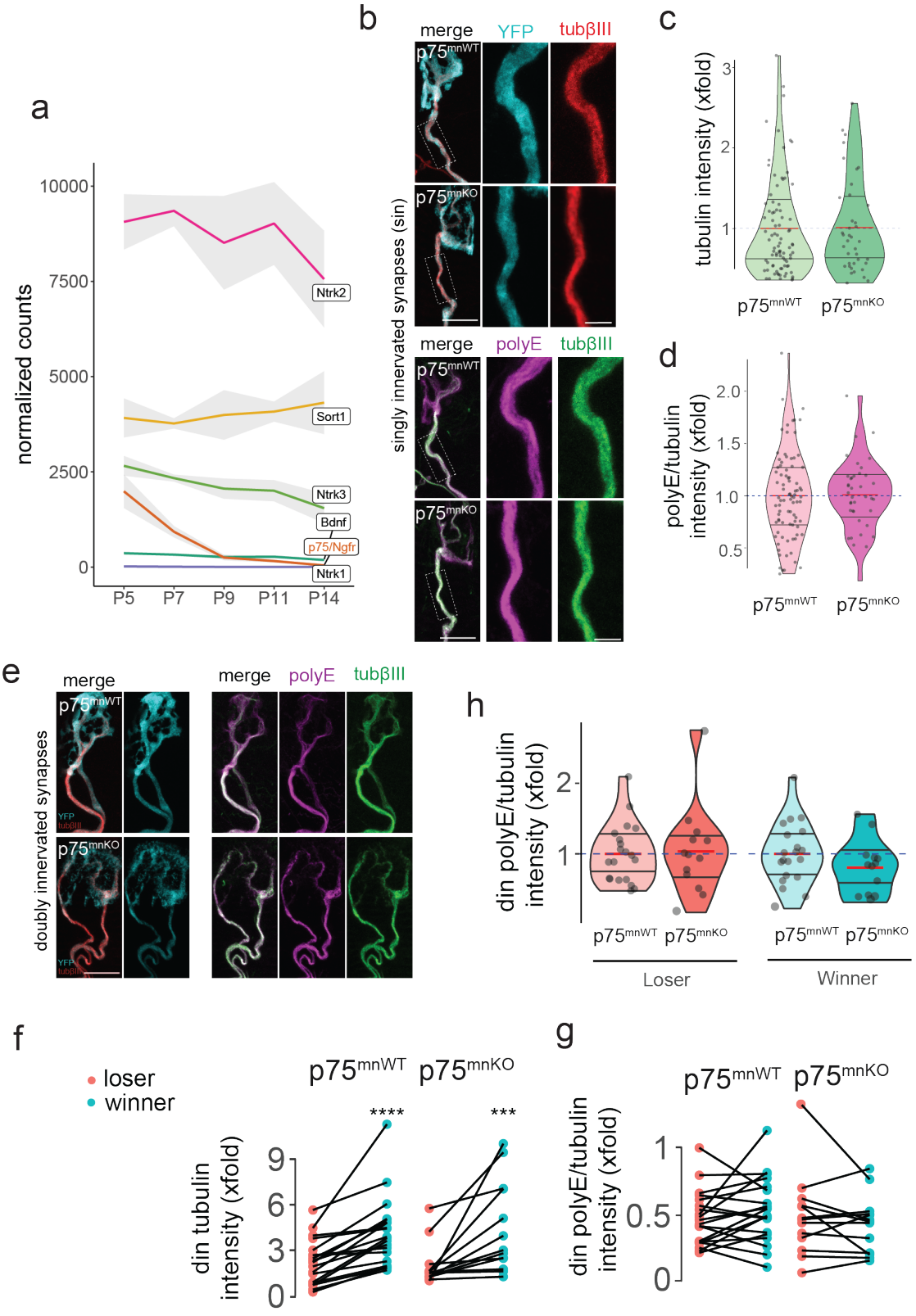

Figure 3.22: ***p75 motor neuron deletion does not affect polyglutamylation.***

Figure 3.22 *(continues from previous page)*: ***a)*** *Normalized read counts of neurothrophic factors expressed in motoneurons at 5 time points of mouse development (mean ± s.e.m). p75 (also known as Ngfr, orange line) mRNA has a sharp decrease in expression at around P9. No changes where detected in overall* ***b)*** *βIII-tubulin normalized on YFP intensities, p = 0.87 (two-tailed Mann-Whitney test) or* ***c)*** *ratio of polyglutamylation on βIII-tubulin, p = 0.91 (two-tailed unpaired t-test) in singly innervated synapses from $p75^{mnKO}$ and $p75^{mnWT}$.* ***d)*** *Axon pairs from doubly innervated synapses (din) from $p75^{mnWT}$ and $p75^{mnKO}$ were segregated into "winners" (win) or "losers" (lose) based on βIII-tubulin mass normalized on YFP intensities, ****$p \leq 0.0001$ *(n= 40 $p75^{mnWT}$ dins, paired Mann Whitney), ***$p \leq 0.001$ *(n= 26 $p75^{mnKO}$ dins, paired Mann Whitney).* ***e)*** *The sorting of dins in "winners" and "losers" according to tubulin intensity did not affect overall polyE intensities in neither $p75^{mnWT}$, p=0.23 (n= 40 dins, paired Mann Whitney) nor $p75^{mnKO}$, p=0.64 (n=26 dins, paired Mann Whitney).* ***f)*** *The ratio of polyE over tubulin mass were not altered in $p75^{mnKO}$ compared to 75^{mnKO} in neither "loser" axons, p=1 (n=20/13, unpaired Mann Whitney) nor "winner" axons, p= 0.17 (n=20/13, unpaired Mann Whitney). Statistical testing of sin was performed based on axons (n= 86/34) for the comparison among genotypes. A total of 6 control and 4 knock-out animals were used in sin and din analysis; data are expressed as x-fold of control animals from staining on the same experimental batch, violin bars are mean and IQR.*

of TNFα binding.

Using TNFα full KO mouse, I prepped NMJ at P9 and quantified tubulin mass and polyglutamylation. In line with previous reports of delayed pruning in TNFα^{KO64}, there was an increase in tubulin mass in the TNFα^{KO} compared to control littermates (Figure 3.23b &c). However, although polyE was increased, the overall ratio of polyglutamylation to tubulin was comparable between TNFα^{KO} and TNFα^{WT} in motor axons (Figure 3.23b &d). It is thus not clear if TNFα exerts its effects through polyglutamylation and it should be further studied in the future.

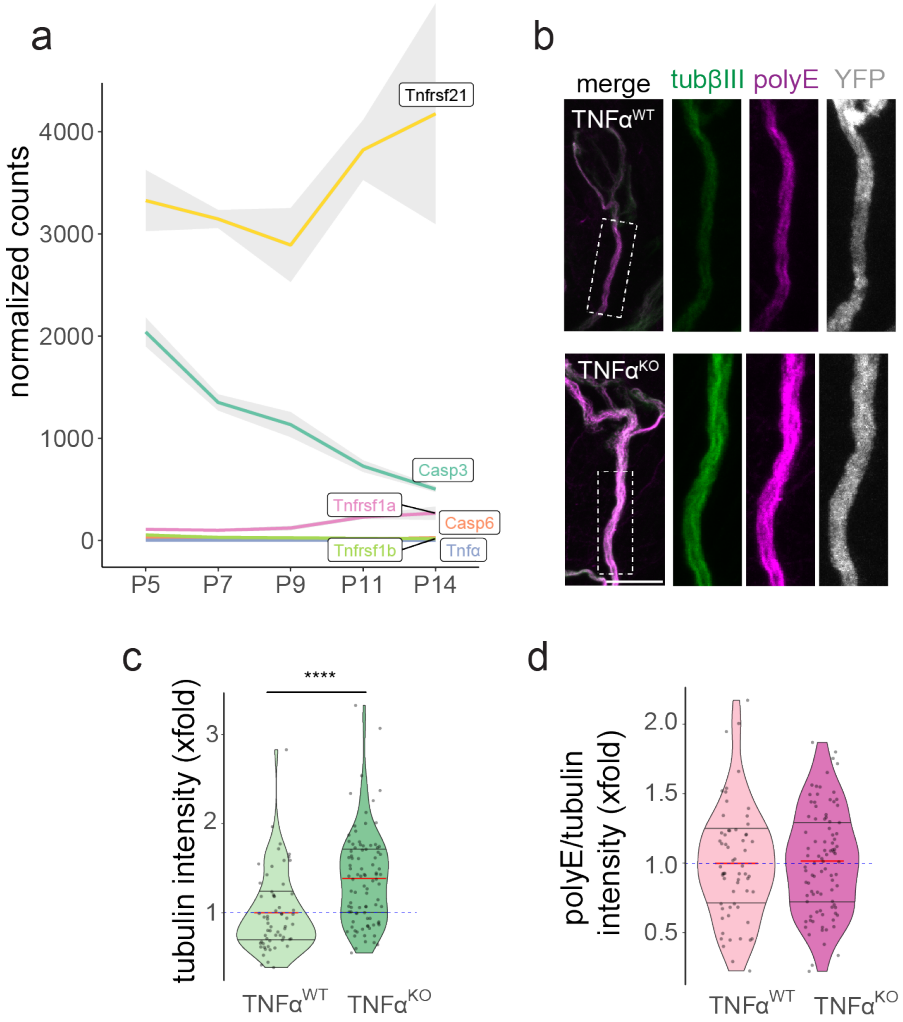

Figure 3.23: ***TNFα deletion does not affect polyglutamylation of MTs.*** ***a)*** *Normalized read counts of genes of the TNF pathway expressed in motoneurons at 5 time points of mouse development (mean ± s.e.m).* ***b*** *βIII-tubulin normalized on YFP and expressed as fold change of wild type control, was increased in $TNF\alpha^{KO}$ compared to $TNF\alpha^{WT}$, **** $p = \leq 0.0001$ (two-tailed Mann Whitney).* ***c)*** *No changes were detected in the ratio of polyglutamylation on βIII-tubulin, $p = 0.81$ (two-tailed unpaired t-test) in singly innervated synapses from$TNF\alpha^{KO}$ and $TNF\alpha^{WT}$. Statistical testing was performed based on axons (n= 61/91) for the comparison amongst genotypes from a total of 8 animals; data are expressed as mean and IQR.*

4 Discussion

The shaping of neuronal circuits to form a mature nervous system is a highly conserved and fundamental occurrence of early postnatal development[3,4]. The establishment of functional neuronal networks requires the fine-tuned removal of synapses[283]. This process is characterized by two phases, an initial overproduction, followed by an extensive loss of both pre- and postsynaptic structures. Despite decades of research, a clear mechanistic understanding of mammalian pruning is lacking. Taking advantage of the prominent role of the cytoskeleton in these morphogenic events and using the well-studied NMJ system, in this PhD project I had the following goals:

- Establish a cell-specific sequencing technique amenable for mining the paths involved in the pruning process
- Investigate the role of glutamylases and deglutamylases in synapse elimination and their effect on the MT cytoskeleton
- Identify the intrinsic molecular pathways that guide axonal pruning

9 functional glutamylases in mammals and 6 deglutamylases

4.1 Glutamylases and deglutamylases pace axonal pruning

To delineate the contributions of the Tubulin Code on synapse elimination, my first goal was to obtain the expression profile of deglutamylases and glutamylases in motor neurons across the pruning period in mice.

As mammals have 9 functional glutamylases and 6 deglutamylases, the abundance of members in both the CCP and the TTLL families raises the question if there is redundancy in their activity. Growing evidence suggests that these enzymes have acquired specialised activity to either initiate the glutamylation process to form a glutamate "seed", or elongate the glutamates into a polyE chain, starting from this initial seed[113,151,159]. However, it is not know if they would exert different outcomes to axon pruning.
Armed with this dataset I first assessed the expression patterns of glutamylases and deglutamylases in mice across 5 data points spanning from P5 to P14 (Figure 3.4g). From this it merged that TTLL7 was the highest expressed initiator, while TTLL1 the highest expressed elongator in motor neurons (Figure 3.3c &g). The lack of effect of TTLL7 in mammalian axon pruning (Figure 3.4g), but the prominent role of TTLL1 (Figure 3.10f) suggests rather a divergence in function within glutamylases to acquire specific roles of either “seeders” or “elongators”. This divergence might ensure implementing a step-wise action performed by different enzymes, to coordinate function and localization of the effectors and thus obtain more control over the pruning phenotype.
Apart from being segregated into initiators or elongators, glutamylation enzymes seem to have a preference to modify either α or β-tubulin substrates. In particular, TTLL7 catalyzes the addition of the first branch point on the β-tubulin isotypes[143,275]. Consistent with this, genetic ablation of TTLL7 glutamylase from motor neuron specifically depleted the β-monoglutamate signature. Despite being highly expressed, TTLL7 absence in motor neurons did affect axon pruning, nor did it perturb MT mass or MT dynamics (Figure 3.4 &3.5). It is not however excluded that TTLL7 could have a role in the mature nervous system, since our motor neuron translatome indicated that TTLL7 expression increases over time (Figure 3.3c &g) and it is known to be the highest expressed glutamylase in the adult CNS[275].
My findings confirm that polyglutamylation is catalyzed by TTLL1 (Figure 3.6 a &d). However, contrary to TTLL7, TTLL1 deletion had robust effects on delaying axon pruning (Figure 3.10e &f), have higher MT cytoskeletal content (Figure 3.6a &e) and show more persistent MT growth than

controls (Figure 3.10d). Consistent with the preference for α-tubulin as a substrate[151], TTLL1 is unable to add the first glutamate seed on β-tubulin, since its motor neuron genetic deletion didn't affect βmonoE abundance (Figure 3.6g). To date, an antibody specific against αmonoE to confirm if TTLL1 can simply elongate or also function as initiator, is missing. TTLL1 is, however, generally classified as an elongator, which raises the question of which TTLL would instead add the seed for TTLL1 to elongate. The translatome sequencing results point to TTLL5 for undertaking this role. TTLL5 was the only other seeder, apart from TTLL7, enriched in motor neurons compared to spinal cord tissue (Figure 3.7), and the second most expressed glutamylase initiator in motoneurons overall (Figure 3.3c &g). Of the other neuronal enriched glutamylases, TTLL11 is classified as an "elongator" while TTLL12 is predicted to lack glutamylation activity[284]. Both TTLL1 and TTLL5 seem to preferentially modify the α-tubulin isoforms instead of β-tubulin counterparts[143]. Thus, future work should corroborate whether TTLL5 is responsible for the addition of the first branch point on α-tubulin, therefore functioning upstream of TTLL1.

Could TTLL1 specificity not be limited to a general preference to modify α-tubulin substrates, but rather act on specific tubulin isotypes, such as Tuba4A? In line with this, impairing the polyglutamylation ability of Tuba4A in Tuba4a^{KI} mouse increases MT mass and delays pruning (Figure 3.8g &h), phenocopying the results of TTLL1^{mnKO} (Figure 3.6e & 3.10f).

Despite Tuba4a not being the most abundantly expressed tubulin isotype in motor neurons at the developmental age tested (Figure 3.8a), it is however the isotype with the highest relative increase from P5 to P14 (Figure 3.8b), namely by 63%. Impairing Tuba4a's ability to be polyglutamylated has substantial effects on the MT cytoskeleton, as it led to a significant increase in overall βIII-tubulin mass (Figure 3.8g). The seemingly unexpected increase of βIII-tubulin, although Tuba4a was manipulated, can be explained by the nature of the MT assembly: α- and β-tubulin subunits are obligate heterodimers when assembled into the MT protofilament[285]. One the explanation for the increase in βIII-tubulin, is that they could form heterodimers with αIV-tubulin. Since Tub4a^{KI} cannot be polyglutamylated, these spe-

cific type of MT filaments enriched in βIII and αIV-tubulin dimers, could be spared by Spastin severing.Hence, manipulation of α-tubulin has an indirect effect on β-tubulin and cytoskeleton, resulting in overall stabilized cytoskeleton (Figure 3.8g). However, considering that the α - β heterodimer assembly occurs with a 1:1 stoichiometry, the results on cytoskeleton are quite striking and cannot be explained solely through its effects on βIII-tubulin. In fact, Tuba4a expression covers for only roughly 5% of the total expression of tubulins in motorneurons at P14, while Tub3b has the highest proportion of expression of the β isoforms during motor neuron development (16.7% at P14) and its expression steadily increases from P5 to P14 with a net increase of 47% (Figure 3.8a &d).
Interestingly, a distinct characteristic of Tuba4a is that it acts as being permanently detyrosinated, due to the lack of the C-terminal tyrosine residue in its gene sequence[113]. Thus, the interplay between detyrosination and hypoglutamylation in this *knock-in* mouse could alter overall MT mechanics and behaviour, and/or protein recruitment. The precise mechanism are worth investigating further and would be instrumental to decipher the underlying cause of neurodegenerative phenotypes associated with mutation in several tubulin genes, including three β tubulins (Tubb3, Tubb4a, Tubb2a)[286–289] and the α tubulin, Tuba4a, whose mutations are found in familial forms of amyotrophic lateral sclerosis (ALS)[290].

4.2 Synapse elimination is under rheaostatic control of local PolyE levels

Deleting TTLL1 delays axonal pruning in the PNS (Figure 3.10e &f) and the CNS (Figure 3.11). Conversely, deleting CCP1 speeds up the process (Figure 3.15f). These observations uncovers a rheostatic balance between these two enzymes' activity during development. Hence, the winning branch has a more active set of CCP1 to remove polyE and avoid destabilization, while TTLL1 in loser branches is activated to recruit Spastin to MTs. I further show how CCP1 deletion alone, in the absence of Spastin, is sufficient

to induce hyperglutamylation of MTs in young mice when acutely deleted (Figure 3.17a - e). This suggests that CCP1 is the main controller of polyglutamylation in motor axons, while CCP6 might only contribute to a minor degree in this cell type and at this developmental stage. This is congruent with our motor neuron translatome data where CCP6 has 60 times lower expression than CCP1 (Figure 3.14b). This difference between the developmental stages and the adult can explain why CCP6 deletion in CNS expands the brain regions that become hyperglutamylated and thus more susceptible to neurodegeneration, when CCP1 is concomitantly absent[266]. Indeed CCP6 expression increases over time (Figure 3.14c), pointing to a more predominant role in the mature nervous system rather than in developmental stages.

4.3 Commonalities and differences of glutamylases and deglutamylases in adult and young mice

Hyperglutamylation or hypoglutamylation determined different outcomes for MT cytoskeleton in adult animals compared to young mice undergoing pruning. In the absence of TTLL1, MTs are hypoglutamylated in both adult (Figure 3.9a &b), and in young animals (Figure 3.6a &d) and as expected from its canonical enzymatic activity[144]. On the other hand, MT mass is unaltered in adult TTLL1^{mnKO} and WT (Figure 3.9a &c), but is increased in TTLL1^{mnKO} motor neuron axons compared to their littermate controls. This suggests that control over MT mass by TTLL1 could be developmentally confined: at older ages, the cytoskeleton in motor neurons is fully stabilized, hence presumably homeostatic mechanisms come into play when the pruning period is over, to maintain the integrity of the mature cytoskeleton. Similarly, the MT content in Spastin^{KO} is also unchanged compared to controls in adults (Figure 3.9d), but not in young mice[74]: a further evidence that these two enzymes act in concert in the same enzymatic pipeline, which puts Spastin downstream TTLL1.

Absence of CCP1/6 in mature motor axons, on the other hand, causes significant hyperglutamylation (Figure 3.18a &b) as reported in adult cerebellum of the Purkinje cell degeneration or *pcd* mouse and in whole brain of mice lacking CCP1 and CCP6[266,291], but fails to do so in young animals (Figure 3.15a &c). Unlike TTLL1, CCP1/6 deletion also reduced overall MT mass (Figure 3.18a & c) and affected neuronal transport in adults (Figure 3.19). Transport defects are possibly a consequence of hyperglutamylation neurotoxicity[154,266]. Indeed, abnormal axonal swellings appear as soon as 1 month of age in motor neurons lacking CCP1/6 (Figure 3.19a), reminiscent of perturbations in axonal transport[292,293]. Furthermore, at 6 months mice start to present motor deficits, indicating a cell-autonomous role for this gene deletion, similarly to the Purkinje-cell degeneration induced by L7-promoter-mediated *Cre* deletion of floxed CCP1[266]. These results also recapitulate the involvement of the motor neurons in the human disease caused by the biallelic damaging variants of the CCP1/AGTPBP1 gene, also known as childhood-onset neurodegeneration with cerebellar atrophy (CONDCA), affecting cerebellum, spinal motor neurons, and peripheral nerves[294,295]. These data further suggest that hypo- or hyper- glutamylation is handled differently by neuronal cells, with a net susceptibility for hyperglutamylation. Further, it seems that while tubulin content can be homeostatically regulated, hyperglutamylation fails to do so, since tubulin content falls into a steady state in adult TTLL1$^{\mathrm{mnKO}}$ and to comparable levels as wildtype, but glutamylation doesn't. This knowledge has important repercussions for strategies aiming to target neurodegeneration by modulating glutamylation levels.

4.4 CCP1 – Spastin cooperation determines the extent of polyglutamylation in axons

The analysis of the cytoskeleton of both adult and young animals was invaluable in highlighting the differences in phenotype caused by the absence of deglutamylases, and obtaining a clearer mechanism of action. While

CCP1/6 deletion in both time points reduced MT mass (Figure 3.15a &e , Figure 3.18a & c), only in the adult this resulted in increased polyglutamylation (Figure 3.18a & b). It is more likely that the discrepancies in polyE levels between adult and young derive from Spastin activity itself, rather than CCP1 having a different enzymatic behavior in the two ages. In fact, Spastin expression decreased over time (Figure 3.17a), stressing the importance of this severase in the pruning period and only to a marginal extent in the adult. Accordingly, the high activity of Spastin at P9 does not allow for polyglutamylation to accumulate in CCP1/6 deletion (Figure 3.15f). Indeed, albeit Spastin deletion is unable to rescue hyperglutamylation caused by the absence of CCP1 in adult[266], acute deletion of both CCP1 and Spastin, induced hyperglutamylation at P9 (Figure 3.17c &d). This goes to show how the combination of different expression patterns of the severing enzymes, directly or in combination with downstream regulatory effects that remain to be elucidated, adds a second layer of regulation that dramatically changes the net effects on MT fate. This could, in part, explain the different vulnerabilities to neurodegeneration of specific neuronal populations at specific ages.

4.5 Cytoskeleton organization and dynamics are affected by the polyglutamylation state of MTs

The tight enzymatic regulation is not limited to time but also space, as postulated by the "tubulin code": a set of positional information placed on MT thanks to the post-translational decorations to generate a set of instructions for MAPs and cargos[113,114].

MT orientation combined with specific PTMs that ultra-structurally tend to organize in bundles, can bias molecular motor interaction with MTs and guide directionality of neuronal transport in either anterograde or retrograde direction[262]. An updated view of the modality of how MTs are posttranslationally modified, aided by more potent super resolution techniques such

as motor paint[262] and STED[296], deviates from seeing the filaments carrying multiple intermingled modifications. Instead, bundles of filaments carry the same modification for a good span of their length, effectively creating sub population of MTs[79,113]. My findings indicate that decreasing polyE through TTLL1 genetic deletion reduces the acetylation ratio over MT mass (Figure 3.6c & f). Vice-versa, deleting CCP1/6 increased this ratio (Figure 3.15b &d). This suggests that 1) PTMs affect each other's abundance, 2) acetylated MTs could reside in a separate bundles from polyglutamylated ones, as previously shown for acetylation and tyrosination[262]. This raises the question if this control is direct or indirect. Does one PTM limit the abundance of another, or is this relative change dependent on other MAPs recruitments, such as it could be for Spastin and polyglutamylation? How does the PTM landscape affect MT dynamics? This will be discussed in the next section.

4.6 The tubulin code affects MT dynamics

Using mice nerve-muscle explants I monitored dynamics of MT growth with EB3 imaging, as well as neuronal transport with mito-keima[297], and cytoskeleton organization with high resolution confocal imaging. Together, they provided an in depth idea of the status of the cytoskeleton and the repercussion of manipulating enzymes that change the state of PTM of MTs. Motor neurons devoid of CCP1/6 have overall reduced MT dynamics (Figure 3.16a &b). Through comparison of different parameters, it emerges that there are possibly two different subpopulations of MTs: a highly dynamic subpopulation with an increased rate of assembly and disassembly which is presumably highly polyglutamylated; and a more stable population with overall longer filaments, that could be mainly acetylated (Figure 4.1). In CCP1/6$^{\mathrm{mnKO}}$, MT filaments showed higher persistence of MT growth (Figure 3.16d), and overall higher run length of mito-lysosomal organelles during transport (Figure 3.20d), suggesting that MT are longer[107]. Although these independent experiments suggest that a subset of MTs are longer in the knockout, a formal confirmation on MT length status needs further vali-

dation through direct measures, either ultrastructurally (e.g. through EM) or via direct labelling of tubulin dimers. These however, are challenging in the mice nerve-muscle explant model system, due to the 3D nature of their geometry and the high MT abundance and density in the motor axons (up to 15 filaments per μm^2, in axons with diameter of 4 to 50μm^2**??**). This will surely be the goal of future research and could be achieved through a combination of exciting new fluorescent probes and emerging techniques which I discuss in the chapter 4.12. The longer filaments can acquire this length if protected from the activity of severases, such as Spastin. This can occur either through acetylation, which allows MT to become more flexible and resist mechanic stress[133,298], or alternatively through the ability of polyE to change affinity for MAP2 or other MAPs such as Tau[200,299,300], thereby altering the electrostatic capacities of the MT lattice.

The existence of a subpopulation with a higher frequency of unstable and highly dynamic MT in the CCP1/6^{mnKO} is in line with the higher pause rate seen in the keima transport (Figure 3.20b). There is a correlation between the pause frequency of organelles and MT length, such that, the shorter the MTs, the more often an organelle pauses. Pause time is inversely correlated with the abundance of MT[107]. Pause duration of molecular motors increases with the lower abundance of MT, since the lack of overlap between MT filaments delays the engagement of motors with the next MT filament[108,110]. This result is consistent with the lower MT mass in the CCP1/6^{mnKO} compared to wild-type control mice both in young and adult mice (Figure 3.15a &e , Figure 3.18a & c).
Given these indications of a highly altered MT architecture, I additionally investigated how PTM status in de/glutamylases mouse models affects neuronal transport.

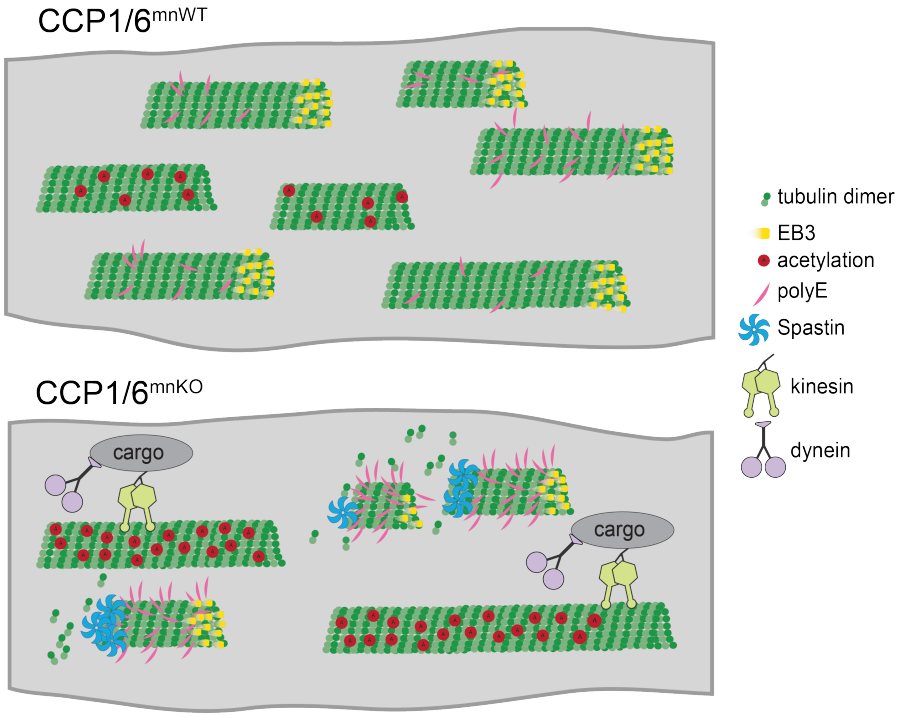

Figure 4.1: ***The interaction of Spastin and polyE affects MT mass and dynamics***. *Model of cytoskeletal differences in CCP1/6mnKO compared to wild-type controls. The absence of deglutamylases impedes the enzymatic removal of polyE, which causes polyE amounts to accumulate on a subset of MT filaments. Spastin is recruited and actively severs MTs. This causes a burst in the availability of soluble free-tubulin, which might trigger rescue events and allow freshly Spastin-cut MTs to grow*[301]*. EB3 is thus biased to bind on this "dynamic" population of MTs. Instead, the PTM acetylation accumulates on a different subset of MTs, which protects from Spastin-severing, thanks to its stabilizing properties. The acetylated MT are thus more inert and less prone to EB3 binding. This explains the higher acetylation ratio, but the reduced EB3 comets, polyE ratio and tubulin mass in the CCP1/6mnKO. Kinesin-1, which is responsible for the majority of organelle's transport, favours movement on acetylated MTs*[182, 258, 262]*. Our transport analysis suggests that acetylated MTs might be longer on average.*

4.7 Effect of PTMs tubulin code on neuronal transport and organization during pruning

PTMs affect the recruitment of MAPs, including MT severing enzymes and motor proteins and their cargos[113,114]. To our surprise, organelle flux (either mitochondria or mito-lysosomes) was not affected in axons devoid of TTLL1 during the pruning period in mice (Figure 3.12). Possibly, this result is due to the fact that an increase in MT does not boost additional delivery of organelles. This is either due to the limitation of cargo or motor proteins availability, which could be the case if the transport is already running at full capacity in this axonal context.

A second explanation comes from the entity of the experimental paradigm: axonal transport was characterized through *ex vivo* muscle-nerve explants at the intercostal nerve. Differences in transport due to the enzymatic manipulation of TTLL1 could diverge instead at the terminal axons, and in particular at doubly innervated synapses where the outcome of the competition is being decided[12,22]. Although technically more challenging, testing the effects of polyE on transport in competing terminal axons could be achieved nevertheless by retracing the same axons after *post-hoc* staining with βIII-tubulin, and categorizing winner and losers according to the total amount of cytoskeletal mass. A more accurate alternative method is sequential photobleaching to determine the extent of the synapse territory occupation[74], since synaptic territory is predictive of competition outcome[20]. Either paradigm are worth investigating in the future.

The obvious delay of axonal pruning in TTLL1$^{\mathrm{mnKO}}$ (Figure 3.6f &g) implies that this glutamylase affects synapse elimination through a different modality.

Apart from the effects on neuronal transport, an important consequence of cytoskeletal organization in axons is MT's abundance at specific locations. This affects the availability of resources at metabolically strategic locations such as synapses in dendrites or axons[225]. This can occur by means of MT architecture, to boost cargo delivery at synaptic boutons and strengthen specific synapses. In fact, MTs in presynaptic areas are shorter and more

dynamic, in order to promote cargo pausing and delivery[225,238,302]. In addition, TTLL1 could play important roles in recruiting Spastin to presynapses. Spastin, thanks to its property to bind both ER proteins, such as REEP1 and atlastin[205,207,208], and MT through the MTDB domain[192], could redistribute ER by co-aligning MT filaments with ER to drive movement of ER tubules[303–305]. This could be potentially occurring in axons at Nodes of Ranvier of pruning motor axons. While ultrastructural analysis showed no difference in total ER volume at inter-nodal areas (Figure 3.13c), preliminary results indicate there was potentially an increase of total ER at nodes of Ranvier (Figure 3.13d). In this respect, two functional Spastin isoforms have been detected. M1, which enables interaction with ER through its N-terminal hydrophobic domain; and m87, which is preponderantly responsible for MT binding. Previously, it has been shown that m87 is more expressed than m1 in the adult CNS[174,213], while the translatome data show that the opposite is true in young pruning neurons (Figure 3.13a). This result underscores the importance of ER at these developmental stages, to possibly modulate calcium buffering and calcium events at nodes of Ranvier[306]. Terminal branches and synapses are subjected to high levels of calcium influx, thus buffering by ER might be crucial in these locations to maintain homeostasis.

To recapitulate, my findings indicate that the change in polyglutamylation might alter the MT structural organization and cause a redistribution of organelles, such as ER or mitochondria, by using Spastin as an interaction node between MT and ER. Regulation of pruning through redistribution of organelles is a previously unknown mechanism of action contributing to axon pruning, and is worth exploring and exploring in the future.

4.8 Effect of PTMs tubulin code and neuronal transport in adult

Axons require both the continuous delivery of new organelles and the clearance of aged ones, both of which rely on a proper axonal transport and MT

organization[225]. Motivated by the compelling evidence that hyperglutamylation is associated with neurodegeneration[266], and by the observation that hyperglutamylation is absent in young mice, I examined how transport is affected when MTs are hyperglutamylated in the adult in the absence of CCP1/6 in motor neurons.

My results show the altered neuronal transport of both anterograde and retrograde mitochondria and mito-lysosomes (Figure 3.19d - f). The higher rate of mito-lysosomes anterogradely but the lower rate retrogradely (corresponding roughly to 1 lysosome per minute difference between conditions) indicates that these organelles accumulate at synapses. This is also corroborated by a higher mitophagy index quantified in the distal NMJ (Figure 3.19g - i). The effects on lysosomes are intriguing, since lysosomal dysfunctions have also been reported in Spastin^{KO} models[210,278,307] and in HSP models, a neurodegenerative disease where the majority of mutations reside in Spastin gene[308–311]. Additionally, CCP1 has been shown to physically interact with parkin[312], a key gene involved in mitochondria autophagy and quality control[313–315]. This suggests that CCP1 and Spastin might converge onto the same downstream pathway and, when dysfunctional, affect the quality control machinery.

Axonal transport abnormalities and axon swelling have also been reported in patients with HSP[316]. Mitochondria and lysosomes are mainly transported by the kinesin-1 family of motors[112,236,317] and mutations in one of its members, KIF5A, are also associated with hereditary spastic paraplegia[318,319]. It is reported that polyE affects kinesin motility: hyperglutamylation enhances the motility of kinesin-1 in single molecule assays[120,320] but it decreases binding affinity and processivity of kinesin-1 motors in mouse cultured hippocampal neurons[267,321]. These discrepancies in transport might in part be explained by the fact that Spastin MT severing efficacy is graded according to polyE side chain length[157]. It would be interesting to also test the effects of polyE length on motor recruitment.

Thus, disrupting deglutamylase activity affects axonal transport, possibly by changing the binding affinities of MAPs and motors to the cytoskeleton by changing the electrostatic properties of the MT lattice through hyperglu-

tamylation[190]. This could also affect mitochondria's health by interacting with the mitochondria quality control machinery. Hence, downstream of glutamylation, severing enzymes alter cell physiology through a MT dependent and independent means.

4.9 Dissecting the role of neuronal activity in modulating polyE levels

Mechanistically, the combination of neuronal activity[15], pre- and post- synaptic connection strength[27,28,65–67] and the synchronization neuron-muscle activity[26], play a fundamental part in the recessive phase of synapse elimination. Especially at the NMJs, neuronal activity has direct effects on pruning. Post-synaptic blockade through α-btx acts as presynaptic punishment that destabilizes cytoskeleton and reduces overall MT mass[227]. Here we show that neurotransmission blockade alters the levels of polyglutamylation on MTs (Figure 3.21). Only blocking neurotransmission and not also the effector (Spastin) recapitulates hypoglutamylation, as in the genetic deletion of CCP1/6. By removing both the effector of polyglutamylation (Spastin), and the instructor (neuronal activity), thus uncoupling the two, we could identify the contributions from each signal. We show that neurotransmission modulates the activity of glutamylases or deglutamylases in such a way that in losing synapses, the lack of activity prompts hyperglutamylation of MTs. Our cumulative evidence so far suggests that this process could be mediated through the activation of the glutamylase TTLL1, which in turn recruits Spastin that dismantles MT cytoskeleton. Since glutamylases and deglutamylases are in a rheostatic relation, the reversed scenario is also likely: in winning axons, neurotransmission activates CCP1 to remove glutamylation from tubulin tails; this prevents cytoskeleton destabilization through Spastin.

It should be taken into consideration that neurotransmission blockade through BTX is a pharmacological intervention, and furthermore acts post-synaptically. A more refined approach to test how neuronal activity affects glutamylation

modifying enzymes, would be to use genetic models to block axons from the pre-synaptic side, offering a more direct readout on the axonal cytoskeleton. This is possible through conditional deletion of Choline-acetyltransferase (Chat), the enzyme responsible for the production of the neurotransmitter Acetylcholine. Care should be placed so that the deletion targets only a subset of motorneurons, since total Chat deletion is fatal at birth[25,322]. Furthermore, it is the relative strength of competing synapses that offers a competitive advantage in one of the motor branches[15]. Such partial deletion can be achieved by a careful dosage of intraventricular injection of *Cre* construct[323] to a mouse line where Chat is *floxed*, as explained in the section 5.6, and could be pursued in the future to corroborate these results.
Overall our data strongly suggest that the activity of CCPs and TTLLs is under the control of neurotransmission and, likewise, these MT modifying enzymes have an instructive role in guiding the outcome of synapse elimination.

4.10 Roles of glutamylases in CNS pruning

Pruning, either dendritic or axonal, occurs extensively in the nervous system[8–10]. Although we are starting to uncover molecular candidates involved in the process (Chapter 2.3), it remains an open question how canonical and generalized these pathways are and whether they occur in different neuronal locations. To bridge this gap, we set to explore if glutamylases are also involved in pruning of the CNS.
We found that both spine density of hippocampal granule cells and axon length of the infra pyramidal bundle are affected in the TTLL1^{KO} model (Figure 3.11). Thus we infer that polyglutamylation not only affects pruning of NMJ in PNS, but guides remodeling of both dendritic spines and axonal cytoskeleton. These findings widen the scope of action of glutamylases as key drivers of synapse elimination.

4.11 Translatome-driven search of molecular factors affecting synapse elimination

A final objective of my work was to uncover molecular cues that mediate the elimination of redundant connections through polyglutamylation.
Neurotrophins and related members are key candidates to explore, due to their prominent role in providing trophic support and previous evidence in being involved in synapse elimination[45,53,55,56,64]. Motor neuron deletion of neurotrophic related factor p75, did not affect mass (Figure 3.22b &c) or MT glutamylation, in neither singly (Figure 3.22b &d) or doubly innervated synapses (Figure 3.22 e &h). Possibly, this lack of response is due to the presence of the p75 co-receptor, Sortilin in this mouse line (Sort1, Figure 3.22a). It was previously shown that concomitant pharmacological targeting of both p75 and Sortilin are needed to exert pruning effects on NMJ[45,55,56], while full $p75^{KO}$ didn't have any effect[53]. At the time of analysis, a genetic double mutant was lacking, but it could be worth to explore in the future.
I also explored the role of TNFα, a cytokine that acts as a retrograde factor to induce presynaptic axonal elimination during the development of mouse neuromuscular synapses[64]. The lack of expression of TNFα in motor neurons seen in the transcriptome data is consistent with its derivation from postsynaptic muscle cells[64] (Figure 3.23a). Although this cytokine can bind to different receptors, it is possible that in young motor neurons it exerts its function through either TNFRSF1A/TNFR1 (the highest expressed) or TNFRSF1B/TNFBR (Figure 3.23a). Consistent with TNFα punitive properties, the full knock-out of TNFα increases overall MT mass in motor axons (Figure 3.23b &c), which leads to NMJ pruning delays[64].
However, to my surprise, polyE increased proportionally to tubulin (Figure 3.23b &d). An expected linear outcome would have been a lower ratio of polyE to tubulin in the full knock-out and subsequently less Spastin recruitment and pruning delay. An explanation for this steady state might be due to the nature of the animal model, which is a complete knock-out of the "punishment" signal. Since at the NMJ, the resolution of polyinnervation occurs through relative strength of competing synapses[15], the absence of a

biased synaptic strength between inputs in TNFα^{KO} might prevent triggering the activation of glutamylases in a branch selective manner. The nature of this "activity dependent switch", which senses the lack of activity and triggers synapse-selective pruning, is still unknown at the NMJ, but has shown to be mediated by the JAK2-STAT1 pathway in CNS callosal axons. JAK2 is localized at the inactive presynaptic terminals and transmits punishment signals from active connections to drive elimination of inactive ones[324]. To understand if the same or more complex mechanisms are at play at the NMJ still requires further investigation.

4.12 General conclusions and future perspectives

I highlight a carefully orchestrated sequence of events, where downstream of neuronal transmission the less active of two competing synapses is eliminated[15]. I show that the fate of the losing branch is marked by recruitment of glutamylases to add polyglutamylation to remove the MT cytoskeleton. Through docking to negatively charged polyE, added sequentially to α-tubulin tails by TTLL1, Spastin dismantles the cytoskeleton of axonal branches targeted for degradation (Figure 4.2).

I further show that this process affects pruning by regulating cytoskeletal mass through rheostatic mechanisms of glutamylases and deglutamylases. Polyglutamylation is not simply a permissive factor but determines the pruning paces instructively, both in the PNS at the NMJ, and in the CNS where it contributes to the removal of spines in the hippocampal granule cell and in the shortening of the IBP. This speaks to the importance of this mechanism in affecting these large scale recessive events during development. The modulation of the activity of this family of enzymes is under the control of neuronal activity, a known master regulator of pruning which dictates the competition outcomes according to experience.

It is quite striking how each enzyme of the molecular signaling here de-

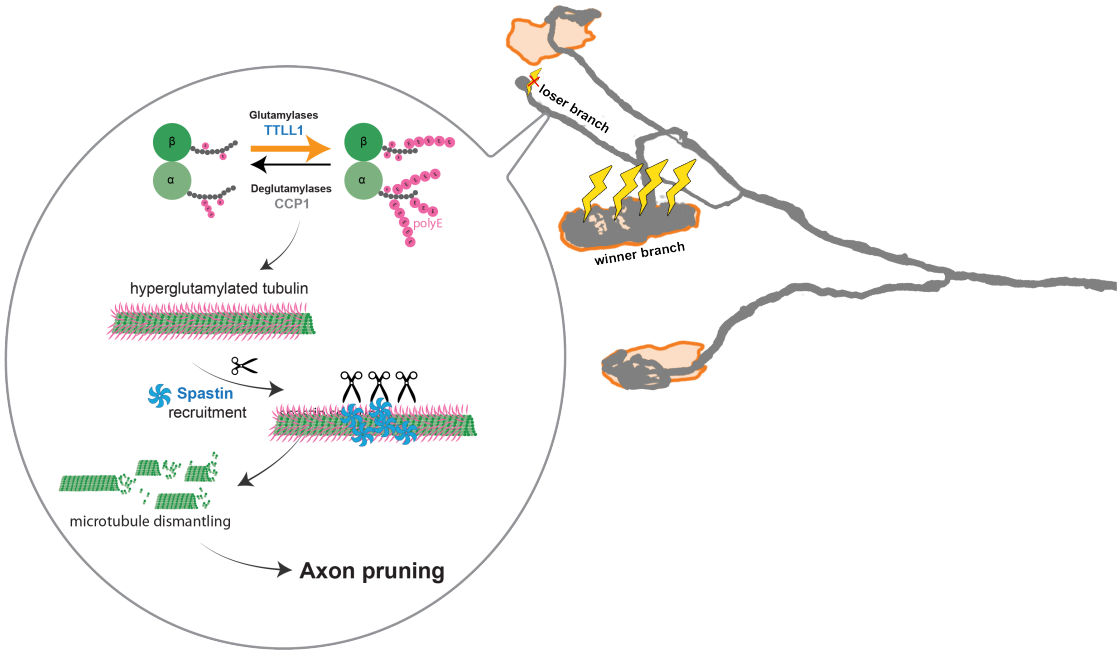

Figure 4.2: ***Glutamylases and deglutamylases rheostatically regulate developmental pruning***. *Suboptimal neural activity in a losing axonal branch triggers the activation of TTLL1 glutamylase. This enzyme hyperglutamylates the α-tubulin tail of MTs, a PTM which acts as a recruitment signal for Spastin. Spastin then severs the MT lattice and causes cytoskeletal dismantling and selective axonal branch removal. Reconstruction of terminal motor axon branches is modified from Brill et al. (2016)*

scribed, is linked with neurodegenerative disease: Spastin and HSP, CCP1 and infantile-onset neurodegeneration[294], Tuba4a with ALS[290]. All converge to the cytoskeleton, underscoring its central role both in physiology and in pathology, and the importance of obtaining a clear mechanistic understanding of this process.

The cytoskeleton architecture is highly dependent on the molecular context. The motoneuron-specific translatome obtained through the Ribotag was fundamental to uncover differences in response to the absence of CCP1 in young *vs* adult mice and the repercussion for MT architecture, pruning and axonal transport.

Future effort will be spent to mine and experimentally validate the translatome data across the different ages and conditional knock-out models, in order to gain new insights into the molecular pathways that drive the pruning process.

It is not excluded that TTLLs and CCPs might contribute to pruning independently of cytoskeleton. Although no other substrates except tubulin are currently known for TTLL1, other TTLLs can modify other substrates, such as the nucleosome assembly proteins NAP1 and NAP2, the MT +TIP protein EB1, the myosin light chain kinase (MLCK) and others[325–327]. Motoneuron transcriptome of TTLL1 or CCP1 knock-out mice could help differentiate between the extent of the contribution of these pathways to pruning. Ribotag sequencing could be additionally utilized to directly compare "losing" versus "winning" axon branches. This could be achieved by a selective presynaptic activity blockade of competing synapses (as explained in MM section 5.6), through deletion of the Chat gene in a subset of motoneurons. The altered relative synaptic strength of competing terminals by the inhibition of Acetylcholine synthesis, coupled with Ribotag sequencing, would enable the generation of a dataset of blocked (pulled down) and unblocked (total input) synapses. Then, the direct comparison of these datasets could help elucidate which molecular pathways are elicited downstream of neural activity.

An open question is how these enzymes are able to produce opposite outcomes to competition, despite sharing a common main axonal branch. Tak-

ing advantage of the extremely polarized nature of the motoneurons, Ribotag could also be implemented to generate a compartment-specific translatome of motor neurons of axons and soma. This can be achieved by dissecting and separately isolating mRNA from soma, residing in spinal cord, and mRNA from synapses located in the TRG muscle. This would help extricating the local contributions and uncover local translation events at synapses. Combined with the dataset of blocked neurotransmission in a motoneuron subset, we could obtain a direct comparison of compartmentalized and "winner vs loser" synapses. However, extremely low amounts of in-translation-mRNAs are expected in synapses, which could be a caveat for the Ribotag technique. Possibly, this could be bypassed by complementing Ribotag pull-down with single-cell sequencing mRNA amplification techniques, prior to sequencing. New and exciting technological advancements are on the horizon and will help to validate top candidates emerging from the omics datasets: techniques such as STED or Airy-scan that allow for *in situ* investigation of MTs at nanoscale resolution in animal models. Coupling them with expansion microscopy might help to super-resolve MT structure in more challenging conditions, such as the bundled axonal cytoskeleton of murine NMJ. On the other hand, other techniques could add the dynamic component of MT regulation: motor paint[262] for visualizing molecular motors dynamics, while new probes amenable for visualization MT PTMs in real time[328] will help to elucidate how they affect tubulin dynamics in cells, and possibly in animal models *in vivo*. Combined, they provide exciting avenues for the Tubulin Code and untangle how it shapes large scale morphogenic events.

5 Materials and methods

5.1 Buffers, Solutions, Reagents and Equipment

5.1.1 Buffers

0.1 M Phosphate buffer	0.1M NaH_2PO_4	500 ml
	0.1 M Na_2HPO_4	500 ml
	Total	1 l

PBS pH 7.4 10x	Sodium phosphate monobasic dihydrate	18.6 mM	71505	Sigma
	Sodium phosphate dibasic	84.1 mM	S5136	Sigma
	Sodium chloride	1.75 M	3957.1	Roth

4% Paraformaldehyde in PBS	Paraformaldehyde	4%	158127	Sigma
	PBS, pH 7.4, 10x	1x	-	-

DMEM, high glucose, GlutaMax	61965059	Thermo Fisher
Fetal bovine serum (FBS)	10100147	Thermo Fisher
PBS pH 7.4	10010015	Thermo Fisher

EM fixative pH 7.2	Glutaraldehyde	2.5 %	16300	EM Sciences
	Paraformaldehyde	4 %	15700	EM Sciences
	Sodium cacodylate buffer	0.1 M	11654	EM Sciences

5.1 Buffers, Solutions, Reagents and Equipment

4% Paraformaldehyde in 0.1 M PB	PFA	40 g	Sigma-Aldrich, P6148
	NaOH	125 µl	Roth, KK71.1
	0.1 M PB	up to 1 l	
	Total	1 l	

Lysis buffer	Gitocher Buffer	15 µl
	β-mercaptoethanol	1.5 µl
	Proteinase K	0.75 µl
	H_2O	125.25 µl
	Total	150 µl

Agarose gel	50 x TAE buffer	2 ml	Roth, CL86.1
	Agarose	1 g	SeaKem, 50004
	Gel Red	10 µl	VWR International,730-2957
	H_2O	up to 100 ml	
	Total	100 ml	

Blocking solution	BSA	5 g
	Triton X-100	500 µl
	0.1 M PB	up to 100 ml
	Total	100 ml

Ringer's solution 1x	Sodium chloride	125 mM	3957.1	Roth
	Potassium chloride	2.5 mM	7447-40-7	Merck
	Sodium phosphate monobasic dihydrate	1.25 mM	71505	Sigma
	Sodium bicarbonate	26 mM	S5761	Sigma
	Calcium chloride dihydrate	2 mM	C7902	Sigma
	Magnesium chloride hexahydrate	1 mM	630628	Sigma
	D-(+)-glucose	20 mM	G7021	Sigma
	oxygenate with carbogen (95% O2 / 5% CO2)	-	-	-

5.1.2 Antibodies

Primary Antibodies

Antigen	Species	#	Dilution	Company
ChAT	Goat	AB144P	1:500	Sigma
Gfap	Chicken	ab4674	1:2000	Abcam
GFP	Chicken	ab13970	1:1000	Abcam
GT335	Mouse	AG-20B-0020	1:200	Adipogen
polyE tubulin	Rabbit	IN105	1:1000	Adipogen
acetylated tubulin	Mouse	611B1	1:1000	Abcam
Neurofilament heavy polypeptide	Chicken	ab4680	1:500	Abcam
β-monoE	Rabbit	-	1:500	gift from Janke Lab
HA	Mouse	H6908	1:50	Sigma-Aldrich
βIII-Tubulin AF488	Mouse	801203	1:200	Biolegend
βIII-Tubulin AF555	Mouse	560339	1:200	BD Biosciences
βIII-Tubulin AF594	Mouse	657408	1:200	Biolegend
βIII-Tubulin AF647	Mouse	657406	1:200	Biolegend
α-BTX AF488	Mouse	B13422	1:50	Invitrogen
α-BTX AF594	Mouse	B13423	1:50	Invitrogen
α-BTX AF647	Mouse	B35450	1:50	Invitrogen
α-BTX-biotin	Mouse	B1196	1:50	Invitrogen

Table 5.1: *The primary antibodies.*

Secondary Antibodies

Antigen	Species	#	Dilution	Company
α-rabbit IgG-F(ab')2 AF488	Goat	A-11070	1:1000	Thermo Fisher
α-rabbit IgG-F(ab')2 AF549	Goat	A-11072	1:1000	Thermo Fisher
α-rabbit IgG-F(ab')2 AF647	Goat	A-21246	1:1000	Thermo Fisher
α-chicken IgY AF488	Goat	A-11039	1:1000	Thermo Fisher
α-chicken IgY AF647	Goat	A-21449	1:1000	Thermo Fisher
α-goat IgG AF594	Donkey	A-32758	1:1000	Thermo Fisher
α-mouse IgG AF594	Goat	A-21125	1:1000	Thermo Fisher
α-mouse IgG AF647	Donkey	715-605-151	1:2000	Jackson Immunofluorescence
α-rabbit IgG AF555	Donkey	A-31572	1:2000	Thermo Fisher
α-rabbit IgG AF568	Goat	A-11011	1:1000	Thermo Fisher
α-rabbit IgG AF594	Goat	A-11012	1:1000	Thermo Fisher
α-rabbit IgG AF405	Goat	A-31556	1:1000	Thermo Fisher
α-rabbit IgG AF488	Goat	A-11008	1:1000	Thermo Fisher

Table 5.2: *The secondary antibodies.*

5.1.3 Primers

Primer	Sequence (5' – 3')	Product (bp)
Cre	GCCGAAATTGCCAGGATCAG (fw) AGCCACCAGCTTGCATGATC (rv)	650 bp
Chat-Cre	GTTTGCAGAAGCGGTGGG (wt-fw) CCTTCTATCGCCTTCTTGACG (mut-fw) AGATAGATAATGAGAGGCTC (rv)	wt: 200 bp mut: 148 bp
GFP	CACGCTTCAAAAGCGCACGTCTG (fw) GTTGTGCCCAGTCATAGCCGAATAG (rv)	280 bp
CCP1	TTAAGCAGTGGCTGCCGGAGTGC (fw) GTCTACAGCCACGTGCTCAGCAAAGG (rv)	wt: 296 bp mut: 405 bp
CCP6	GAATGGCAATGAGATCACCACTCTCCAGC (fw) CTGTTGGGTGTCTGAGGCAAACACTTCC (rv)	wt: 202 bp mut: 337 bp
TTLL1	CCCAGGTAGACCAGAAGAGGGAGGC (fw) TCTTGGCTTCTCTTGCTTGGGACCC (rv)	wt: 124 bp mut: 310 bp
TTLL1-KO	GAACTCGACACCACCTGCAACCAACC (fw) CAATGTGCTTGGCGGTTCAGGATCCC (rv)	wt: 1300 bp ko: 520 bp
TTLL7	CGACCGAGAACCTAGCTACTGCTCATT (fw) CGCTATGAAATAACCCTGATGCTGAAG (rv)	wt: 317 bp mut: 422 bp
Spastin	AAGTCATGGCAGTCTTTCTGGCT (41-fw) CACATGGTGGCTCATAACCATTTA (89-fw) ATTTGCAAAAACTACTTGCTATTAAATTCC (169- rv)	wt: 223 bp mut: 270 bp ko: 432 bp
YFP	CACATGAAGCAGCACGACTT (wt) TGCTCAGGTAGTGGTTGTCG (rv)	378 bp
P75	TGTCAGGCGTTACAAGAAACA (fw) GAAGGATCCATAACTTCGTATAGC (mut-rv) TCTTTAAGCTGGAGCAATGACT (wt-rv)	wt: 250 bp mut: 209 bp

Table 5.3: *The primers.*

Primer	Sequence (5' – 3')	Product (bp)
TNFα	TAGCCAGGAGGGAGAACAGA (fw) AGTGCCTCTTCTGCCAGTTC (wt-rv) CGTTGGCTACCCGTGATATT (mut-rv)	wt: 183 bp mut: 318 bp
Ribotag	GGG AGG CTT GCT GGA TAT G (fw) TTT CCA GAC ACA GGC TAA GTA CAC (rv)	wt: 243 bp mut: 290 bp
CagTomato	CTGTTCCTGTACGGCATGG (fw-wt) AAGGGAGCTGCAGTGGAGTA (rv-wt) GGCATTAAAGCAGCGTATCC (fw-mut) CCGAAAATCTGTGGGAAGTC (rv-mut)	wt: 297 bp mut: 196 bp
Chat	GCCCTGCCAGTCAACTCTA (fw) GAAATCCTGACAGATTCCAACA (wt-rv) TTTCCGCCTCAGGACTCTTC (mut-rv)	wt: 550 bp mut: 400 bp

5.1.4 Microscopy reagents and equipment

Item	#	Company
FV1000	-	Olympus
20xO/N.A. 0.85	UPlanSApo	Olympus
FV3000	-	Olympus
20x/N.A. 0.75	UPlanSApo	Olympus
40x/N.A. 0.95	UApo N340	Olympus
60xO/N.A. 1.42	PlanApo	Olympus
100xW/N.A. 1.0	LumPlanFL	Olympus
10x/N.A. 0.4	UPlanSApo	Olympus
20xW/N.A. 0.5	LumPlanFL	Olympus
Lambda 10-3	LB10-NWIQ	Sutter
4x/N.A. 0.16	UPlanFL N	Olympus
4x/N.A. 0.28	XLFluor 4x/340	Olympus

Table 5.4: *Microscopy reagents.*

5.1.5 Other equipment

Item	#	Company
Vibratome	VT1200	Leica
Cryostat	CM1860	Leica
Injector	Nanoliter 2000	World Precision Instruments
Bioanalyzer	RNA 6000 Nano	Agilent
Ultrasound	Vevo 2100	Visualsonics

Table 5.5: *Other equipment.*

5.1.6 Softwares

Item	#	Company
GraphPad Prism	8.2.1	GraphPad Software
Illustrator CS5	15.0.2	Adobe
ImageJ/Fiji	1.52f	Schindelin et al. (2012)
Microsoft Excel	2016	Microsoft Office
Photoshop	12.0.4	Adobe
µManager	1.48v	www.micro-manager.org
RStudio	2022.07.1 Build 554	github.com/rstudio/rstudio
R	4.2.1	www.r-project.org

Table 5.6: *The softwares.*

5.1.7 Chemicals and other reagents

Item	#	Company
DAPI	D9542	Sigma
DNA polymerase I	M0209	New England BioLabs
GoTaq(R) G2 Hot Start Green Master Mix	M7423	Promega
Heparin sodium salt	H3149	Sigma
Hoechst 33342	H3570	Molecular Probes
Proteinase K	351100902	Biozym
Streptavidin-Alexa Fluor 405	S32351	Thermo Fisher Scientific
Vectashield Mounting medium	H-1000	Vector Laboratories
β-Mercaptoethanol	M6250	Sigma
RNAsin Plus Inhibitor	N2615	Promega
M-MLV Reverse Transcriptase Buffer	M170A	Promega
Reverse Transcriptase M-MLV	M170A	Promega
QIAEX II Gel Extraction Kit	20021	Qiagen

Table 5.7: *The chemicals.*

5.2 Mouse lines, husbandry and genotyping

The experiments were carried using mice of both sexes. The animals were housed in individually ventilated cages with food and water ad libitum, and kept together with littermates. Every experiment was performed conform to the regulations of the local authorities of the government of upper Bavaria.

By crossbreeding conditional knock-out mice with a line of mice with Cre-recombinase expression under the Chat promotor[329] (ChAT-IRES-Cre, Jackson #6410), we have generated motor neuron KO mice for the following genes:

- p75 (Jackson #031162)
- Glutamylases (gifted from Dr. C. Janke, Institut Curie, Paris, France):
  - TTLL1[266]
  - TTLL7[151]
- Deglutamylases (gifted from Dr. C. Janke, Institut Curie, Paris, France):
  - CCP1[330]
  - CCP6[266]

Additional mouse lines used were:

- TNFα full knock out (Jackson #005540)
- full neuronal deleted TTLL1 (*Nestin*-Cre derived deletion by crossing to TTLL1$^{\mathrm{fl/fl}266}$)
- Tuba4a knock-in, mutation that prevents polyglutamylation of tubulin tails[331]

Homozygous conditional mutants (which were at least heterozygous for *Cre*), or constitutive mutants (homozygous for deletion) were used as experimental animals, and referred to as CCP1/6$^{\mathrm{mnKO}}$, TTLL1$^{\mathrm{mnKO}}$, TTLL7$^{\mathrm{mnKO}}$, p75$^{\mathrm{mnKO}}$, TTLL1$^{\mathrm{KO}}$, TNFα^{KO}, Tuba4A$^{\mathrm{KI}}$; while homozygous conditional littermates (*Cre-negative*) or full wild-types were used as controls, named

hereafter CCP1/6$^{\mathrm{mnWT}}$, TTLL1$^{\mathrm{mnWT}}$ or TTLL7$^{\mathrm{mnWT}}$, p75$^{\mathrm{mnWT}}$, TTLL1$^{\mathrm{WT}}$, TNFα^{WT}, Tuba4A$^{\mathrm{WT}}$.

The mice have been used for the quantitative immunohistochemistries, following the protocol indicated in the section 5.3. They have also been used for the study of axonal transport following injections of AAV9-hSyn-mitoKeima (CCP1/6$^{\mathrm{mnWT}}$, TTLL1$^{\mathrm{mnWT}}$). Thy1-YFP transgenic mice[332] (cytoplasmic YFP in all motor neurons, Jackson #3709) were used to assess pruning speed in CCP1/6$^{\mathrm{mnWT}}$, TTLL1$^{\mathrm{mnKO}}$, TTLL7$^{\mathrm{mnKO}}$ compared to their littermates CCP1/6$^{\mathrm{mnWT}}$, TTLL1$^{\mathrm{mnWT}}$, TTLL7$^{\mathrm{mnWT}}$.

MT dynamics of EB3 comet density has been analyzed on Thy1-EB3-YFP-J045[11] transgenic animals, either CCP1/6$^{\mathrm{mnWT}}$, TTLL1$^{\mathrm{mnWT}}$ or TTLL7$^{\mathrm{mnWT}}$ and littermates CCP1/6$^{\mathrm{mnWT}}$, TTLL1$^{\mathrm{mnKO}}$ or TTLL7$^{\mathrm{mnKO}}$.

Conditional knockout of CCP1 and Spast[74] in motor neurons, monitored by ROSA-CAG-TdTomato reporter[333] (Jackson; #7914; CCP1$^{\mathrm{fl/fl}}$ Spast$^{\mathrm{fl/fl}}$ TdTomato) was generated by injection of AAV9-CMV-iCre. Block of neurotransmission was analyzed in constitutive spastin knockout[74] (Spast$^{\mathrm{KO}}$) mice and wild-type controls injected with α-BTX. 'Ribotagging' of motor neurons was conducted in homozygous Rpl22 mice[270] (Ribotag$^{\mathrm{fl/fl}}$; Jackson, #11029) crossbred to Chat-IRES-Cre mice.

Genotyping was performed to discriminate between hetero and homozygous mice. The genomic DNA has been extracted from biopsies of the tail, using lysis buffer containing 67 mM Tris, pH 8.8, 16.6 mM $(NH_4)_2SO_4$, 6.5 mM $MgCl_2$, 5 mM β-mercaptoethanol, 10% Triton-X-100, and 50 µg/ml of Proteinase K. The sample was incubated for 5 h at 55 °C, followed by an inactivation step of 5 minutes at 95 °C. PCR was then performed using a standard protocol and the amplificated DNA was separated on a 1.5 or 2% agarose gel.

5.3 Immunofluoresce staining of triangularis sterni muscle

Immunohistochemistry is a technique that allows the detection of specific proteins by exploiting the principle of antigen-antibody conjugation, associated with a detection system (usually a fluorophore). The immunostaining of the mouse muscles has been prepared as following. The mouse thorax has been fixed in 4% paraformaldehyde (PFA) for 1 hour in phosphate buffer (PB) 0.1 M put on ice, and the triangularis muscle was dissected and extracted[334]. Muscles were then incubated in 5% CHAPS detergent in 0.1 M PB for 1h at 37 °C. The primary antibody (see table 5.1) has been diluted in a blocking solution made of 5% BSA, 0.5% Triton in 0.1 M PB, and incubated at 4°C. The incubation times were dependent on the type of tissue and antibodies used. In particular, overnight for postnatal muscles, 3 days for adult tissues or when the antibody against anti-acetylated tubulin was used.

To label postsynaptic nicotinic AChRs, x-fluorophore conjugated α-BTX (5.2) was added to the primary antibody mixture. All antibodies used in this study are listed in table 5.1 and 5.2. The muscles have then been washed in PB 0.1M and incubated for 1h at room temperature with the corresponding secondary antibodies. The sample was then washed in PB 0.1M, and the muscles then mounted on glass slides (Vectashield from Vector Laboratories or Prolong-Glass from Thermo Fisher). At this point, the samples were imaging ready and the image stacks have been recorded by confocal microscopy (more details in section 5.9.2).

5.4 Immunohistochemistry and analysis of the infrapyramidal bundles

Immunostaining was carried out as described previously[31]. Briefly, mice were transcardially perfused with PBS and ice-cold 4% PFA in PBS and brains were post-fixed in 4% PFA in PBS overnight, embedded in paraf-

fin blocks and 7 μm thick coronal sections were cut. Sections were boiled in unmasking solution (Citrate-Based Antigen Unmasking Solution, Vector Laboratories), blocked with 1% BSA and incubated overnight at 4°C with primary antibodies in PBS with 1% BSA and 0.2% Tween 20. Subsequently, samples were washed 3 times with PBS with 0.2% Tween 20 and incubated for 2 hours at room temperature with fluorescent secondary antibodies in PBS with 1% BSA and 0.2% Tween 20, washed three times with PBS with 0.2% Tween 20 and embedded in Mowiol with 1 μg/ml Hoechst. Fluorescent images were taken using a confocal microscope (Leica SP8 and Leica Stellaris).
IPB was visualized by anti-calbindin D28K (Swant, 1:300) immuno-staining of 7 μm coronal sections of P56 WT and TTLL1^{KO} mouse brains embedded in paraffin. Images taken using a confocal microscope (Leica SP8 and Leica Stellaris) were analyzed by ImageJ software. IPB length was quantified using the ratio of IPB length to the length of the CA3 as described previously[276].

5.5 DiOlistics labeling of hippocampal granule cells and dendritic spine density analysis

For the visualization of dendritic spines in WT and TTLL1^{KO} brains DiOlistic approach was used as described previously[31]. In brief, mice were perfused with 20 ml of 4% PFA/PBS, and brains were isolated and post-fixed in 4% PFA/PBS for 30 minutes. Then, brains were washed in PBS for 30 minutes and incubated in 15% sucrose for 30 minutes then again other 30 minutes in 30% sucrose. 250 μm thick coronal slices were cut with vibratome, washed in PBS and incubated for 5 minutes in 15% sucrose and subsequently in 30% sucrose. The solution was removed and DiI was introduced into the brain slices by DiI-labeled tungsten particles with the use of a Gene Gun helium-powered system from Bio-Rad and 120 Psi pressure[31] . After the labeling, the slices were washed in PBS to remove residual tungsten particles and kept for 30 minutes in PBS in the dark to let the dye

diffuse. Slices were mounted onto a glass slice in 0.5% n-propyl gallate/90% glycerol/PBS (NPG) and the next day imaged by Leica Stellaris confocal microscope. Analysis of the dendritic spines density was performed using Neurolucida software (MBF Bioscience) in 3 different WT and TTLL1^{KO} brains (at least 10 labelled granule cell dendrites were analysed per brain).

5.6 Neonatal AAV9 or α-BTX injections

I injected viral vectors into neonatal pups following the same procedures as previously published[74, 227, 323, 335] and as shown in Figure 5.1. First of all, P3 pups have been anesthetized with isofluorane (Abbott). 3µl of viral vector was then injected into the right lateral ventricle, by a nanoliter injector (World Precision Instruments; Micro4 MicroSyringe Pump Controller connected with Nanoliter 2000) connected to a fine glass pipette (Drummond; 3.5", #3-000-203-G/X). The injection rate, at a rate of 30 nl/s, was guided by ultrasound (Visualsonics, Vevo® 2100). Trypan blue 0.05 % (wt/vol) was added to the viral solution in order to visualize the process of filling of the injected ventricles. Only whole litters were injected. The pups have then been let recover on a heating mat before being returned to their mother into the home cage. At appropriate age, they were sacrificed for the experiments. AAV9-hSyn-iCre, AAV9-mito-Keima viral vectors have been injected at a titer of 1x10^{13} to 2x 10^{14}.

The expression of TdTomato reporter allele (homozygous) in the motor neurons of the triangularis sterni muscle has been used to verify the Cre-mediated deletion in conditional knock-out of CCP1 and Spast. The recombination was considered positive when the fluorescence intensity of TdTomato was in the upper 25 % range. On the other hand, it was considered negative when the fluorescence level was in the lowest 25% quartile. The other axons were excluded from the analysis.

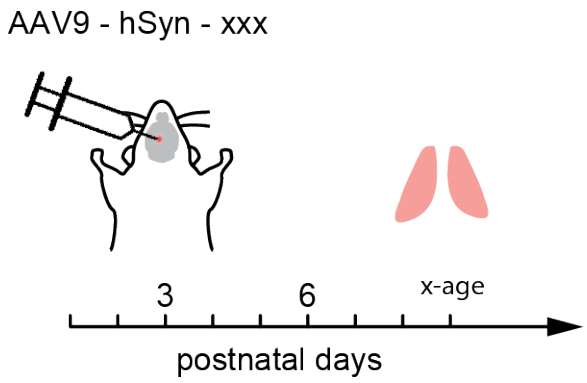

Figure 5.1: ***Intraventraventricular injection of viral vectors.*** *Motor neuron expression was obtained through the use of human Synapsin promoter (hSyn) and the adeno-associated capsid serotype of AAV9 to drive the expression of the construct of interest (such as iCre, mito-keima etc.) in neuronal cells, specifically motor neurons of triangularis sterni muscle. Injection was executed at P3 to achieve broad targeting of neurons, followed by tissue preparation at specific age according to the experimental requirements.*

The postsynaptic neurotransmission in the triangularis sterni muscle of BI6 or Spast^{KO} and Spast^{WT}mice was inhibited with 1 µl of 50 mg/µl α-BTX conjugated to Alexa Fluor 594 (purchased from Invitrogen; B13423), injected in the thorax (at P7) using a pulled glass capillary, as previously described[74, 227, 323] and as shown in schematic 5.2. Visualization was possible because α-BTX was conjugated to Alexa Fluor 594 (purchased from Invitrogen, B13423). As control, we used the contralateral side of the thorax, untreated.

To verify the degree of blockade and the level of the absence of denervation, we performed a post-hoc staining of the triangularis sterni muscle with BTX-AF488 or AF594 (>100 NMJs per mouse, n=3). The immunostaining was conducted following the protocol indicated in the the section 5.3, with anti-βIII-tubulin and anti-polyE antibodies.

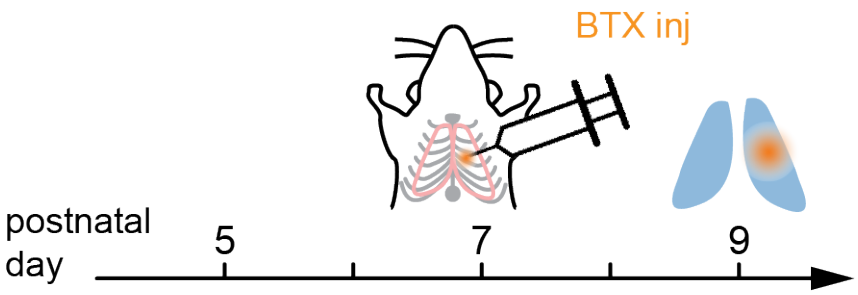

Figure 5.2: *Unilateral injection into Triangularis sterni muscle with β-BTX. Injection was executed on P7 old mice followed by triangularis sterni muscle extraction and staining at P9. In some cases, post-hoc staining using a different fluorochrome conjugated β-BTX was used to confirm extent of blocked synapses.*

5.7 Ribosomal pull down and RNA sequencing

The ribotagging protocol allows for the isolation of cell specific mRNA in translation as shown in Figure 5.3. For each group we have dissected three spinal cords, from homozygous Rpl22 mice[270] crossbred to Chat-IRES-Cre mice. The samples were kept at -80°C. The spinal cords have been homogenized in the following buffer: 50 mM TrisCl (pH 7.5), 100 mM KCl (Sigma #P9541), 12mM $MgCl_2$ (Sigma 63068), 1%NP-40 (Roche, #11332473001),1 mM DTT (Sigma #646563), 1X Protease Inhibitors (Sigma #11697498001), 1mg/ml Heparin (Sigma #H3393), 100µg/ml cycloheximide (Sigma # C7698), RNAse OUT (Thermofisher #10777019). The mRNA-ribosome complex was then precipitated using the polyclonal HA-antibody (Sigma #H6908) and Dynabeads Protein G (Life Technologies 10004D)[270]. The mRNA bound to the ribosome has been isolated using the RNeasy Plus Micro Kit purchased from Qiagen (#74034), following the manufacturer instructions. The non-precipitated fraction was used as "input" spinal cord control.

RNA was then checked for quantity and integrity (RIN $>$ 9) with the Bioanalyzer (Agilent RNA 6000 Nano). We then sequenced the motor neuron mRNA in pair-end using the Illumina HiSeq4000 Kit, at a depth of 40 million reads per sample. The raw sequencing data (fastq files) have been aligned to the mouse genome (mm9). The read counts were extracted with the htseq-count (option "intersectionStrict"). The low expressed RNAs (less

than 10 reads) have been excluded from the analysis. We used the DESeq2 software package[336] to analyse the differential gene expression. We performed a likelihood ratio test on the timeline analysis. Plots were created using ggplot2 and custom statistical software scripts in R.

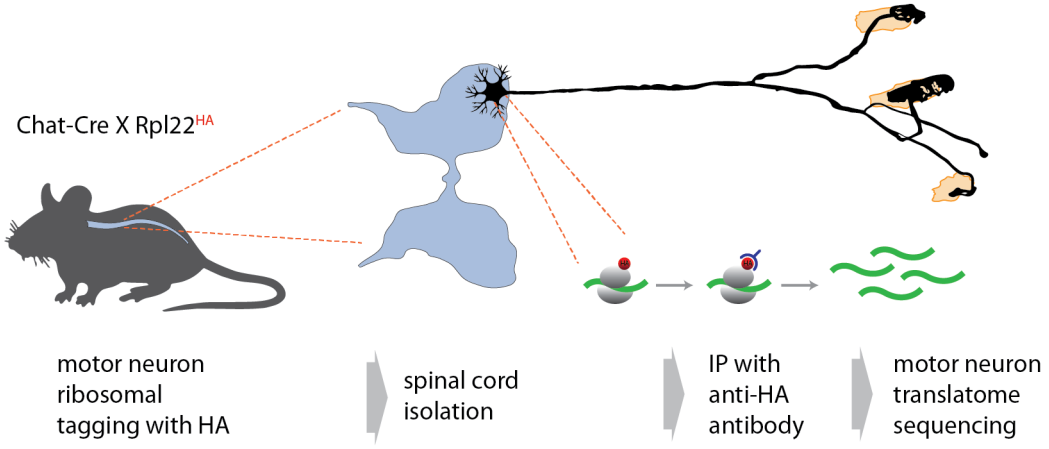

Figure 5.3: ***Ribotag protocol schematic.*** *To achieve precipitation of the motor neuron derived mRNA, the L22 ribosomal subunit encoded by Rpl22 gene, is tagged with hemagglutining (HA). Toward this, the Chat-Cre mouse line is crossed to $Rpl22^{fl/fl}$ mouse line, where the C-terminal exon of endogenous Rpl22 gene has the HA cassette flanked by two lox-P sites. Isolated spinal cord are subsequently immuno-precipiated with anti-HA antibody to obtain ribosome-bound mRNA from motor neurons. The purified mRNA is sequenced and analysed. Reconstruction of terminal motor axon branches is modified from Brill et al. (2016)*

5.8 Reverse Transcription (RT)-qPCR

The Reverse Transcription Polymerase Chain Reaction (RT-PCR) is an amplification technique to measure the amount of specific RNA molecules (in our case, gene expression). It consists in the reverse transcription of

RNA into complementary DNA (cDNA), followed by its amplification and quantification using the quantitative Polymerase Chain Reaction (qPCR) method. The RNA template is converted into its cDNA form by using the Reverse Transciptase (RT) enzyme, and then used as the template for the exponential amplification by qPCR.

In our case, the cDNA was obtained with the following protocol: 100 ng of ribotagged motor neurons mRNA, 100 µM of random hexamer primers (Roche, # 11034731001) 1 μl RNAsin Plus Inhibitor (Promega #N2615) have been filled up with water to a final volume of 14 µl. The mixture was incubated at 70 °C for 5 minutes, followed by a cooling step for 10 minutes on ice. We then added to the mixture 5 µl of M-MLV Reverse Transcriptase Buffer (Promega, #M531A), 10 mM of NTPs and 200 units of reverse transcriptase M-MLV (Promega, #M170A). The mix was then incubated for 1.5 hours at 37 °C. The cDNA was purified using QIAEX II Gel Extraction Kit (Qiagen, #20021). It was mixed with 2 µl of QiaEX-II suspension (Silica-Matrix) and 80 µl of QX-I buffer, incubated for 20 min at 25 °C in a shaker at 1000 rpm and then centrifuged at 13.000 x g for 2 minutes. The supernatant was discarded and the matrix has been washed two times with 90 µl of PE buffer. The column was then again centrifuged at 13000 g for 2 minutes. The supernatant was discarded and the pellet was left to dry shaking at 300 rpm at 25 °C for 10 minutes, with the lid open. The cDNA was then eluted with 20 µl of elution buffer (1 mM Tris, pH 8.5), incubated at 25 °C shaking at 1000 rpm to homogenize the pellet. Finally, the sample was centrifugated at 13000 g for 2 minutes and the supernatant containing the clear cDNA was collected. All steps have been conducted on ice in order to limit the degradation of the oligonucleotides.

The qPCR reactions have been performed in a LightCyler 1.3 Real-Time PCR system, (Roche, S/N: 140 6143). $MgCl_2$ concentration varied between 1-3 mM and the annealing temperature was dependent on the primer pair used, as optimized in a past study[178] and confirmed through primer efficiency curves. The primer sequences that we utilized were the following (5' to 3'):

For each reaction well, we mixed the cDNA template at a concentration of

Gene	Accession #	Primer sequence	Tm (°C)	Size (bp)	Efficiency (%)
Chat	NM_009891.2	TTCTAGCTGTGAGGAGGTGC (fw) CCCAAACCGCTTCACAATGG (rv)	64.6 65.2	145	93
Gfap	NM_001131020.1	TCGCACTCAATACGAGGCAG (fw) TTGGCGGCGATAGTCGTTAG (rv)	65.3 65.3	151	90
Myod1	NM_010866.2	TACAGTGGCGACTCAGATGC (fw) GTAGTAGGCGGTGTCGTAGC (rv)	65 64.8	117	90
Olig2	NM_016967.2	ATTACAGACCGAGCCAACACC (fw) GGGCGGGCAGAAAAAGATCA (rv)	65.5 66.4	202	92
Sqor	NM_021507.5	GTCCTTGTCAGTCCGTTCCA (fw) CAGCTGGATTCCAAGAGCGA (rv)	65 65.4	160	92
Syde1	NM_027875.1	AGAAGGCCCCAACATCCAAG (fw) GGCCTGTGCGAGTACTTCTT (rv)	65.4 65.3	155	100

Table 5.8: *The primers for qPCR.*

1 ng/µl, the forward and reverse primers to 0.5 µM, 2 µl of FastStart DNA Master SYBR Green I (Roche, #03 003 230 001), 1-3 mM $MgCl_2$ and water to a final volume of 20µl. Each sample was run in duplicate or triplicate. The controls with no cDNA and no RT were always included for each primer pair.

5.9 Microscopy

5.9.1 Live imaging of axonal transport or EB3 comet densities in nerve-muscle explants

The live imaging of EB3 comet and mitochondrial or mito-lysosome transport analyses have been performed on acute explants of the triangularis sterni muscle-nerve tissue, as previously indicated[11,337,338]. The thorax of euthanized mice has been obtained by removing the skin over the rib cage, severing the ribs close to the spinal column and removing the diaphragm to

release the explant. Oxygenated cold Ringer's solution (in mM: 125 NaCl, 2.5 KCl, 1.25 NaH_2PO_4, 26 $NaHCO_3$, 2 $CaCl_2$, 1 $MgCl_2$, and 20 glucose, oxygenated with 95% O_2 / 5% CO_2) has been used for the further dissections. In particular, we removed the remains of thymus, pleura, lung and pectoral muscles over the rib cage to avoid muscle contraction during imaging. The explant was then fixed with 0.25mm insect pins (purchased from Fine Science Tools) on Sylgard-coated 3.5 cm petri dish. The inside of the thorax faced up to expose the intercostal nerves and the terminal motor neuron branches, and synapses. During imaging, the sample was continuously and steadily perfused with oxygenated Ringer's solution at 33-36°C, maintained constant thanks to a heated stage connected to an automatic temperature controller (Warner Instruments; TC- 344C).

An Olympus BX51WI epifluorescence microscope has been used to perform live imaging, equipped with ×20/0.5 NA and ×100/1.0 NA water-immersion objectives, an automated filter wheel (Sutter Instruments; Lambda 10–3), a charge-coupled device camera (Visitron Systems; CoolSnap HQ2), and controlled by µManager version 1.4(Edelstein, Tsuchida et al. 2014).

For MT dynamics EB3 imaging studies, we usually acquired 200 frames per movie at 0.5 Hz and with an exposure time of 500 ms, with the YFP filter set (F36-528; AHF Analysentechnik). Total imaging time never exceeded 2 hours. For mito-lysosome tracking and mitochondria, the time lapses were acquired at a 0.9 Hz frame rate for 60 min with an exposure time of 300-400 ms, using the Keima filter set (AHF, #F76- 504).

5.9.2 Confocal microscopy

The confocal microscope is an optical microscope which makes use of a spatial pinhole to eliminate the interference of scattered light from the out-of-focus planes of the specimen, therefore increasing optical resolution and contrast. The image is detected by a point-by-point scanning, also allowing for a 3D reconstruction of the object. The confocal microscope that we have used is an Olympus FV1000 (or FV3000) equipped with x20/0.8 NA and

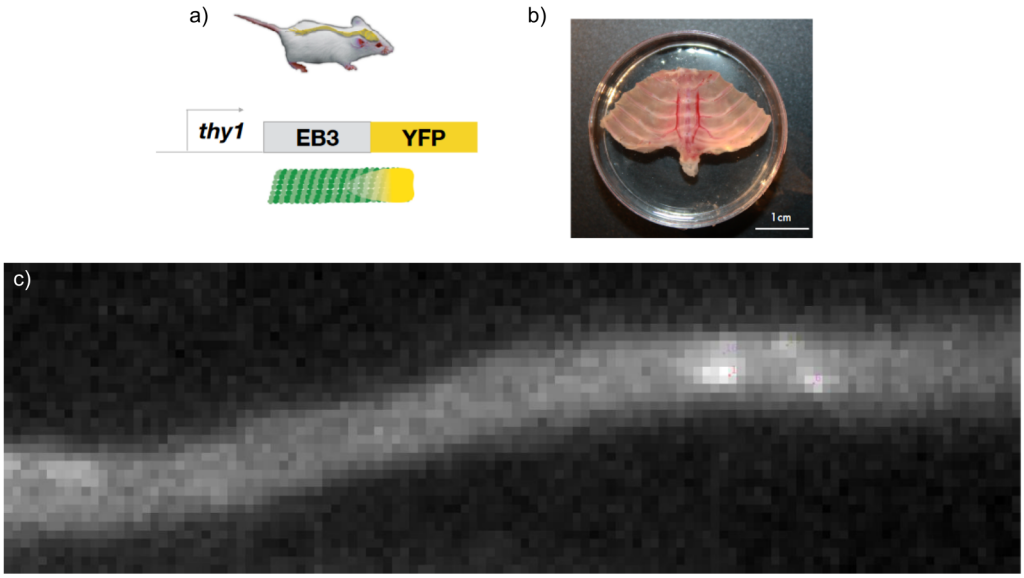

Figure 5.4: ***Dissection and live imaging of muscle-nerve explants.*** ***a)*** *MT dynamics are quantified from transgenic line where Thy1 promoter drives neuronal expression of a fused EB3-YFP cassette.* ***b)*** *Murine thorax is dissected and pinned to a Sylgard dish facing up to expose the most superficial nerves of M. triangularis sterni. The explant is submerged in 37°C Ringer's solution which is continuously perfused and oxigenated throughout the live imaging protocol. Image taken from Kerschensteiner et al. (2008).* ***c)*** *Example of EB3 comets (bright dots) on a terminal axon of Triangularis sterni muscle.*

x60/1.42 NA oil-immersion objectives. Tissue sections have been scanned either on an upright confocal microscope (Olympus equipped with 1x/0.28, 10x/0.4, 20xO/0.85, 40xO/1.35 and 60xO/1.42 objectives, or using an inverted confocal microscope (FV3000 from Olympus) equipped with 4x/0.16, 20x/0.75 and 40x/0.95 objectives.

5.9.3 Electron microscopy

P11 TTLL1$^{\text{mnKO}}$ and TTLL1$^{\text{mnWT}}$ mice have been perfused with 5 ml of HBSS and heparin (19.6 U/ml), and 30 ml of EM fixative. Triangularis sterni muscle was isolated and fixed with EM fixative for 8 hours at 4°C and subsequently moved to 2% OsO 4 and 1.5% ferrocyanide solution, and then dehydrated with ethanol/acetone and Epon embedded. The sections have been stained with 4% uranyl acetate for 30 minutes, and with lead citrate for 5 minutes. Images have then been taken with transmission electron microsopy at 20000x magnification.
Data have been analyzed in blind for genotype state. EM images have been analyzed with the software VaST[339] (Volume Annotation and Segmentation Tool). Total mitochondrial volume and total ER volume were quantified from 20 micrograph slices for each axon, and consisted of μm^3 area of organelle of interest, normalized on total axoplasmic area (either internodal or nodal area).

5.10 Data analysis

We have used the software ImageJ / FiJi to analyse the images. First of all, movies of EB3 comets have been filteret to remove the out-of-focus frames. Images were then aligned with the TurboReg plugin that corrects the shifts during the image acquisition with the following parameters: rigid-nody (to avoid image distortions); quality set on “Accurate”. The EB3

trajectories were analyzed manually with the MTrackJ plugin (from E. Meijering, Biomedical Imaging Group, Erasmus Medical Center, Rotterdam). We only considered the EB3 comets that appeared for at least 3 consecutive frames, otherwise discarded. To determine the "transport flux", namely the number of anterogradely and retrogradely transported mitochondria or mitolysosomes, we measured the number of fluorescent particles that per minute crossed a vertical line placed across the axon.

The tracking of the particles (mitochondria and mito-lysosomes) has been performed manually with the "Manual Tracking" plugin. We also determined several transport parameters using a custom made Python script: average speed (total distance travelled divided by total the observation time); average moving speed (average speed excluding the time spent pausing); run length (distance travelled between the stops). The stop was defined when a previously moving particle moved less than 0.091 µm/s.

5.11 Calculation of the mitofagy index

The mitofagy index[340,341] is a metric that describes the extent of mitochondria targeted for degradation through fusion with lysosomes. This quantification was obtained by injecting the mitoKeima reporter as described in section 5.6. The mitoKeima reporter[279] (Figure 5.5) allows concomitant examination of mitochondrial and lysosomal organelles *in vivo*. A drop in pH resulting from the fusion of mitochondria to acidic lysosomes when the latter are targeted for degradation, induces a measurable excitation shift. This allows to measure not only the extent of mitophagy that occurs in a cell, but also the intracellular location of these events.

In neutral environments, such as healthy mitochodria, Keima's excitation optimum is around 440 nm wavelengths (Keima-'green'). In an acidic environment, such as mitolysosomes, this excitation shifts to 586 nm wavelengths (Keima-'red'). Concomitant acquisition of both excitation wavelenghts allows for a ratiometric calculation.
To calculate the mitofagy index in NMJs, nerve-muscle explants were prepared as described in section 5.9.1. Live imaging acquisitions were conducted

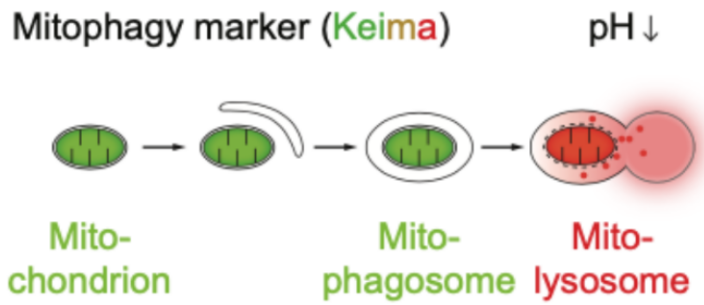

Figure 5.5: ***Schematic of mito-Keima reporter.*** *The fluorescence spectral shift from 440 nm (Keima-'green') to 586 nm (Keima-'red') induced by an increase in acidity, allows for a ratiometric quantification which is proportional to amount of mitophagy within a cell.*

as in 5.9.1 using a Keima filter cube (AHF, #F76-504) and with a 0.75 - 0.9 Hz frame rate. A z-stack was acquired during live imaging by sequential acquisition of the short (440nm) and long (586nm) wavelengths at each z-position. The z-stack was required to obtain a 3D image of the NMJ since its thickness is such that the entire synapse cannot be obtain from a single frame. This also implies that all z-positions are only partially in focus, and many parts remain blurry due to the limitations of widefield microscopy. Even though this could be overcome through optical sectioning of confocal microscopy, it was not possible with our fixation protocols to preserve fluorescence of the keima reporter.
It is therefore important to limit the analysis to only those regions which are in focus throughout the z-stack. This must be performed on each image of the stack. Prior to the analysis, every image was first cropped and background subtracted. Each image of the stack has been thresholded to create a "mask" (a binary image) that identifies the focused regions. I have used the following thresholding algorithms:

- **Niblack thresholding**[342].

$$t = m_{\mathrm{N}} + (k \times std_{\mathrm{N}})$$

The algorithm computes thresholds (t) for each pixels based on the sum of the mean (mN) and standard deviation (stdN) of the neighbouring pixels. The neighbouring pixels were set as the ones in a subregion of the image 10 times smaller than the original image. k was set to 0.2.

- **Background correction**[343]. The algorithm performs background correction to eliminate uneven illumination effects, and then performs thresholding by clustering using the Otsu's method[344].

The choice the algorithm was determined based on the context of each image and the amount of blurriness it contained. An example of the thresholding process is shown in Figure 5.6a-b.

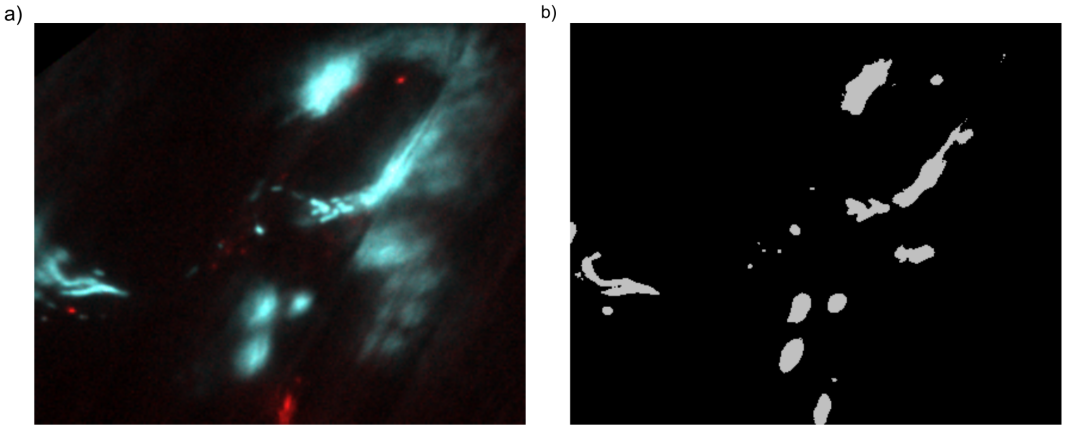

Figure 5.6: *Image thresholding image by Niblack algorithm. a) Single frame of 2-channel composite z-stack of NMJ from live imaging widefield acquisition (blue: 440 nm excitation keima; red: 586 nm excitation keima). Note that the picture is only partially in focus, with many parts being blurry. b) Binary image displaying the focused parts of the original image. This image will be used as mask to select the pixels in focus.*

The binary image (mask) is made of pixels which have a value of 0 (dark pixels) or 1 (bright pixels). By directly multiplying each image of the stack with its corresponding binary mask, all the out of focus parts of the stack

are removed.
In the next step, each thresholded 3D stack is transformed into a single image by maximum intensity projection[345,346](MIP). The result of MIP is an image, one per channel (blue and red), where each pixel represents the maximum value at that pixel position along the stack. The red and blue MIPs are shown in Figure 5.7a-b. The two MIPs are then divided (blue / red) to calculate the ratio between the blue and red pixel intensities. The values are then binned and displayed in a histogram (Figure5.7c). The discrete histogram is then fitted with a Gaussian function of the form:

$$a \times exp(-(x-\mu)^2/(2 \times \sigma^2)))$$

where a corresponds to the maximum height of the Gaussian, μ is the mean and σ is the standard deviation. The mitofagy index is defined as the fraction of the number of "red" pixels over the total number of pixels ("red" + "blue"). I defined "red" pixels as the ones whose value (blue / red ratio) is more than 4σ away from the Gaussian mean fitted on the histogram. The division of the pixels in the two categories is shown in Figure 5.7d. The mitofagy index, in this particular example, resulted 0.098.

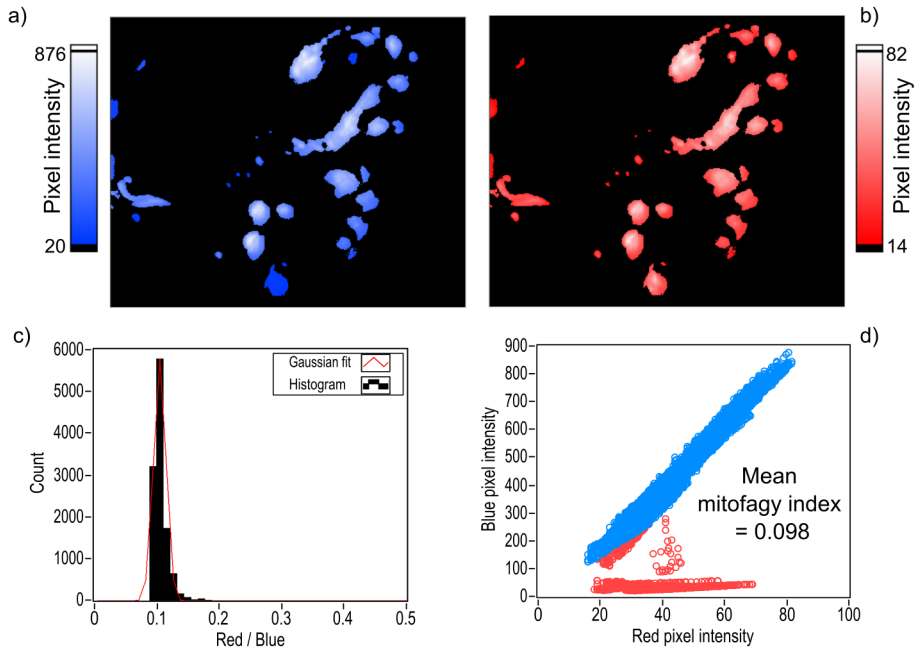

Figure 5.7: ***Calculation of the mitofagy index on NMJs.*** *Max intensity projection of the blue (a) and red (b) channels. c) Histogram of the ratio between red and blue pixels (black bars). The Gaussian fit is displayed as a red continuous line. d) Scatter plot of blue vs red pixels after the determination of the 4σ threshold.*

Figure 5.8 is an example of the resulting image processing where extent of mitophagy can be visually assessed. Yellow regions in the NMJ indicate areas of high mitophagy, whereas violet regions indicate a low red/blu ratio, i.e. low amount of mitophagy.

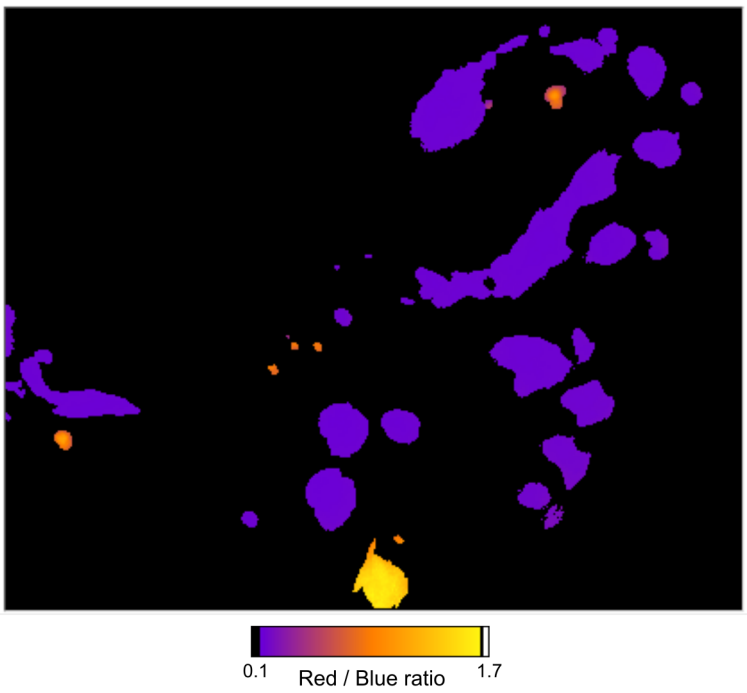

Figure 5.8: ***Extent of mitophagy at NMJ with ratiometric analysis.*** *Maximum intensity projection of the red/blue ratio of an NMJ. High levels of mitophagy result in yellow areas, while neglegible mitophagy results in violet areas.*

5.12 Image quantification and processing

The pruning speed was determined by analyzing the images with ImageJ[347], counting the number of innervating terminal branches at which end we could measure BTX-stained NMJ. We quantified the tubulin and PTM content by

averaging three background subtracted mean gray values per axon. The ROI was determined from the optical sections, as described in previous work[74]. The maximum intensity projections (MIP) have been generated from the image stacks (obtained by confocal microscopy) using ImageJ, and further processed in Adobe Photoshop for visual purposes only.
Importantly, all analyses have been performed in blind, with the experimenter blinded to the treatment and the genotypes, both during imaging and scoring.

5.13 Statistics and reproducibility

Data have been statistically analzsed using the softwares R and Graphprism. Every experiment included at least 3 biological replicates. Normality was assessed visually with QQ plot of residuals, and density plots, and with Shapiro-Wilk's test. We have used a two-tailed Students t-test for normally distributed data, otherwise the Mann-Whitney test was used for non-Parametric data. $P < 0.05$ was considered significant. Bar graphs show mean + SEM. Violin plots depict mean and IQR. Multiple comparisons were assessed statistically with One way ANOVA for parametric or Dunn's test for pairwise comparison for non parametric data, followed by Bonferroni post hoc test correction.

6 Abbreviations

AAV9	adeno-associated virus serotype 9
AChR	acetylcholine receptor
AF	alexa fluor
APLP	APP-like protein
APP	amyloid precursor protein
BDNF	brain-derived neurotrophic factor
BSA	bovine Serum albumine
BTX	bungarotoxin
CCP	cytochrome c peroxidase 1
cDNA	complementary DNA
ChaT	choline acetyl transferase
CNS	central nervous system
CRMP2	collapsin response mediator protein 2
DAG	diacylglycerol
DNA	deoxyribonucleic acid
Dock180	dedicator of cytokinesis 180kDa
DR6	death receptor 6
DTT	dithiothreitol
EB3	end-binding protein
EPPs	end plate potentials
FGFBP1	fibroblast growth factor binding protein 1
GAP	GTPase activating protein
GDNF	glial cell line-derived neurotrophic factor
GO	gene ontology
GT	glutamylated tubulin

IP3	inositol triphosphate
IPB	infra pyramidal bundle
KO	knock-out
mEPSCs	miniature excitatory postsynaptic currents
MHC1	major histocompatibility complex 1
MIP	maximum intensity projection
MT	microtubule
NA	numerical aperture
NCAM	neural cell adhesion molecule
NF-L	neurofilament light chain
NGF	nerve growth factor
NMDA	R
NMJ	neuromuscular junction
NT	neurotrophin-3
PAK	Serine/threonine-protein kinase
PB	phosphate buffer
PCA	principal component analysis
PDK1	phosphoinositide-dependent kinase 1
PK	protein kinase
proBDNF	precursor BDNF
PTM	post-translational modifications
RT-PCR	reverse transcription polymerase chain reaction
SNAP25	synaptosomal-associated protein 25 kDa
SNARE	SNAP receptor proteins
TNF	tumor necrosis factor
trkB	tropomyosin receptor kinase B
TTLL	tubulin tyrosine ligase like
WT	wild type
YFP	yellow fluorescent protein

Bibliography

[1] Azevedo, F. A, Carvalho, L. R, Grinberg, L. T, Farfel, J. M, Ferretti, R. E, Leite, R. E, Filho, W. J, Lent, R, & Herculano-Houzel, S. (2009) Equal numbers of neuronal and nonneuronal cells make the human brain an isometrically scaled-up primate brain. *The Journal of comparative neurology* **513**, 532–541.

[2] Cohen-Cory, S. (2002) The developing synapse: construction and modulation of synaptic structures and circuits. *Science* **298**, 770–776.

[3] Tapia, J. C, Wylie, J. D, Kasthuri, N, Hayworth, K. J, Schalek, R, Berger, D. R, Guatimosim, C, Seung, H. S, & Lichtman, J. W. (2012) Pervasive Synaptic Branch Removal in the Mammalian Neuromuscular System at Birth. *Neuron* **74**, 816–829.

[4] Lichtman, J. W & Colman, H. (2000) Synapse elimination and indelible memory. *Neuron* **25**, 269–278.

[5] Sengpiel, F & Kind, P. C. (2002) The role of activity in development of the visual system. *Current biology : CB* **12**.

[6] Penzes, P, Cahill, M. E, Jones, K. A, Vanleeuwen, J. E, & Woolfrey, K. M. (2011) Dendritic spine pathology in neuropsychiatric disorders. *Nature neuroscience* **14**, 285–293.

[7] Sellgren, C. M, Gracias, J, Watmuff, B, Biag, J. D, Thanos, J. M, Whittredge, P. B, Fu, T, Worringer, K, Brown, H. E, Wang, J, Kaykas, A, Karmacharya, R, Goold, C. P, Sheridan, S. D, & Perlis, R. H. (2019) Increased synapse elimination by microglia in schizophrenia patient-derived models of synaptic pruning. *Nature neuroscience* **22**, 374–385.

[8] Chen, C & Regehr, W. G. (2000) Developmental remodeling of the retinogeniculate synapse. *Neuron* **28**, 955–966.

[9] Lohof, A. M, Delhaye-Bouchaud, N, & Mariani, J. (1996) Synapse elimination in the central nervous system: functional significance and cellular mechanisms. *Reviews in the neurosciences* **7**, 85–101.

[10] Lichtman, J. W. (1977) The reorganization of synaptic connexions in the rat submandibular ganglion during post-natal development. *The Journal of physiology* **273**, 155–177.

[11] Kleele, T, Marinković, P, Williams, P. R, Stern, S, Weigand, E. E, Engerer, P, Naumann, R, Hartmann, J, Karl, R. M, Bradke, F, Bishop, D, Herms, J, Konnerth, A, Kerschensteiner, M, Godinho, L, & Misgeld, T. (2014) An assay to image neuronal microtubule dynamics in mice. *Nature Communications* **5**.

[12] Sanes, J. R & Lichtman, J. W. (1999) Development of the vertebrate neuromuscular junction. *Annual review of neuroscience* **22**, 389–442.

[13] Brown, M. C, Jansen, J. K, & Van Essen, D. (1976) Polyneuronal innervation of skeletal muscle in new-born rats and its elimination during maturation. *The Journal of Physiology* **261**, 387.

[14] Bagust, J, Lewis, D. M, & Westerman, R. A. (1974) The properties of motor units in a fast and a slow twitch muscle during post-natal development in the kitten. *The Journal of Physiology* **237**, 75.

[15] Buffelli, M, Burgess, R. W, Feng, G, Lobe, C. G, Lichtman, J. W, & Sanes, J. R. (2003) Genetic evidence that relative synaptic efficacy biases the outcome of synaptic competition. *Nature* **424**, 430–434.

[16] Buffelli, M, Busetto, G, Bidoia, C, Favero, M, & Cangiano, A. (2004) Activity-dependent synaptic competition at mammalian neuromuscular junctions. *Physiology (Bethesda)* **19**, 85–91.

[17] Balice-Gordon, R. J & Lichtman, J. W. (1990) In vivo visualization of the growth of pre- and postsynaptic elements of neuromuscular junctions in the mouse. *The Journal of neuroscience : the official journal of the Society for Neuroscience* **10**, 894–908.

[18] Personius, K. E & Balice-Gordon, R. J. (2002) Activity-dependent synaptic plasticity: insights from neuromuscular junctions. *The Neuroscientist : a review journal bringing neurobiology, neurology and psychiatry* **8**, 414–422.

[19] Balice-Gordon, R. J & Lichtman, J. W. (1994) Long-term synapse loss induced by focal blockade of postsynaptic receptors. *Nature* **372**, 519–524.

[20] Keller-Peck, C. R, Walsh, M. K, Gan, W. B, Feng, G, Sanes, J. R, & Lichtman, J. W. (2001) Asynchronous synapse elimination in neonatal motor units: studies using GFP transgenic mice. *Neuron* **31**, 381–394.

[21] Bishop, D. L, Misgeld, T, Walsh, M. K, Gan, W. B, & Lichtman, J. W. (2004) Axon branch removal at developing synapses by axosome shedding. *Neuron* **44**, 651–661.

[22] Balice-Gordon, R. J & Lichtman, J. W. (1993) In vivo observations of pre- and postsynaptic changes during the transition from multiple to single innervation at developing neuromuscular junctions. *Journal of Neuroscience* **13**, 834–855.

[23] Walsh, M. K & Lichtman, J. W. (2003) In vivo time-lapse imaging of synaptic takeover associated with naturally occurring synapse elimination. *Neuron* **37**, 67–73.

[24] Wyatt, R. M & Balice-Gordon, R. J. (2003) Activity-dependent elimination of neuromuscular synapses. *Journal of neurocytology* **32**, 777–794.

[25] Misgeld, T, Burgess, R. W, Lewis, R. M, Cunningham, J. M, Lichtman, J. W, & Sanes, J. R. (2002) Roles of Neurotransmitter in Synapse Formation. *Neuron* **36**, 635–648.

[26] Favero, M, Busetto, G, & Cangiano, A. (2012) Spike timing plays a key role in synapse elimination at the neuromuscular junction. *Proceedings of the National Academy of Sciences of the United States of America*.

[27] Chang, Q, Gonzalez, M, Pinter, M. J, & Balice-Gordon, R. J. (1999) Gap Junctional Coupling and Patterns of Connexin Expression among Neonatal Rat Lumbar Spinal Motor Neurons. *The Journal of Neuroscience* **19**, 10813.

[28] Personius, K. E, Chang, Q, Mentis, G. Z, O'Donovan, M. J, & Balice-Gordon, R. J. (2007) Reduced gap junctional coupling leads to uncorrelated motor neuron firing and precocious neuromuscular synapse elimination. *Proceedings of the National Academy of Sciences of the United States of America* **104**, 11808–11813.

[29] Sperry, R. W. (1963) Chemoaffinity in the orderly growth of nerve fiber patterns and connections . *Proceedings of the National Academy of Sciences of the United States of America* **50**, 703.

[30] Riccomagno, M. M, Hurtado, A, Wang, H, MacOpson, J. G, Griner, E. M, Betz, A, Brose, N, Kazanietz, M. G, & Kolodkin, A. L. (2012) The RacGAP β2-Chimaerin selectively mediates axonal pruning in the hippocampus. *Cell* **149**, 1594–1606.

[31] Ziak, J, Weissova, R, Jeřábková, K, Janikova, M, Maimon, R, Petrasek, T, Pukajova, B, Kleisnerova, M, Wang, M, Brill, M. S, Kasparek, P, Zhou, X, Alvarez-Bolado, G, Sedlacek, R, Misgeld, T, Stuchlik, A, Perlson, E, & Balastik, M. (2020) CRMP 2 mediates Sema3F-dependent axon pruning and dendritic spine remodeling. *EMBO Rep.* **21**.

[32] Venkova, K, Christov, A, Kamaluddin, Z, Kobalka, P, Siddiqui, S, & Hensley, K. (2014) Semaphorin 3A signaling through neuropilin-1 is an early trigger for distal axonopathy in the SOD1G93A mouse model of amyotrophic lateral sclerosis. *Journal of neuropathology and experimental neurology* **73**, 702–713.

[33] Winter, F. D, Vo, T, Stam, F. J, Wisman, L. A, Bär, P. R, Niclou, S. P, van Muiswinkel, F. L, & Verhaagen, J. (2006) The expression of the chemorepellent Semaphorin 3A is selectively induced in terminal Schwann cells of a subset of neuromuscular synapses that display limited anatomical plasticity and enhanced vulnerability in motor neuron disease. *Molecular and Cellular Neuroscience* **32**, 102–117.

[34] Xu, N.-J & Henkemeyer, M. (2009) Ephrin-B3 reverse signaling through grb4 and cytoskeletal regulators mediates axon pruning. *Nat. Neurosci.* **12**, 268–276.

[35] Burke, R. E. (1999) Chapter 15 Revisiting the Notion of 'motor unit types'. *Progress in Brain Research* **123**, 167–175.

[36] Stark, E, Roux, L, Eichler, R, & Buzsáki, G. (2015) Local generation of multineuronal spike sequences in the hippocampal CA1 region. *Proceedings of the National Academy of Sciences of the United States of America* **112**, 10521–10526.

[37] McCann, C. M, Nguyen, Q. T, Neto, H. S, & Lichtman, J. W. (2007) Rapid synapse elimination after postsynaptic protein synthesis inhibition in vivo. *The*

Journal of neuroscience : the official journal of the Society for Neuroscience **27**, 6064–6067.

[38] Purves, D & Lichtman, J. W. (1985) Principles of neural development. p. 433.

[39] Oppenheim, R. W. (1991) Cell death during development of the nervous system. *Annual review of neuroscience* **14**, 453–501.

[40] Barde, Y. A. (1989) Trophic factors and neuronal survival. *Neuron* **2**, 1525–1534.

[41] Lu, B. (2003) BDNF and activity-dependent synaptic modulation. *Learning and memory (Cold Spring Harbor, N.Y.)* **10**, 86–98.

[42] Gall, C. M & Isackson, P. J. (1989) Limbic Seizures Increase Neuronal Production of Messenger RNA for Nerve Growth Factor. *Science* **245**, 758–761.

[43] Zafra, F, Lindholm, D, Castren, E, Hartikka, J, & Thoenen, H. (1992) Regulation of brain-derived neurotrophic factor and nerve growth factor mRNA in primary cultures of hippocampal neurons and astrocytes. *The Journal of neuroscience : the official journal of the Society for Neuroscience* **12**, 4793–4799.

[44] Hurtado, E, Cilleros, V, Nadal, L, Simó, A, Obis, T, Garcia, N, Santafé, M. M, Tomàs, M, Halievski, K, Jordan, C. L, Lanuza, M. A, & Tomàs, J. (2017) Muscle contraction regulates bdnf/trkb signaling to modulate synaptic function through presynaptic cPKCα and cPKCβi. *Frontiers in Molecular Neuroscience* **10**, 147.

[45] Je, H. S, Yang, F, Ji, Y, Potluri, S, Fu, X.-Q, Luo, Z.-G, Nagappan, G, Chan, J. P, Hempstead, B, Son, Y.-J, & Lu, B. (2013) ProBDNF and Mature BDNF as Punishment and Reward Signals for Synapse Elimination at Mouse Neuromuscular Junctions. *Journal of Neuroscience*.

[46] Blöchl, A & Thoenen, H. (1996) Localization of cellular storage compartments and sites of constitutive and activity-dependent release of nerve growth factor (NGF) in primary cultures of hippocampal neurons. *Molecular and cellular neurosciences* **7**, 173–190.

[47] Goodman, C. S. (2003) Mechanisms and Molecules that Control Growth Cone Guidance. *Annual Review of Neuroscience* **19**, 341–377.

[48] Wang, X. H & Poo, M. M. (1997) Potentiation of developing synapses by postsynaptic release of neurotrophin-4. *Neuron* **19**, 825–835.

[49] Lohof, A. M, Ip, N. Y, & Poo, M. M. (1993) Potentiation of developing neuromuscular synapses by the neurotrophins NT-3 and BDNF. *Nature* **363**, 350–353.

[50] Favero, M, Buffelli, M, Cangiano, A, & Busetto, G. (2010) The timing of impulse activity shapes the process of synaptic competition at the neuromuscular junction. *Neuroscience* **167**, 343–353.

[51] Garcia, N, Santafe, M. M, Tomàs, M, Lanuza, M. A, Besalduch, N, & Tomàs, J. (2010) Involvement of brain-derived neurotrophic factor (BDNF) in the functional elimination of synaptic contacts at polyinnervated neuromuscular synapses during development. *Journal of neuroscience research* **88**, 1406–1419.

[52] Stoop, R & Poo, M. M. (1996) Synaptic modulation by neurotrophic factors: differential and synergistic effects of brain-derived neurotrophic factor and ciliary neurotrophic factor. *The Journal of neuroscience : the official journal of the Society for Neuroscience* **16**, 3256–3264.

[53] Garcia, N, Tomàs, M, Santafe, M. M, Lanuza, M. A, Besalduch, N, & Tomàs, J. (2011) Blocking p75NTR receptors alters polyinnervationz of neuromuscular synapses during development. *Journal of Neuroscience Research* **89**, 1331–1341.

[54] Wang, X. H, Berninger, B, & Poo, M. M. (1998) Localized synaptic actions of neurotrophin-4. *The Journal of neuroscience : the official journal of the Society for Neuroscience* **18**, 4985–4992.

[55] Nykjaer, A, Lee, R, Teng, K. K, Jansen, P, Madsen, P, Nielsen, M. S, Jacobsen, C, Kliemannel, M, Schwarz, E, Willnow, T. E, Hempstead, B. L, & Petersen, C. M. (2004) Sortilin is essential for proNGF-induced neuronal cell death. *Nature* **427**, 843–848.

[56] Teng, H. K, Teng, K. K, Lee, R, Wright, S, Tevar, S, Almeida, R. D, Kermani, P, Torkin, R, Chen, Z. Y, Lee, F. S, Kraemer, R. T, Nykjaer, A, & Hempstead, B. L. (2005) ProBDNF induces neuronal apoptosis via activation of a receptor complex of p75NTR and sortilin. *The Journal of neuroscience : the official journal of the Society for Neuroscience* **25**, 5455–5463.

[57] Jansen, P, Giehl, K, Nyengaard, J. R, Teng, K, Lioubinski, O, Sjoegaard, S. S, Breiderhoff, T, Gotthardt, M, Lin, F, Eilers, A, Petersen, C. M, Lewin, G. R,

Hempstead, B. L, Willnow, T. E, & Nykjaer, A. (2007) Roles for the proneurotrophin receptor sortilin in neuronal development, aging and brain injury. *Nature neuroscience* **10**, 1449–1457.

[58] Pérez, V, Bermedo-Garcia, F, Zelada, D, Court, F. A, Pérez, M. Á, Fuenzalida, M, Ábrigo, J, Cabello-Verrugio, C, Moya-Alvarado, G, Tapia, J. C, Valenzuela, V, Hetz, C, Bronfman, F. C, & Henríquez, J. P. (2019) The p75NTR neurotrophin receptor is required to organize the mature neuromuscular synapse by regulating synaptic vesicle availability. *Acta Neuropathologica Communications* **7**, 1–18.

[59] Pousinha, P. A, José Diogenes, M, Alexandre Ribeiro, J, & Sebastião, A. M. (2006) Triggering of BDNF facilitatory action on neuromuscular transmission by adenosine A2A receptors. *Neuroscience letters* **404**, 143–147.

[60] Simó, A, Cilleros-Mañé, V, Just-Borràs, L, Hurtado, E, Nadal, L, Tomàs, M, Garcia, N, Lanuza, M. A, & Tomàs, J. (2019) nPKCϵ Mediates SNAP-25 Phosphorylation of Ser-187 in Basal Conditions and After Synaptic Activity at the Neuromuscular Junction. *Molecular neurobiology* **56**, 5346–5364.

[61] Li, Y, Soos, T. J, Li, X, Wu, J, DeGennaro, M, Sun, X, Littman, D. R, Birnbaum, M. J, & Polakiewicz, R. D. (2004) Protein kinase C Theta inhibits insulin signaling by phosphorylating IRS1 at Ser(1101). *The Journal of biological chemistry* **279**, 45304–45307.

[62] Taetzsch, T, Tenga, M. J, & Valdez, G. (2017) Muscle Fibers Secrete FGFBP1 to Slow Degeneration of Neuromuscular Synapses during Aging and Progression of ALS. *The Journal of neuroscience : the official journal of the Society for Neuroscience* **37**, 70–82.

[63] Nguyen, Q. T, Parsadanian, A. S, Snider, W. D, & Lichtman, J. W. (1998) Hyperinnervation of neuromuscular junctions caused by GDNF overexpression in muscle. *Science* **279**, 1725–1729.

[64] Fu, X.-Q, Peng, J, Wang, A.-H, & Luo, Z.-G. (2020) Tumor necrosis factor alpha mediates neuromuscular synapse elimination. *Cell Discov.* **6**, 9.

[65] Covault, J & Sanes, J. R. (1985) Neural cell adhesion molecule (N-CAM) accumulates in denervated and paralyzed skeletal muscles. *Proceedings of the National Academy of Sciences of the United States of America* **82**, 4544–4548.

[66] Moscoso, L. M, Cremer, H, & Sanes, J. R. (1998) Organization and Reorganization of Neuromuscular Junctions in Mice Lacking Neural Cell Adhesion Molecule, Tenascin-C, or Fibroblast Growth Factor-5. *Journal of Neuroscience* **18**, 1465–1477.

[67] Rafuse, V. F, Polo-Parada, L, & Landmesser, L. T. (2000) Structural and functional alterations of neuromuscular junctions in NCAM-deficient mice. *The Journal of neuroscience : the official journal of the Society for Neuroscience* **20**, 6529–6539.

[68] Tetruashvily, M. M, Melson, J. W, Park, J. J, Peng, X, & Boulanger, L. M. (2016) Expression and alternative splicing of classical and nonclassical MHCI genes in the hippocampus and neuromuscular junction. *Molecular and cellular neurosciences* **72**, 34–45.

[69] Tetruashvily, M. M, McDonald, M. A, Frietze, K. K, & Boulanger, L. M. (2016) MHCI promotes developmental synapse elimination and aging-related synapse loss at the vertebrate neuromuscular junction. *Brain, behavior, and immunity* **56**, 197–208.

[70] Roche, S. L, Sherman, D. L, Dissanayake, K, Soucy, G, Desmazieres, A, Lamont, D. J, Peles, E, Julien, J. P, Wishart, T. M, Ribchester, R. R, Brophy, P. J, & Gillingwater, T. H. (2014) Loss of Glial Neurofascin155 Delays Developmental Synapse Elimination at the Neuromuscular Junction. *The Journal of Neuroscience* **34**, 12904.

[71] Watts, R. J, Hoopfer, E. D, & Luo, L. (2003) Axon pruning during drosophila metamorphosis. *Neuron* **38**, 871–885.

[72] Zhai, Q, Wang, J, Kim, A, Liu, Q, Watts, R, Hoopfer, E, Mitchison, T, Luo, L, & He, Z. (2003) Involvement of the ubiquitin-proteasome system in the early stages of wallerian degeneration. *Neuron* **39**, 217–225.

[73] Williams, D. W & Truman, J. W. (2005) Cellular mechanisms of dendrite pruning in drosophila: insights from in vivo time-lapse of remodeling dendritic arborizing sensory neurons. *Development* **132**, 3631–3642.

[74] Brill, M. S, Kleele, T, Ruschkies, L, Wang, M, Marahori, N. A, Reuter, M. S, Hausrat, T. J, Weigand, E, Fisher, M, Ahles, A, Engelhardt, S, Bishop, D. L, Kneussel, M, & Misgeld, T. (2016) Branch-Specific Microtubule Destabilization

Mediates Axon Branch Loss during Neuromuscular Synapse Elimination. *Neuron* **92**, 845–856.

[75] Maor-Nof, M, Homma, N, Raanan, C, Nof, A, Hirokawa, N, & Yaron, A. (2013) Axonal pruning is actively regulated by the microtubule-destabilizing protein kinesin superfamily protein 2a. *Cell Reports* **3**, 971–977.

[76] Lee, H.-h, Jan, L. Y, & Jan, Y.-n. (2009) P60-Like 1 Regulate Dendrite Pruning of Sensory Neuron During Metamorphosis. *Pnas* **106**, 6536–6368.

[77] Kreutzberg, G. W. (1969) Neuronal dynamics and axonal flow. IV. Blockage of intra-axonal enzyme transport by colchicine. *Proceedings of the National Academy of Sciences of the United States of America* **62**, 722–728.

[78] Akhmanova, A & Hoogenraad, C. C. (2015) Microtubule minus-end-targeting proteins. *Current Biology*.

[79] Kapitein, L. C & Hoogenraad, C. C. (2015) Building the Neuronal Microtubule Cytoskeleton. *Neuron* **87**, 492–506.

[80] Dent, E. W. (2020) Dynamic microtubules at the synapse. *Current Opinion in Neurobiology* **63**, 9–14.

[81] Park, J. H & Roll-Mecak, A. (2018) The tubulin code in neuronal polarity. *Current Opinion in Neurobiology* **51**, 95–102.

[82] Meiring, J. C, Shneyer, B. I, & Akhmanova, A. (2020) Generation and regulation of microtubule network asymmetry to drive cell polarity. *Current Opinion in Cell Biology* **62**, 86–95.

[83] Jaworski, J, Kapitein, L. C, Gouveia, S. M, Dortland, B. R, Wulf, P. S, Grigoriev, I, Camera, P, Spangler, S. A, Di Stefano, P, Demmers, J, Krugers, H, Defilippi, P, Akhmanova, A, & Hoogenraad, C. C. (2009) Dynamic Microtubules Regulate Dendritic Spine Morphology and Synaptic Plasticity. *Neuron* **61**, 85–100.

[84] Burton, P. R & Paige, J. L. (1981) Polarity of axoplasmic microtubules in the olfactory nerve of the frog. *Neurobiology* **78**, 3269–3273.

[85] Stepanova, T, Slemmer, J, Hoogenraad, C. C, Lansbergen, G, Dortland, B, Zeeuw, C. I. D, Grosveld, F, Cappellen, G. V, Akhmanova, A, Galjart, N, De Zeeuw, C. I, & van Cappellen, G. (2003) Visualization of microtubule growth

in cultured neurons via the use of EB3-GFP (end-binding protein 3-green fluorescent protein). *J. Neurosci.* **23**, 2655–2664.

[86] Caplow, M & Shanks, J. (2000) Single Monolayer. *Molecular Biology of the Cell* **7**, 663–675.

[87] Mitchison, T & Kirschner, M. (1984) Dynamic instability of microtubule growth. *Nature 1984 312:5991* **312**, 237–242.

[88] Akhmanova, A & Steinmetz, M. O. (2019) Microtubule minus-end regulation at a glance. *Journal of cell science* **132**.

[89] Desai, A & Mitchison, T. J. (1997) Microtubule polymerization dynamics. *Annual review of cell and developmental biology* **13**, 83–117.

[90] Baas, P. W, Rao, A. N, Matamoros, A. J, & Leo, L. (2016) Stability properties of neuronal microtubules. *Cytoskeleton* **73**, 442–460.

[91] Akhmanova, A & Hoogenraad, C. C. (2005) Microtubule plus-end-tracking proteins: Mechanisms and functions. *Current Opinion in Cell Biology* **17**, 47–54.

[92] Akhmanova, A & Steinmetz, M. O. (2008) Tracking the ends: A dynamic protein network controls the fate of microtubule tips. *Nature Reviews Molecular Cell Biology* **9**, 309–322.

[93] Conde, C & Cáceres, A. (2009) Microtubule assembly, organization and dynamics in axons and dendrites. *Nature Reviews Neuroscience* **10**, 319–332.

[94] Dent, E. W. (2017) Of microtubules and memory: implications for microtubule dynamics in dendrites and spines. *Molecular biology of the cell* **28**, 1–8.

[95] Pacheco, A & Gallo, G. (2016) Actin filament-microtubule interactions in axon initiation and branching. *Brain research bulletin* **126**, 300–310.

[96] Baas, P. W, Nadar, C. V, & Myers, K. A. (2006) Axonal Transport of Microtubules: the Long and Short of It. *Traffic* **7**, 490–498.

[97] Conde, C & Cáceres, A. (2009) Microtubule assembly, organization and dynamics in axons and dendrites. *Nature Reviews Neuroscience* **10**, 319–332.

[98] Stiess, M, Maghelli, N, Kapitein, L. C, Gomis-Rüth, S, Wilsch-Bräuninger, M, Hoogenraad, C. C, Tolić-Nørrelykke, I. M, & Bradke, F. (2010) Axon extension

occurs independently of centrosomal microtubule nucleation. *Science* **327**, 704–707.

[99] Sulimenko, V, Hájková, Z, Klebanovych, A, & Dráber, P. (2017) Regulation of microtubule nucleation mediated by γ-tubulin complexes. *Protoplasma* **254**, 1187–1199.

[100] Yau, K. W, VanBeuningen, S. F, Cunha-Ferreira, I, Cloin, B. M, VanBattum, E. Y, Will, L, Schätzle, P, Tas, R. P, VanKrugten, J, Katrukha, E. A, Jiang, K, Wulf, P. S, Mikhaylova, M, Harterink, M, Pasterkamp, R. J, Akhmanova, A, Kapitein, L. C, & Hoogenraad, C. C. (2014) Microtubule minus-end binding protein CAMSAP2 controls axon specification and dendrite development. *Neuron* **82**, 1058–1073.

[101] Feng, C, Thyagarajan, P, Shorey, M, Seebold, D. Y, Weiner, A. T, Albertson, R. M, Rao, K. S, Sagasti, A, Goetschius, D. J, & Rolls, M. M. (2019) Patronin-mediated minus end growth is required for dendritic microtubule polarity. *The Journal of Cell Biology* **218**, 2309.

[102] Wang, Y, Rui, M, Tang, Q, Bu, S, & Yu, F. (2019) Patronin governs minus-end-out orientation of dendritic microtubules to promote dendrite pruning in Drosophila. *eLife*.

[103] Yalgin, C, Ebrahimi, S, Delandre, C, Yoong, L. F, Akimoto, S, Tran, H, Amikura, R, Spokony, R, Torben-Nielsen, B, White, K. P, & Moore, A. W. (2015) Centrosomin represses dendrite branching by orienting microtubule nucleation. *Nature neuroscience* **18**, 1437–1445.

[104] Sánchez-Huertas, C, Freixo, F, Viais, R, Lacasa, C, Soriano, E, & Lüders, J. (2016) Non-centrosomal nucleation mediated by augmin organizes microtubules in post-mitotic neurons and controls axonal microtubule polarity. *Nature communications* **7**.

[105] Cunha-Ferreira, I, Chazeau, A, Buijs, R. R, Stucchi, R, Will, L, Pan, X, Adolfs, Y, van der Meer, C, Wolthuis, J. C, Kahn, O. I, Schätzle, P, Altelaar, M, Pasterkamp, R. J, Kapitein, L. C, & Hoogenraad, C. C. (2018) The HAUS Complex Is a Key Regulator of Non-centrosomal Microtubule Organization during Neuronal Development. *Cell reports* **24**, 791–800.

[106] Chalfie, M & Thomson, J. N. (1979) Organization of neuronal microtubules in the nematode Caenorhabditis elegans. *The Journal of cell biology* **82**, 278–289.

[107] Yogev, S, Cooper, R, Fetter, R, Horowitz, M, & Shen, K. (2016) Microtubule Organization Determines Axonal Transport Dynamics. *Neuron* **92**, 449–460.

[108] Wortman, J. C, Shrestha, U. M, Barry, D. M, Garcia, M. L, Gross, S. P, & Yu, C. C. (2014) Axonal transport: How high microtubule density can compensate for boundary effects in small-caliber axons. *Biophysical Journal* **106**, 813–823.

[109] Bálint, Š, Vilanova, I. V, Álvarez, Á. S, & Lakadamyali, M. (2013) Correlative live-cell and superresolution microscopy reveals cargo transport dynamics at microtubule intersections. *Proceedings of the National Academy of Sciences of the United States of America* **110**, 3375–3380.

[110] Zajac, A. L, Goldman, Y. E, Holzbaur, E. L, & Ostap, E. M. (2013) Local Cytoskeletal and Organelle Interactions Impact Molecular-Motor-Driven Early Endosomal Trafficking. *Current Biology* **23**, 1173–1180.

[111] Lüders, J. (2021) Nucleating microtubules in neurons: Challenges and solutions. *Developmental Neurobiology* **81**, 273–283.

[112] Hirokawa, N, Niwa, S, & Tanaka, Y. (2010) Molecular motors in neurons: Transport mechanisms and roles in brain function, development, and disease. *Neuron* **68**, 610–638.

[113] Janke, C & Magiera, M. M. (2020) The tubulin code and its role in controlling microtubule properties and functions. *Nature reviews. Molecular cell biology* **21**, 307–326.

[114] Roll-Mecak, A. (2020) The Tubulin Code in Microtubule Dynamics and Information Encoding. *Developmental cell* **54**, 7–20.

[115] Maliekal, T. T, Dharmapal, D, & Sengupta, S. (2022) Tubulin Isotypes: Emerging Roles in Defining Cancer Stem Cell Niche. *Frontiers in Immunology* **13**, 2648.

[116] Akhmanova, A & Steinmetz, M. O. (2015) Control of microtubule organization and dynamics: Two ends in the limelight. *Nature Reviews Molecular Cell Biology* **16**, 711–726.

[117] Hausrat, T. J, Radwitz, J, Lombino, F. L, Breiden, P, & Kneussel, M. (2021) Alpha- and beta-tubulin isotypes are differentially expressed during brain development. *Developmental neurobiology* **81**, 333–350.

[118] Vemu, A, Atherton, J, Spector, J. O, Moores, C. A, & Roll-Mecak, A. (2017) Tubulin isoform composition tunes microtubule dynamics. *Molecular Biology of the Cell* **28**, 3564–3572.

[119] Nogales, E. (2001) Structural insight into microtubule function. *Annual review of biophysics and biomolecular structure* **30**, 397–420.

[120] Sirajuddin, M, Rice, L. M, & Vale, R. D. (2014) Regulation of microtubule motors by tubulin isotypes and post-translational modifications. *Nature Cell Biology* **16**, 335–344.

[121] Magiera, M. M & Janke, C. (2014) Post-translational modifications of tubulin. *Current biology : CB* **24**.

[122] Lewis, S. A, Gu, W, & Cowan, N. J. (1987) Free intermingling of mammalian beta-tubulin isotypes among functionally distinct microtubules. *Cell* **49**, 539–548.

[123] Kunishima, S, Kobayashi, R, Itoh, T. J, Hamaguchi, M, & Saito, H. (2009) Mutation of the beta1-tubulin gene associated with congenital macrothrombocytopenia affecting microtubule assembly. *Blood* **113**, 458–461.

[124] Cuenca-Zamora, E. J, Ferrer-Marín, F, Rivera, J, & Teruel-Montoya, R. (2020) Correction: Cuenca-Zamora, Ernesto José., et al. Tubulin in Platelets: When the Shape Matter. Int. J. Mol. Sci. 2019, 20, 3484. *International Journal of Molecular Sciences 2020, Vol. 21, Page 3577* **21**, 3577.

[125] Saillour, Y, Broix, L, Bruel-Jungerman, E, Lebrun, N, Muraca, G, Rucci, J, Poirier, K, Belvindrah, R, Francis, F, & Chelly, J. (2014) Beta tubulin isoforms are not interchangeable for rescuing impaired radial migration due to Tubb3 knockdown. *Human molecular genetics* **23**, 1516–1526.

[126] Katrukha, E. A, Jurriens, D, Pastene, D. S, & Kapitein, L. C. (2021) Quantitative mapping of dense microtubule arrays in mammalian neurons. *eLife* **10**.

[127] Cappelletti, G, Calogero, A. M, & Rolando, C. (2021) Microtubule acetylation: A reading key to neural physiology and degeneration. *Neuroscience Letters* **755**, 135900.

[128] Shida, T, Cueva, J. G, Xu, Z, Goodman, M. B, & Nachury, M. V. (2010) The major α-tubulin K40 acetyltransferase αTAT1 promotes rapid ciliogenesis and efficient mechanosensation. *Proceedings of the National Academy of Sciences of the United States of America* **107**, 21517–21522.

[129] Hubbert, C, Guardiola, A, Shao, R, Kawaguchi, Y, Ito, A, Nixon, A, Yoshida, M, Wang, X. F, & Yao, T. P. (2002) HDAC6 is a microtubule-associated deacetylase. *Nature* **417**, 455–458.

[130] North, B. J, Marshall, B. L, Borra, M. T, Denu, J. M, & Verdin, E. (2003) The human Sir2 ortholog, SIRT2, is an NAD+-dependent tubulin deacetylase. *Molecular cell* **11**, 437–444.

[131] Neumann, B & Hilliard, M. (2014) Loss of MEC-17 leads to microtubule instability and axonal degeneration. *Cell Reports*.

[132] Xu, Z, Schaedel, L, Portran, D, Aguilar, A, Gaillard, J, Peter Marinkovich, M, Théry, M, & Nachury, M. V. (2017) Microtubules acquire resistance from mechanical breakage through intralumenal acetylation. *Science* **356**, 328–332.

[133] Portran, D, Schaedel, L, Xu, Z, Théry, M, & Nachury, M. V. (2017) Tubulin acetylation protects long-lived microtubules against mechanical ageing. *Nature cell biology* **19**, 391–398.

[134] Kreis, T. E. (1987) Microtubules containing detyrosinated tubulin are less dynamic. *The EMBO journal* **6**, 2597–2606.

[135] Ersfeld, K, Wehland, J, Plessmann, U, Dodemont, H, Gerke, V, & Weber, K. (1993) Characterization of the tubulin-tyrosine ligase. *The Journal of cell biology* **120**, 725–732.

[136] Hallak, M. E, Rodriguez, J. A, Barra, H. S, & Caputto, R. (1977) Release of tyrosine from tyrosinated tubulin. Some common factors that affect this process and the assembly of tubulin. *FEBS letters* **73**, 147–150.

[137] Aillaud, C, Bosc, C, Peris, L, Bosson, A, Heemeryck, P, Van Dijk, J, Le Friec, J, Boulan, B, Vossier, F, Sanman, L. E, Syed, S, Amara, N, Couté, Y, Lafanechère,

L, Denarier, E, Delphin, C, Pelletier, L, Humbert, S, Bogyo, M, Andrieux, A, Rogowski, K, & Moutin, M. J. (2017) Vasohibins/SVBP are tubulin carboxypeptidases (TCPs) that regulate neuron differentiation. *Science* **358**, 1448–1453.

[138] Nieuwenhuis, J, Adamopoulos, A, Bleijerveld, O. B, Mazouzi, A, Stickel, E, Celie, P, Altelaar, M, Knipscheer, P, Perrakis, A, Blomen, V. A, & Brummelkamp, T. R. (2017) Vasohibins encode tubulin detyrosinating activity. *Science* **358**, 1453–1456.

[139] Landskron, L, Bak, J, Adamopoulos, A, Kaplani, K, Moraiti, M, van den Hengel, L. G, Song, J.-Y, Bleijerveld, O. B, Nieuwenhuis, J, Heidebrecht, T, Henneman, L, Moutin, M.-J, Barisic, M, Taraviras, S, Perrakis, A, & Brummelkamp, T. R. (2022) Posttranslational modification of microtubules by the matcap detyrosinase. *Science* **376**, eabn6020.

[140] Baas, P. W & Black, M. M. (1990) Individual microtubules in the axon consist of domains that differ in both composition and stability. *The Journal of cell biology* **111**, 495–509.

[141] Peris, L, Wagenbach, M, Lafanechère, L, Brocard, J, Moore, A. T, Kozielski, F, Job, D, Wordeman, L, & Andrieux, A. (2009) Motor-dependent microtubule disassembly driven by tubulin tyrosination. *Journal of Cell Biology* **185**, 1159–1166.

[142] Eddé, B, Rossier, J, Le Caer, J. P, Desbruyères, E, Gros, F, & Denoulet, P. (1990) Posttranslational glutamylation of alpha-tubulin. *Science* **247**, 83–85.

[143] Devambez, I, Van Dijk, J, Benlefki, S, Layalle, S, Grau, Y, Rogowski, K, Parmentier, M. L, & Soustelle, L. (2017) Identification of DmTTLL5 as a Major Tubulin Glutamylase in the Drosophila Nervous System. *Scientific Reports* **7**.

[144] Janke, C, Rogowski, K, Wloga, D, Regnard, C, Kajava, A. V, Strub, J. M, Temurak, N, Van Dijk, J, Boucher, D, Van Dorsselaer, A, Suryavanshi, S, Gaertig, J, & Eddé, B. (2005) Tubulin polyglutamylase enzymes are members of the TTL domain protein family. *Science* **308**, 1758–1762.

[145] Ikegami, K, Heier, R. L, Taruishi, M, Takagi, H, Mukai, M, Shimma, S, Taira, S, Hatanaka, K, Morone, N, Yao, I, Campbell, P. K, Yuasa, S, Janke, C, Macgregor, G. R, & Setou, M. (2007) Loss of alpha-tubulin polyglutamylation in ROSA22 mice is associated with abnormal targeting of KIF1A and modulated synaptic

function. *Proceedings of the National Academy of Sciences of the United States of America* **104**, 3213–3218.

[146] van Dijk, J, Rogowski, K, Miro, J, Lacroix, B, Eddé, B, & Janke, C. (2007) A Targeted Multienzyme Mechanism for Selective Microtubule Polyglutamylation. *Molecular Cell* **26**, 437–448.

[147] Rogowski, K, Juge, F, van Dijk, J, Wloga, D, Strub, J. M, Levilliers, N, Thomas, D, Bré, M. H, Van Dorsselaer, A, Gaertig, J, & Janke, C. (2009) Evolutionary Divergence of Enzymatic Mechanisms for Posttranslational Polyglycylation. *Cell* **137**, 1076–1087.

[148] Wloga, D, Rogowski, K, Sharma, N, Van Dijk, J, Janke, C, Eddé, B, Bré, M. H, Levilliers, N, Redeker, V, Duan, J, Gorovsky, M. A, Jerka-Dziadosz, M, & Gaertig, J. (2008) Glutamylation on α-Tubulin Is Not Essential but Affects the Assembly and Functions of a Subset of Microtubules in Tetrahymena thermophila. *Eukaryotic Cell* **7**, 1362.

[149] Ikegami, K & Setou, M. (2009) TTLL10 can perform tubulin glycylation when co-expressed with TTLL8. *FEBS letters* **583**, 1957–1963.

[150] Sferra, A, Nicita, F, & Bertini, E. (2020) Microtubule Dysfunction: A Common Feature of Neurodegenerative Diseases. *International journal of molecular sciences* **21**, 1–36.

[151] Bodakuntla, S, Yuan, X, Genova, M, Gadadhar, S, Leboucher, S, Birling, M.-C, Klein, D, Martini, R, Janke, C, & Magiera, M. M. (2021) Distinct roles of α- and β-tubulin polyglutamylation in controlling axonal transport and in neurodegeneration. *The EMBO Journal* **40**, e108498.

[152] Audebert, S, Desbruyeres, E, Gruszczynski, C, Koulakoff, A, Gros, F, Denoulet, P, & Edde, B. (1993) Reversible polyglutamylation of alpha- and beta-tubulin and microtubule dynamics in mouse brain neurons. *Molecular biology of the cell* **4**, 615–626.

[153] Kimura, Y, Kurabe, N, Ikegami, K, Tsutsumi, K, Konishi, Y, Kaplan, O. I, Kunitomo, H, Iino, Y, Blacque, O. E, & Setou, M. (2010) Identification of tubulin deglutamylase among Caenorhabditis elegans and mammalian cytosolic carboxypeptidases (CCPs). *The Journal of biological chemistry* **285**, 22936–22941.

[154] Rogowski, K, van Dijk, J, Magiera, M. M, Bosc, C, Deloulme, J. C, Bosson, A, Peris, L, Gold, N. D, Lacroix, B, Grau, M. B, Bec, N, Larroque, C, Desagher, S, Holzer, M, Andrieux, A, Moutin, M. J, & Janke, C. (2010) A family of protein-deglutamylating enzymes associated with neurodegeneration. *Cell* **143**, 564–578.

[155] Berezniuk, I, Lyons, P. J, Sironi, J. J, Xiao, H, Setou, M, Angeletti, R. H, Ikegami, K, & Fricker, L. D. (2013) Cytosolic Carboxypeptidase 5 Removes α- and γ-Linked Glutamates from Tubulin. *Journal of Biological Chemistry* **288**, 30445–30453.

[156] Tort, O, Tanco, S, Rocha, C, Bieche, I, Seixas, C, Bosc, C, Andrieux, A, Moutin, M.-J, Aviles, F. X, Lorenzo, J, & Janke, C. (2014) The cytosolic carboxypeptidases CCP2 and CCP3 catalyze posttranslational removal of acidic amino acids. *Molecular Biology of the Cell* **25**, 3017–3027.

[157] Lacroix, B, Van Dijk, J, Gold, N. D, Guizetti, J, Aldrian-Herrada, G, Rogowski, K, Gerlich, D. W, & Janke, C. (2010) Tubulin polyglutamylation stimulates spastin-mediated microtubule severing. *Journal of Cell Biology* **189**, 945–954.

[158] Roll-Mecak, A, Roll-Mecak, & Antonina. (2018) Microtubule cryptography: the effects of tubulin diversity on polymer structure, dynamics and readout by cellular effectors. *APS* **2018**, F51.006.

[159] Mahalingan, K. K, Keith Keenan, E, Strickland, M, Li, Y, Liu, Y, Ball, H. L, Tanner, M. E, Tjandra, N, & Roll-Mecak, A. (2020) Structural basis for polyglutamate chain initiation and elongation by TTLL family enzymes. *Nature Structural and Molecular Biology* **27**, 802–813.

[160] McNally, F. J & Roll-Mecak, A. (2018) Microtubule-severing enzymes: From cellular functions to molecular mechanism. *Journal of Cell Biology* **217**, 4057–4069.

[161] Westermann, S & Weber, K. (2003) Post-translational modifications regulate microtubule function. *Nature reviews. Molecular cell biology* **4**, 938–947.

[162] Dixit, R, Ross, J. L, Goldman, Y. E, & Holzbaur, E. L. (2008) Differential regulation of dynein and kinesin motor proteins by tau. *Science* **319**, 1086–1089.

[163] Vershinin, M, Carter, B. C, Razafsky, D. S, King, S. J, & Gross, S. P. (2007) Multiple-motor based transport and its regulation by Tau. *Proceedings of the National Academy of Sciences of the United States of America* **104**, 87–92.

[164] Moughamian, A. J, Osborn, G. E, Lazarus, J. E, Maday, S, & Holzbaur, E. L. (2013) Ordered Recruitment of Dynactin to the Microtubule Plus-End is Required for Efficient Initiation of Retrograde Axonal Transport. *Journal of Neuroscience* **33**, 13190–13203.

[165] Nakagawa, H, Koyama, K, Murata, Y, Morito, M, Akiyama, T, & Nakamura, Y. (2000) EB3, a novel member of the EB1 family preferentially expressed in the central nervous system, binds to a CNS-specific APC homologue. *Oncogene* **19**, 210–216.

[166] Su, L. K & Qi, Y. (2001) Characterization of human MAPRE genes and their proteins. *Genomics* **71**, 142–149.

[167] Mustyatsa, V. V, Boyakhchyan, A. V, Ataullakhanov, F. I, & Gudimchuk, N. B. (2017) EB-family proteins: Functions and microtubule interaction mechanisms. *Biochemistry (Mosc.)* **82**, 791–802.

[168] Schuyler, S. C & Pellman, D. (2001) Microtubule "plus-end-tracking proteins": The end is just the beginning. *Cell* **105**, 421–424.

[169] Diamantopoulos, G. S, Perez, F, Goodson, H. V, Batelier, G, Melki, R, Kreis, T. E, & Rickard, J. E. (1999) Dynamic Localization of CLIP-170 to Microtubule Plus Ends Is Coupled to Microtubule Assembly. *Journal of Cell Biology* **144**, 99–112.

[170] Stone, M. C, Roegiers, F, & Rolls, M. M. (2008) Microtubules have opposite orientation in axons and dendrites of Drosophila neurons. *Molecular biology of the cell* **19**, 4122–4129.

[171] Roll-Mecak, A & McNally, F. J. (2010) Microtubule-severing enzymes. *Current Opinion in Cell Biology* **22**, 96–103.

[172] Kuo, Y. W & Howard, J. (2021) Cutting, Amplifying, and Aligning Microtubules with Severing Enzymes. *Trends in cell biology* **31**, 50–61.

[173] Howard, J & Hyman, A. A. (2007) Microtubule polymerases and depolymerases. *Current opinion in cell biology* **19**, 31–35.

[174] Wood, J. D, Landers, J. A, Bingley, M, McDermott, C. J, Thomas-McArthur, V, Gleadall, L. J, Shaw, P. J, & Cunliffe, V. T. (2006) The microtubule-severing protein Spastin is essential for axon outgrowth in the zebrafish embryo. *Human Molecular Genetics* **15**, 2763–2771.

[175] Srayko, M, O'Toole, E. T, Hyman, A. A, & Müller-Reichert, T. (2006) Katanin disrupts the microtubule lattice and increases polymer number in C. elegans meiosis. *Current biology : CB* **16**, 1944–1949.

[176] McNally, K. P, Bazirgan, O. A, & McNally, F. J. (2000) Two domains of p80 katanin regulate microtubule severing and spindle pole targeting by p60 katanin. *Journal of cell science* **113 (Pt 9)**, 1623–1633.

[177] Errico, A, Ballabio, A, & Rugarli, E. I. (2002) Spastin, the protein mutated in autosomal dominant hereditary spastic paraplegia, is involved in microtubule dynamics. *Human molecular genetics* **11**, 153–163.

[178] Yu, Y, Lee, C, Kim, J, & Hwang, S. (2005) Group-specific primer and probe sets to detect methanogenic communities using quantitative real-time polymerase chain reaction. *Biotechnology and Bioengineering* **89**, 670–679.

[179] Sherwood, N. T, Sun, Q, Xue, M, Zhang, B, & Zinn, K. (2004) Drosophila spastin regulates synaptic microtubule networks and is required for normal motor function. *PLoS biology* **2**.

[180] Yu, W, Qiang, L, Solowska, J. M, Karabay, A, Korulu, S, & Baas, P. W. (2008) The microtubule-severing proteins spastin and katanin participate differently in the formation of axonal branches. *Molecular biology of the cell* **19**, 1485–1498.

[181] Roll-Mecak, A & Vale, R. D. (2006) Making more microtubules by severing: A common theme of noncentrosomal microtubule arrays? *Journal of Cell Biology* **175**, 849–851.

[182] Kuo, Y. W, Trottier, O, Mahamdeh, M, & Howard, J. (2019) Spastin is a dual-function enzyme that severs microtubules and promotes their regrowth to increase the number and mass of microtubules. *Proceedings of the National Academy of Sciences of the United States of America* **116**, 5533–5541.

[183] Schaedel, L, John, K, Gaillard, J, Nachury, M. V, Blanchoin, L, & Thery, M. (2015) Microtubules self-repair in response to mechanical stress. *Nature Materials* **14**, 1156–1163.

[184] Vemu, A, Szczesna, E, Zehr, E. A, Spector, J. O, Grigorieff, N, Deaconescu, A. M, & Roll-Mecak, A. (2018) Severing enzymes amplify microtubule arrays through lattice GTP-tubulin incorporation. *Science* **361**.

[185] Aumeier, C, Schaedel, L, Gaillard, J, John, K, Blanchoin, L, & Théry, M. (2016) Self-repair promotes microtubule rescue. *Nature cell biology* **18**, 1054–1064.

[186] Triclin, S, Inoue, D, Gaillard, J, Htet, Z. M, DeSantis, M. E, Portran, D, Derivery, E, Aumeier, C, Schaedel, L, John, K, Leterrier, C, Reck-Peterson, S. L, Blanchoin, L, & Théry, M. (2021) Self-repair protects microtubules from destruction by molecular motors. *Nature materials* **20**, 883–891.

[187] VanDelinder, V, Adams, P. G, & Bachand, G. D. (2016) Mechanical splitting of microtubules into protofilament bundles by surface-bound kinesin-1. *Scientific reports* **6**.

[188] Schaedel, L, Triclin, S, Chrétien, D, Abrieu, A, Aumeier, C, Gaillard, J, Blanchoin, L, Théry, M, & John, K. (2019) Lattice defects induce microtubule self-renewal. *Nature physics* **15**, 830–838.

[189] Lawrence, E. J, Arpag, G, Arnaiz, C, & Zanic, M. (2021) Ssna1 stabilizes dynamic microtubules and detects microtubule damage. *eLife* **10**.

[190] Valenstein, M. L & Roll-Mecak, A. (2016) Graded Control of Microtubule Severing by Tubulin Glutamylation. *Cell* **164**, 911–921.

[191] Sun, X, Park, J. H, Gumerson, J, Wu, Z, Swaroop, A, Qian, H, Roll-Mecak, A, & Li, T. (2016) Loss of RPGR glutamylation underlies the pathogenic mechanism of retinal dystrophy caused by TTLL5 mutations. *Proceedings of the National Academy of Sciences of the United States of America* **113**, E2925–E2934.

[192] Roll-Mecak, A & Vale, R. D. (2008) Structural basis of microtubule severing by the hereditary spastic paraplegia protein spastin. *Nature* **451**, 363–367.

[193] Kelle, D, Kırımtay, K, Selçuk, E, & Karabay, A. (2019) Elk1 affects katanin and spastin proteins via differential transcriptional and post-transcriptional regulations. *PloS one* **14**.

[194] Henson, B. J, Zhu, W, Hardaway, K, Wetzel, J. L, Stefan, M, Albers, K. M, & Nicholls, R. D. (2012) Transcriptional and post-transcriptional regulation of

SPAST, the gene most frequently mutated in hereditary spastic paraplegia. *PloS one* **7**.

[195] Nakazeki, F, Tsuge, I, Horie, T, Imamura, K, Tsukita, K, Hotta, A, Baba, O, Kuwabara, Y, Nishino, T, Nakao, T, Nishiga, M, Nishi, H, Nakashima, Y, Ide, Y, Koyama, S, Kimura, M, Tsuji, S, Naitoh, M, Suzuki, S, Izumi, Y, Kawarai, T, Kaji, R, Kimura, T, Inoue, H, & Ono, K. (2019) MiR-33a is a therapeutic target in SPG4-related hereditary spastic paraplegia human neurons. *Clinical Science* **133**, 583–595.

[196] Jiang, T, Cai, Z, Ji, Z, Zou, J, Liang, Z, Zhang, G, Liang, Y, Lin, H, & Tan, M. (2020) The lncRNA MALAT1/miR-30/Spastin Axis Regulates Hippocampal Neurite Outgrowth. *Frontiers in Cellular Neuroscience* **14**.

[197] Ji, Z. S, Liu, Q. L, feng Zhang, J, Yang, Y. H, Li, J, Zhang, G. W, Tan, M. H, Lin, H. S, & Guo, G. Q. (2020) SUMOylation of spastin promotes the internalization of GluA1 and regulates dendritic spine morphology by targeting microtubule dynamics. *Neurobiology of disease* **146**.

[198] Sardina, F, Pisciottani, A, Ferrara, M, Valente, D, Casella, M, Crescenzi, M, Peschiaroli, A, Casali, C, Soddu, S, Grierson, A. J, & Rinaldo, C. (2020) Spastin recovery in hereditary spastic paraplegia by preventing neddylation-dependent degradation. *Life science alliance* **3**.

[199] Qiang, L. (2006) Tau Protects Microtubules in the Axon from Severing by Katanin. *Journal of Neuroscience* **26**, 3120–3129.

[200] Siahaan, V, Krattenmacher, J, Hyman, A. A, Diez, S, Hernndez-Vega, A, Lansky, Z, & Braun, M. (2019) Kinetically distinct phases of tau on microtubules regulate kinesin motors and severing enzymes. *Nature Cell Biology 2019 21:9* **21**, 1086–1092.

[201] Zempel, H & Mandelkow, E.-M. (2015) Tau missorting and spastin-induced microtubule disruption in neurodegeneration: Alzheimer Disease and Hereditary Spastic Paraplegia. *Molecular Neurodegeneration* **10**, 68.

[202] Fink, J. K. (2013) Hereditary spastic paraplegia: Clinico-pathologic features and emerging molecular mechanisms. *Acta Neuropathologica* **126**, 307–328.

[203] Arribat, Y, Grepper, D, Lagarrigue, S, Qi, T, Cohen, S, & Amati, F. (2020) Spastin mutations impair coordination between lipid droplet dispersion and reticulum. *PLOS Genetics* **16**, e1008665.

[204] Qiang, L, Piermarini, E, & Baas, P. W. (2019) New hypothesis for the etiology of SPAST-based hereditary spastic paraplegia. *Cytoskeleton* **76**.

[205] Park, S. H, Zhu, P. P, Parker, R. L, & Blackstone, C. (2010) Hereditary spastic paraplegia proteins REEP1, spastin, and atlastin-1 coordinate microtubule interactions with the tubular ER network. *The Journal of clinical investigation* **120**, 1097–1110.

[206] Guo, E. Z & Xu, Z. (2015) Distinct mechanisms of recognizing endosomal sorting complex required for transport III (ESCRT-III) protein IST1 by different microtubule interacting and trafficking (MIT) domains. *The Journal of biological chemistry* **290**, 8396–8408.

[207] Evans, K, Keller, C, Pavur, K, Glasgow, K, Conn, B, & Lauring, B. (2006) Interaction of two hereditary spastic paraplegia gene products, spastin and atlastin, suggests a common pathway for axonal maintenance. *Proceedings of the National Academy of Sciences of the United States of America* **103**, 10666–10671.

[208] Sanderson, C. M, Connel, J. W, Edwards, T. L, Bright, N. A, Duley, S, Thompson, A, Luzio, J. P, & Reid, E. (2006) Spastin and atlastin, two proteins mutated in autosomal-dominant hereditary spastic paraplegia, are binding partners. *Human molecular genetics* **15**, 307–318.

[209] Allison, R, Lumb, J. H, Fassier, C, Connell, J. W, Martin, D. T, Seaman, M. N, Hazan, J, & Reid, E. (2013) An ESCRT-spastin interaction promotes fission of recycling tubules from the endosome. *The Journal of cell biology* **202**, 527–543.

[210] Allison, R, Edgar, J. R, Pearson, G, Rizo, T, Newton, T, Günther, S, Berner, F, Hague, J, Connell, J. W, Winkler, J, Lippincott-Schwartz, J, Beetz, C, Winner, B, & Reid, E. (2017) Defects in ER-endosome contacts impact lysosome function in hereditary spastic paraplegia. *The Journal of cell biology* **216**, 1337–1355.

[211] Connell, J. W, Allison, R. J, Rodger, C. E, Pearson, G, Zlamalova, E, & Reid, E. (2020) ESCRT-III-associated proteins and spastin inhibit protrudin-dependent polarised membrane traffic. *Cellular and molecular life sciences : CMLS* **77**, 2641–2658.

[212] Reid, E, Connell, J, Edwards, T. L, Duley, S, Brown, S. E, & Sanderson, C. M. (2005) The hereditary spastic paraplegia protein spastin interacts with the ESCRT-III complex-associated endosomal protein CHMP1B. *Human molecular genetics* **14**, 19–38.

[213] Claudiani, P, Riano, E, Errico, A, Andolfi, G, & Rugarli, E. I. (2005) Spastin subcellular localization is regulated through usage of different translation start sites and active export from the nucleus. *Experimental cell research* **309**, 358–369.

[214] Renvoisé, B, Parker, R. L, Yang, D, Bakowska, J. C, Hurley, J. H, & Blackstone, C. (2010) SPG20 Protein Spartin Is Recruited to Midbodies by ESCRT-III Protein Ist1 and Participates in Cytokinesis. *Molecular Biology of the Cell* **21**, 3293.

[215] Chaudhary, R, Agarwal, V, Rehman, M, Kaushik, A. S, & Mishra, V. (2022) Genetic architecture of motor neuron diseases. *Journal of the Neurological Sciences* **434**.

[216] Hazan, J, Fonknechten, N, Mavel, D, Paternotte, C, Samson, D, Artiguenave, F, Davoine, C. S, Cruaud, C, Dürr, A, Wincker, P, Brottier, P, Cattolico, L, Barbe, V, Burgunder, J. M, Prud'homme, J. F, Brice, A, Fontaine, B, Heilig, R, & Weissenbach, J. (1999) Spastin, a new AAA protein, is altered in the most frequent form of autosomal dominant spastic paraplegia. *Nature Genetics* **23**, 296–303.

[217] Mohan, N, Qiang, L, Morfini, G, & Baas, P. W. (2021) Therapeutic Strategies for Mutant SPAST-Based Hereditary Spastic Paraplegia. *Brain sciences* **11**.

[218] Solowska, J. M, Morfini, G, Falnikar, A, Himes, B. T, Brady, S. T, Huang, D, & Baas, P. W. (2008) Quantitative and functional analyses of spastin in the nervous system: implications for hereditary spastic paraplegia. *The Journal of neuroscience : the official journal of the Society for Neuroscience* **28**, 2147–2157.

[219] Leo, L, Weissmann, C, Burns, M, Kang, M, Song, Y, Qiang, L, Brady, S. T, Baas, P. W, & Morfini, G. (2017) Mutant spastin proteins promote deficits in axonal transport through an isoform-specific mechanism involving casein kinase 2 activation. *Human Molecular Genetics* **26**, 2321–2334.

[220] Solowska, J. M, Rao, A. N, & Baas, P. W. (2017) Truncating mutations of SPAST associated with hereditary spastic paraplegia indicate greater accumulation and toxicity of the M1 isoform of spastin. *Molecular biology of the cell* **28**, 1728–1737.

[221] Maday, S, Twelvetrees, A. E, Moughamian, A. J, & Holzbaur, E. L. F. (2014) Axonal Transport: Cargo-Specific Mechanisms of Motility and Regulation. *Neuron* **84**, 292–309.

[222] Lin, M. Y & Sheng, Z. H. (2015) Regulation of mitochondrial transport in neurons. *Experimental cell research* **334**, 35–44.

[223] Gibbs, K. L, Greensmith, L, & Schiavo, G. (2015) Regulation of Axonal Transport by Protein Kinases. *Trends in biochemical sciences* **40**, 597–610.

[224] Cyr, J. L & Brady, S. T. (1992) Molecular motors in axonal transport. Cellular and molecular biology of kinesin. *Molecular neurobiology* **6**, 137–155.

[225] Guedes-Dias, P & Holzbaur, E. L. (2019) Axonal transport: Driving synaptic function. *Science* **366**.

[226] Rangaraju, V, Tom Dieck, S, & Schuman, E. M. (2017) Local translation in neuronal compartments: how local is local? *EMBO Rep.* **18**, 693–711.

[227] Wang, M, Kleele, T, Xiao, Y, Plucinska, G, Avramopoulos, P, Engelhardt, S, Schwab, M. H, Kneussel, M, Czopka, T, Sherman, D. L, Brophy, P. J, Misgeld, T, & Brill, M. S. (2021) Completion of neuronal remodeling prompts myelination along developing motor axon branches. *Journal of Cell Biology* **220**.

[228] Gennerich, A & Vale, R. D. (2009) Walking the walk: how kinesin and dynein coordinate their steps. *Current opinion in cell biology* **21**, 59–67.

[229] Verbrugge, S, Kapitein, L. C, & Peterman, E. J. (2007) Kinesin moving through the spotlight: single-motor fluorescence microscopy with submillisecond time resolution. *Biophysical journal* **92**, 2536–2545.

[230] Roy, S, Coffee, P, Smith, G, Liem, R. K, Brady, S. T, & Black, M. M. (2000) Neurofilaments Are Transported Rapidly But Intermittently in Axons: Implications for Slow Axonal Transport. *The Journal of Neuroscience* **20**, 6849.

[231] Wang, L, Ho, C. L, Sun, D, Liem, R. K, & Brown, A. (2000) Rapid movement of axonal neurofilaments interrupted by prolonged pauses. *Nature cell biology* **2**, 137–141.

[232] Miki, H, Setou, M, Kaneshiro, K, & Hirokawa, N. (2001) All kinesin superfamily protein, KIF, genes in mouse and human. *Proceedings of the National Academy of Sciences of the United States of America* **98**, 7004–7011.

[233] Hirokawa, N. (1998) Kinesin and dynein superfamily proteins and the mechanism of organelle transport. *Science* **279**, 519–526.

[234] Nakagawa, T, Tanaka, Y, Matsuoka, E, Kondo, S, Okada, Y, Noda, Y, Kanai, Y, & Hirokawa, N. (1997) Identification and classification of 16 new kinesin superfamily (KIF) proteins in mouse genome. *Proceedings of the National Academy of Sciences of the United States of America* **94**, 9654–9659.

[235] Svoboda, K & Block, S. M. (1994) Force and velocity measured for single kinesin molecules. *Cell* **77**, 773–784.

[236] Hirokawa, N. (2011) From electron microscopy to molecular cell biology, molecular genetics and structural biology: intracellular transport and kinesin superfamily proteins, KIFs: genes, structure, dynamics and functions. *Journal of Electron Microscopy* **60**, S63–S92.

[237] Castle, M. J, Perlson, E, Holzbaur, E. L, & Wolfe, J. H. (2014) Long-distance axonal transport of AAV9 is driven by dynein and kinesin-2 and is trafficked in a highly motile Rab7-positive compartment. *Molecular therapy : the journal of the American Society of Gene Therapy* **22**, 554–566.

[238] Hendricks, A. G, Perlson, E, Ross, J. L, Schroeder, H. W, Tokito, M, & Holzbaur, E. L. (2010) Motor coordination via a tug-of-war mechanism drives bidirectional vesicle transport. *Current biology : CB* **20**, 697–702.

[239] Hall, D. H & Hedgecock, E. M. (1991) Kinesin-related gene unc-104 is required for axonal transport of synaptic vesicles in C. elegans. *Cell* **65**, 837–847.

[240] Okada, Y, Yamazaki, H, Sekine-Aizawa, Y, & Hirokawa, N. (1995) The neuron-specific kinesin superfamily protein KIF1A is a unique monomeric motor for anterograde axonal transport of synaptic vesicle precursors. *Cell* **81**, 769–780.

[241] Lo, K. Y, Kuzmin, A, Unger, S. M, Petersen, J. D, & Silverman, M. A. (2011) KIF1A is the primary anterograde motor protein required for the axonal transport of dense-core vesicles in cultured hippocampal neurons. *Neuroscience letters* **491**, 168–173.

[242] Roberts, A. J, Kon, T, Knight, P. J, Sutoh, K, & Burgess, S. A. (2013) Functions and mechanics of dynein motor proteins. *Nature Reviews Molecular Cell Biology 2013 14:11* **14**, 713–726.

[243] Mallik, R, Rai, A. K, Barak, P, Rai, A, & Kunwar, A. (2013) Teamwork in microtubule motors. *Trends in cell biology* **23**, 575–82.

[244] Ross, J. L, Shuman, H, Holzbaur, E. L, & Goldman, Y. E. (2008) Kinesin and Dynein-Dynactin at Intersecting Microtubules: Motor Density Affects Dynein Function. *Biophysical Journal* **94**, 3115–3125.

[245] Verdeny-Vilanova, I, Wehnekamp, F, Mohan, N, Álvarez, á. S, Borbely, J. S, Otterstrom, J. J, Lamb, D. C, & Lakadamyali, M. (2017) 3D motion of vesicles along microtubules helps them to circumvent obstacles in cells. *Journal of cell science* **130**, 1904–1916.

[246] Mallik, R, Petrov, D, Lex, S. A, King, S. J, & Gross, S. P. (2005) Building complexity: an in vitro study of cytoplasmic dynein with in vivo implications. *Current biology : CB* **15**, 2075–2085.

[247] Lipka, J, Kuijpers, M, Jaworski, J, & Hoogenraad, C. C. (2013) Mutations in cytoplasmic dynein and its regulators cause malformations of cortical development and neurodegenerative diseases. *Biochemical Society transactions* **41**, 1605–1612.

[248] Gill, S. R, Schroer, T. A, Szilak, I, Steuer, E. R, Sheetz, M. P, & Cleveland, D. W. (1991) Dynactin, a conserved, ubiquitously expressed component of an activator of vesicle motility mediated by cytoplasmic dynein. *The Journal of cell biology* **115**, 1639–1650.

[249] Schroer, T. A. (2004) Dynactin. *Annual review of cell and developmental biology* **20**, 759–779.

[250] Derr, N. D, Goodman, B. S, Jungmann, R, Leschziner, A. E, Shih, W. M, & Reck-Peterson, S. L. (2012) Tug-of-war in motor protein ensembles revealed with a programmable DNA origami scaffold. *Science* **338**, 662–665.

[251] Sheng, Z. H & Cai, Q. (2012) Mitochondrial transport in neurons: impact on synaptic homeostasis and neurodegeneration. *Nature reviews. Neuroscience* **13**, 77–93.

[252] Roy, S, Zhang, B, Lee, V. M.-Y, & Trojanowski, J. Q. (2005) Axonal transport defects: a common theme in neurodegenerative diseases. *Acta Neuropathol.* **109**, 5–13.

[253] Berth, S. H & Lloyd, T. E. (2023) Disruption of axonal transport in neurodegeneration. *J. Clin. Invest.* **133**.

[254] Baldwin, K. R, Godena, V. K, Hewitt, V. L, & Whitworth, A. J. (2016) Axonal transport defects are a common phenotype in*Drosophila*models of ALS. *Hum. Mol. Genet.* p. ddw105.

[255] Morfini, G. A, Burns, M, Binder, L. I, Kanaan, N. M, LaPointe, N, Bosco, D. A, Brown, Jr, R. H, Brown, H, Tiwari, A, Hayward, L, Edgar, J, Nave, K.-A, Garberrn, J, Atagi, Y, Song, Y, Pigino, G, & Brady, S. T. (2009) Axonal transport defects in neurodegenerative diseases. *J. Neurosci.* **29**, 12776–12786.

[256] Guo, W, Stoklund Dittlau, K, & Van Den Bosch, L. (2020) Axonal transport defects and neurodegeneration: Molecular mechanisms and therapeutic implications. *Semin. Cell Dev. Biol.* **99**, 133–150.

[257] Kasthuri, N & Lichtman, J. W. (2003) The role of neuronal identity in synaptic competition. *Nature* **424**, 426–430.

[258] Dunn, S, Morrison, E. E, Liverpool, T. B, Molina-Paris, C, Cross, R. A, Alonso, M. C, & Peckham, M. (2008) Differential trafficking of Kif5c on tyrosinated and detyrosinated microtubules in live cells. *Journal of Cell Science* **121**, 1085–1095.

[259] Kaul, N, Soppina, V, & Verhey, K. J. (2014) Effects of α-tubulin K40 acetylation and detyrosination on kinesin-1 motility in a purified system. *Biophysical journal* **106**, 2636–2643.

[260] Liao, G, Kreitzer, G, Cook, T. A, & Gundersen, G. G. (1999) A signal transduction pathway involved in microtubule-mediated cell polarization. *FASEB journal : official publication of the Federation of American Societies for Experimental Biology* **13 Suppl 2**.

[261] Hammond, J. W, Huang, C.-F, Kaech, S, Jacobson, C, Banker, G, & Verhey, K. J. (2010) Posttranslational Modifications of Tubulin and the Polarized Transport of Kinesin-1 in Neurons. *Molecular biology of the cell* **21**, 4042–4056.

[262] Tas, R. P, Chazeau, A, Cloin, B. M, Lambers, M. L, Hoogenraad, C. C, & Kapitein, L. C. (2017) Differentiation between Oppositely Oriented Microtubules Controls Polarized Neuronal Transport. *Neuron* **96**, 1264–1271.e5.

[263] Kahn, O. I, Sharma, V, González-Billault, C, & Baas, P. W. (2015) Effects of kinesin-5 inhibition on dendritic architecture and microtubule organization. *Molecular biology of the cell* **26**, 66–77.

[264] McKenney, R. J, Huynh, W, Vale, R. D, & Sirajuddin, M. (2016) Tyrosination of α-tubulin controls the initiation of processive dynein–dynactin motility. *The EMBO Journal* **35**, 1175–1185.

[265] Nirschl, J. J, Magiera, M. M, Lazarus, J. E, Janke, C, & Holzbaur, E. L. (2016) α-Tubulin Tyrosination and CLIP-170 Phosphorylation Regulate the Initiation of Dynein-Driven Transport in Neurons. *Cell Reports* **14**, 2637–2652.

[266] Magiera, M. M, Bodakuntla, S, Žiak, J, Lacomme, S, Marques Sousa, P, Leboucher, S, Hausrat, T. J, Bosc, C, Andrieux, A, Kneussel, M, Landry, M, Calas, A, Balastik, M, & Janke, C. (2018) Excessive tubulin polyglutamylation causes neurodegeneration and perturbs neuronal transport. *The EMBO Journal* p. e100440.

[267] Lopes, A. T, Hausrat, T. J, Heisler, F. F, Gromova, K. V, Lombino, F. L, Fischer, T, Ruschkies, L, Breiden, P, Thies, E, Hermans-Borgmeyer, I, Schweizer, M, Schwarz, J. R, Lohr, C, & Kneussel, M. (2020) Spastin depletion increases tubulin polyglutamylation and impairs kinesin-mediated neuronal transport, leading to working and associative memory deficits. *PLOS Biology* **18**, e3000820.

[268] Sanes, J. R & Masland, R. H. (2015) The types of retinal ganglion cells: current status and implications for neuronal classification. *Annual review of neuroscience* **38**, 221–246.

[269] Sanz, E, Yang, L, Su, T, Morris, D. R, McKnight, G. S, & Amieux, P. S. (2009) Cell-type-specific isolation of ribosome-associated mRNA from complex tissues. *Proceedings of the National Academy of Sciences* **106**, 13939–13944.

[270] Sanz, E, Bean, J. C, Carey, D. P, Quintana, A, & McKnight, G. S. (2019) RiboTag: Ribosomal Tagging Strategy to Analyze Cell-Type-Specific mRNA Expression In Vivo. *Current Protocols in Neuroscience* **88**, 1–25.

[271] Shigeoka, T, Jung, H, Jung, J, Turner-Bridger, B, Ohk, J, Lin, J. Q, Amieux, P. S, & Holt, C. E. (2016) Dynamic axonal translation in developing and mature visual circuits. *Cell* **166**, 181–192.

[272] Farias, J, Holt, C. E, Sotelo, J. R, & Sotelo-Silveira, J. R. (2020) Axon microdissection and transcriptome profiling reveals the in vivo RNA content of fully differentiated myelinated motor axons. *RNA* **26**, 595–612.

[273] Kim, N, Jun, M.-H, Jeong, J.-Y, & Oh, W.-J. (2022) Optimized protocol for translatome analysis of mouse brain endothelial cells. *PLoS One* **17**, e0275036.

[274] Molina-Gonzalez, I, Holloway, R. K, Jiwaji, Z, Dando, O, Kent, S. A, Emelianova, K, Lloyd, A. F, Forbes, L. H, Mahmood, A, Skripuletz, T, Gudi, V, Febery, J. A, Johnson, J. A, Fowler, J. H, Kuhlmann, T, Williams, A, Chandran, S, Stangel, M, Howden, A. J. M, Hardingham, G. E, & Miron, V. E. (2023) Astrocyte-oligodendrocyte interaction regulates central nervous system regeneration. *Nat. Commun.* **14**, 3372.

[275] Ikegami, K, Mukai, M, Tsuchida, J. I, Heier, R. L, MacGregor, G. R, & Setou, M. (2006) TTLL7 is a mammalian beta-tubulin polyglutamylase required for growth of MAP2-positive neurites. *The Journal of biological chemistry* **281**, 30707–30716.

[276] Bagri, A, Cheng, H.-J, Yaron, A, Pleasure, S. J, & Tessier-Lavigne, M. (2003) Stereotyped pruning of long hippocampal axon branches triggered by retraction inducers of the semaphorin family. *Cell* **113**, 285–299.

[277] Liu, Y. J. (2005) IPC: professional type 1 interferon-producing cells and plasmacytoid dendritic cell precursors. *Annual review of immunology* **23**, 275–306.

[278] Renvoisé, B, Chang, J, Singh, R, Yonekawa, S, FitzGibbon, E. J, Mankodi, A, Vanderver, A, Schindler, A. B, Toro, C, Gahl, W. A, Mahuran, D. J, Blackstone, C, & Pierson, T. M. (2014) Lysosomal abnormalities in hereditary spastic paraplegia types SPG15 and SPG11. *Annals of Clinical and Translational Neurology* **1**, 379–389.

[279] Katayama, H, Kogure, T, Mizushima, N, Yoshimori, T, & Miyawaki, A. (2011) A sensitive and quantitative technique for detecting autophagic events based on lysosomal delivery. *Chem. Biol.* **18**, 1042–1052.

[280] Wolff, A, de Nechaud, B, Chillet, D, Mazarguil, H, Desbruyeres, E, Audebert, S, Edde, B, Gros, F, & Denoulet, P. (1992) Distribution of glutamylated alpha and beta-tubulin in mouse tissues using a specific monoclonal antibody, GT335. *European journal of cell biology.*

[281] Kann, M. L, Soues, S, Levilliers, N, & Fouquet, J. P. (2003) Glutamylated tubulin: Diversity of expression and distribution of isoforms. *Cell Motility and the Cytoskeleton* **55**, 14–25.

[282] Yang, F, Je, H. S, Ji, Y, Nagappan, G, Hempstead, B, & Lu, B. (2009) Pro-BDNF-induced synaptic depression and retraction at developing neuromuscular synapses. *The Journal of cell biology* **185**, 727–741.

[283] Luo, L & O'Leary, D. D. (2005) Axon retraction and degeneration in development and disease. *Annual review of neuroscience* **28**, 127–156.

[284] Brants, J, Semenchenko, K, Wasylyk, C, Robert, A, Carles, A, Zambrano, A, Pradeau-Aubreton, K, Birck, C, Schalken, J. A, Poch, O, de Mey, J, & Wasylyk, B. (2012) Tubulin tyrosine ligase like 12, a TTLL family member with SET- and TTL-like domains and roles in histone and tubulin modifications and mitosis. *PloS one* **7**.

[285] Aiken, J, Buscaglia, G, Bates, E. A, & Moore, J. K. (2017) The α-Tubulin gene TUBA1A in Brain Development: A Key Ingredient in the Neuronal Isotype Blend. *Journal of Developmental Biology 2017, Vol. 5, Page 8* **5**, 8.

[286] Sferra, A, Fattori, F, Rizza, T, Flex, E, Bellacchio, E, Bruselles, A, Petrini, S, Cecchetti, S, Teson, M, Restaldi, F, Ciolfi, A, Santorelli, F. M, Zanni, G, Barresi, S, Castiglioni, C, Tartaglia, M, & Bertini, E. (2018) Defective kinesin binding of TUBB2a causes progressive spastic ataxia syndrome resembling sacsinopathy. *Human Molecular Genetics* **27**, 1892–1904.

[287] Curiel, J, Bey, G. R, Takanohashi, A, Bugiani, M, Fu, X, Wolf, N. I, Nmezi, B, Schiffmann, R, Bugaighis, M, Pierson, T, Helman, G, Simons, C, van der Knaap, M. S, Liu, J, Padiath, Q, & Vanderver, A. (2017) TUBB4a mutations result

in specific neuronal and oligodendrocytic defects that closely match clinically distinct phenotypes. *Human Molecular Genetics* **26**, 4506–4518.

[288] Lohmann, K, Wilcox, R. A, Winkler, S, Ramirez, A, Rakovic, A, Park, J.-S, Arns, B, Lohnau, T, Groen, J, Kasten, M, Brüggemann, N, Hagenah, J, Schmidt, A, Kaiser, F. J, Kumar, K. R, Zschiedrich, K, Alvarez-Fischer, D, Altenmüller, E, Ferbert, A, Lang, A. E, Münchau, A, Kostic, V, Simonyan, K, Agzarian, M, Ozelius, L. J, Langeveld, A. P. M, Sue, C. M, Tijssen, M. A. J, & Klein, C. (2013) Whispering dysphonia (DYT4 dystonia) is caused by a mutation in the tubb4 gene. *Annals of Neurology* **73**, 537–545.

[289] Watanabe, N, Itakaoka, M, Seki, Y, Morimoto, T, Homma, K, Miyamoto, Y, & Yamauchi, J. (2018) Dystonia-4 (DYT4)-associated TUBB4a mutants exhibit disorganized microtubule networks and inhibit neuronal process growth. *Biochemical and Biophysical Research Communications* **495**, 346–352.

[290] Smith, B. N, Ticozzi, N, Fallini, C, Gkazi, A. S, Topp, S, Kenna, K. P, Scotter, E. L, Kost, J, Keagle, P, Miller, J. W, Calini, D, Vance, C, Danielson, E. W, Troakes, C, Tiloca, C, Al-Sarraj, S, Lewis, E. A, King, A, Colombrita, C, Pensato, V, Castellotti, B, de Belleroche, J, Baas, F, ten Asbroek, A. L, Sapp, P. C, McKenna-Yasek, D, McLaughlin, R. L, Polak, M, Asress, S, Esteban-Pérez, J, Muñoz-Blanco, J. L, Simpson, M, van Rheenen, W, Diekstra, F. P, Lauria, G, Duga, S, Corti, S, Cereda, C, Corrado, L, Sorarù, G, Morrison, K. E, Williams, K. L, Nicholson, G. A, Blair, I. P, Dion, P. A, Leblond, C. S, Rouleau, G. A, Hardiman, O, Veldink, J. H, Van Den Berg, L. H, Al-Chalabi, A, Pall, H, Shaw, P. J, Turner, M. R, Talbot, K, Taroni, F, García-Redondo, A, Wu, Z, Glass, J. D, Gellera, C, Ratti, A, Brown, R. H, Silani, V, Shaw, C. E, Landers, J. E, D'Alfonso, S, Mazzini, L, Comi, G. P, Del Bo, R, Ceroni, M, Gagliardi, S, Querin, G, & Bertolin, C. (2014) Exome-wide rare variant analysis identifies TUBA4A mutations associated with familial ALS. *Neuron* **84**, 324–331.

[291] Wang, T, Parris, J, Li, L, & Morgan, J. I. (2006) The carboxypeptidase-like substrate-binding site in Nna1 is essential for the rescue of the Purkinje cell degeneration (pcd) phenotype. *Molecular and Cellular Neuroscience* **33**, 200–213.

[292] Balastik, M, Ferraguti, F, Pires-da Silva, A, Tae, H. L, Alvarez-Bolado, G, Kun, P. L, & Gruss, P. (2008) Deficiency in ubiquitin ligase TRIM2 causes

accumulation of neurofilament light chain and neurodegeneration. *Proceedings of the National Academy of Sciences of the United States of America* **105**, 12016.

[293] Krstic, D & Knuesel, I. (2013) Deciphering the mechanism underlying late-onset Alzheimer disease. *Nature reviews. Neurology* **9**, 25–34.

[294] Shashi, V, Magiera, M. M, Klein, D, Zaki, M, Schoch, K, Rudnik-Schöneborn, S, Norman, A, Lopes Abath Neto, O, Dusl, M, Yuan, X, Bartesaghi, L, De Marco, P, Alfares, A. A, Marom, R, Arold, S. T, Guzmán-Vega, F. J, Pena, L. D, Smith, E. C, Steinlin, M, Babiker, M. O, Mohassel, P, Foley, A. R, Donkervoort, S, Kaur, R, Ghosh, P. S, Stanley, V, Musaev, D, Nava, C, Mignot, C, Keren, B, Scala, M, Tassano, E, Picco, P, Doneda, P, Fiorillo, C, Issa, M. Y, Alassiri, A, Alahmad, A, Gerard, A, Liu, P, Yang, Y, Ertl-Wagner, B, Kranz, P. G, Wentzensen, I. M, Stucka, R, Stong, N, Allen, A. S, Goldstein, D. B, Schoser, B, Rösler, K. M, Alfadhel, M, Capra, V, Chrast, R, Strom, T. M, Kamsteeg, E, Bönnemann, C. G, Gleeson, J. G, Martini, R, Janke, C, & Senderek, J. (2018) Loss of tubulin deglutamylase CCP1 causes infantile-onset neurodegeneration. *The EMBO Journal* p. e100540.

[295] Sheffer, R, Gur, M, Brooks, R, Salah, S, Daana, M, Fraenkel, N, Eisenstein, E, Rabie, M, Nevo, Y, Jalas, C, Elpeleg, O, Edvardson, S, & Harel, T. (2019) Biallelic variants in AGTPBP1, involved in tubulin deglutamylation, are associated with cerebellar degeneration and motor neuropathy. *European Journal of Human Genetics* **27**, 1419–1426.

[296] Hell, S. W & Wichmann, J. (1994) Breaking the diffraction resolution limit by stimulated emission: stimulated-emission-depletion fluorescence microscopy. *Opt. Lett.* **19**, 780.

[297] Guardia, C. M, Farías, G. G, Jia, R, Pu, J, & Bonifacino, J. S. (2016) BORC Functions Upstream of Kinesins 1 and 3 to Coordinate Regional Movement of Lysosomes along Different Microtubule Tracks. *Cell Reports* **17**, 1950–1961.

[298] Zhu, Y, An, X, Tomaszewski, A, Hepler, P. K, & Lee, W. L. (2017) Microtubule cross-linking activity of She1 ensures spindle stability for spindle positioning. *The Journal of cell biology* **216**, 2759–2775.

[299] Qiang, L, Sun, X, Austin, T. O, Muralidharan, H, Jean, D. C, Liu, M, Yu, W, & Baas, P. W. (2018) Tau Does Not Stabilize Axonal Microtubules but Rather Enables Them to Have Long Labile Domains. *Current Biology* **28**, 2181–2189.e4.

[300] Genova, M, Grycova, L, Puttrich, V, Magiera, M. M, Lansky, Z, Janke, C, & Braun, M. (2023) Tubulin polyglutamylation differentially regulates microtubule-interacting proteins. *EMBO J.* **42**, e112101.

[301] Lin, Z, Gasic, I, Chandrasekaran, V, Peters, N, Shao, S, Mitchison, T. J, & Hegde, R. S. (2020) TTC5 mediates autoregulation of tubulin via mRNA degradation. *Science* **367**, 100–104.

[302] Qu, X, Kumar, A, Blockus, H, Waites, C, & Bartolini, F. (2019) Activity-Dependent Nucleation of Dynamic Microtubules at Presynaptic Boutons Controls Neurotransmission. *Current biology : CB* **29**, 4231–4240.e5.

[303] Terasaki, M, Chen, L. B, & Fujiwara, K. (year?) Microtubules and the Endoplasmic Reticulum Are Highly Interdependent Structures.

[304] Kimura, K, Mamane, A, Sasaki, T, Sato, K, Takagi, J, Niwayama, R, Hufnagel, L, Shimamoto, Y, Joanny, J. F, Uchida, S, & Kimura, A. (2017) Endoplasmic-reticulum-mediated microtubule alignment governs cytoplasmic streaming. *Nature cell biology* **19**, 399–406.

[305] Farias, J, Sotelo, J. R, & Sotelo-Silveira, J. (2019) Toward Axonal System Biology: Genome Wide Views of Local mRNA Translation. *Proteomics* **19**, 1–11.

[306] Rizo, T, Gebhardt, L, Riedlberger, J, Eberhardt, E, Fester, L, Alansary, D, Winkler, J, Turan, S, Arnold, P, Niemeyer, B. A, Fischer, M. J, & Winner, B. (2022) Store-operated calcium entry is reduced in spastin-linked hereditary spastic paraplegia. *Brain* **145**, 3131–3146.

[307] Allison, R, Edgar, J. R, & Reid, E. (2019) Spastin MIT Domain Disease-Associated Mutations Disrupt Lysosomal Function. *Frontiers in neuroscience* **13**.

[308] Kasher, P. R, De Vos, K. J, Wharton, S. B, Manser, C, Bennett, E. J, Bingley, M, Wood, J. D, Milner, R, McDermott, C. J, Miller, C. C, Shaw, P. J, & Grierson, A. J. (2009) Direct evidence for axonal transport defects in a novel mouse model of mutant spastin-induced hereditary spastic paraplegia (HSP) and human HSP patients. *Journal of Neurochemistry* **110**, 34–44.

[309] Havlicek, S, Kohl, Z, Mishra, H. K, Prots, I, Eberhardt, E, Denguir, N, Wend, H, Plötz, S, Boyer, L, Marchetto, M. C, Aigner, S, Sticht, H, Groemer, T. W, Hehr,

U, Lampert, A, Schlötzer-schrehardt, U, Winkler, J, Gage, F. H, & Winner, B. (2014) Gene dosage-dependent rescue of HSP neurite defects in SPG4 patients' neurons. *Human Molecular Genetics* **23**, 2527–2541.

[310] Parodi, L, Fenu, S, Barbier, M, Banneau, G, Duyckaerts, C, Tezenas du Montcel, S, Monin, M.-L, Ait Said, S, Guegan, J, Tallaksen, C. M. E, Sablonniere, B, Brice, A, Stevanin, G, Depienne, C, Durr, A, Abada, M, Anheim, M, Bonneau, D, Charles, P, Clavelou, P, Coarelli, G, Coutinho, P, Debs, R, Elleuch, N, Ewenczyk, C, Feki, I, Ferrer, X, Fontaine, B, Goizet, C, Guyant-Marechal, L, Hannequin, D, Heide, S, Kassar, A, Labauge, P, Lagueny, A, Le Ber, I, Lenglet, T, Maldergem, L, Marelli, C, Nguyen, K, Rodriguez, D, Stojkovic, T, Tataru, A, Tchikviladze, M, Tranchant, C, & Vandenberghe, N. (2018) Spastic paraplegia due to SPAST mutations is modified by the underlying mutation and sex. *Brain*.

[311] Wali, G, Sue, C, & Mackay-Sim, A. (2018) Patient-Derived Stem Cell Models in SPAST HSP: Disease Modelling and Drug Discovery. *Brain Sciences* **8**, 142.

[312] Hall, S. G, Kuo, J, Ward, J. M, Zahra, R, Morrison, R. S, & Perkins, G. (2018) CCP1 promotes mitochondrial fusion and motility to prevent Purkinje cell neuron loss in pcd mice. **218**, 206–219.

[313] Jin, S. M & Youle, R. J. (2012) PINK1- and Parkin-mediated mitophagy at a glance. *Journal of cell science* **125**, 795–799.

[314] Vincow, E. S, Merrihew, G, Thomas, R. E, Shulman, N. J, Beyer, R. P, MacCoss, M. J, & Pallanck, L. J. (2013) The PINK1-Parkin pathway promotes both mitophagy and selective respiratory chain turnover in vivo. *Proceedings of the National Academy of Sciences of the United States of America* **110**, 6400–6405.

[315] Ge, P, Dawson, V. L, & Dawson, T. M. (2020) PINK1 and Parkin mitochondrial quality control: a source of regional vulnerability in Parkinson's disease. *Molecular Neurodegeneration 2020 15:1* **15**, 1–18.

[316] Solowska, J. M & Baas, P. W. (2015) Hereditary spastic paraplegia SPG4: What is known and not known about the disease. *Brain* **138**, 2471–2484.

[317] De Pace, R, Britt, D. J, Mercurio, J, Foster, A. M, Djavaherian, L, Hoffmann, V, Abebe, D, & Bonifacino, J. S. (2020) Synaptic vesicle precursors and lysosomes are transported by different mechanisms in the axon of mammalian neurons. *Cell Rep.* **31**, 107775.

[318] Reid, E, Kloos, M, Ashley-Koch, A, Hughes, L, Bevan, S, Svenson, I. K, Graham, F. L, Gaskell, P. C, Dearlove, A, Pericak-Vance, M. A, Rubinsztein, D. C, & Marchuk, D. A. (2002) A kinesin heavy chain (KIF5A) mutation in hereditary spastic paraplegia (SPG10). *American journal of human genetics* **71**, 1189–1194.

[319] Zhao, X, Alvarado, D, Rainier, S, Lemons, R, Hedera, P, Weber, C. H, Tukel, T, Apak, M, Heiman-Patterson, T, Ming, L, Bui, M, & Fink, J. K. (2001) Mutations in a newly identified GTPase gene cause autosomal dominant hereditary spastic paraplegia. *Nature genetics* **29**, 326–331.

[320] Lessard, D. V, Zinder, O. J, Hotta, T, Verhey, K. J, Ohi, R, & Berger, C. L. (2019) Polyglutamylation of tubulin's C-terminal tail controls pausing and motility of kinesin-3 family member KIF1A. *The Journal of biological chemistry* **294**, 6353–6363.

[321] Maas, C, Belgardt, D, Han, K. L, Heisler, F. F, Lappe-Siefke, C, Magiera, M. M, Van Dijk, J, Hausrat, T. J, Janke, C, & Kneussel, M. (2009) Synaptic activation modifies microtubules underlying transport of postsynaptic cargo. *Proceedings of the National Academy of Sciences of the United States of America* **106**, 8731.

[322] Misgeld, T, Burgess, R. W, Lewis, R. M, Cunningham, J. M, Lichtman, J. W, & Sanes, J. R. (2002) Roles of neurotransmitter in synapse formation: Development of neuromuscular junctions lacking choline acetyltransferase. *Neuron* **36**, 635–648.

[323] Wang, M, Misgeld, T, & Brill, M. S. (2022) Neural labeling and manipulation by neonatal intraventricular viral injection in mice. *STAR protocols* **3**.

[324] Yasuda, M, Nagappan-Chettiar, S, Johnson-Venkatesh, E. M, & Umemori, H. (2021) An activity-dependent determinant of synapse elimination in the mammalian brain. *Neuron* **109**, 1333–1349.e6.

[325] Miller, K. E & Heald, R. (2015) Glutamylation of Nap1 modulates histone H1 dynamics and chromosome condensation in Xenopus. *The Journal of cell biology* **209**, 211–220.

[326] Regnard, C, Desbruyères, E, Huet, J. C, Beauvallet, C, Pernollet, J. C, & Eddé, B. (2000) Polyglutamylation of Nucleosome Assembly Proteins. *Journal of Biological Chemistry* **275**, 15969–15976.

[327] Van Dijk, J, Miro, J, Strub, J. M, Lacroix, B, Van Dorsselaer, A, Edde, B, & Janke, C. (2008) Polyglutamylation Is a Post-translational Modification with a Broad Range of Substrates. *Journal of Biological Chemistry* **283**, 3915–3922.

[328] Kesarwani, S, Lama, P, Chandra, A, Reddy, P. P, Jijumon, A. S, Bodakuntla, S, Rao, B. M, Janke, C, Das, R, & Sirajuddin, M. (2020) Genetically encoded live-cell sensor for tyrosinated microtubules. *The Journal of cell biology* **219**.

[329] Rossi, J, Balthasar, N, Olson, D, Scott, M, Berglund, E, Lee, C. E, Choi, M. J, Lauzon, D, Lowell, B. B, & Elmquist, J. K. (2011) Melanocortin-4 receptors expressed by cholinergic neurons regulate energy balance and glucose homeostasis. *Cell Metabolism* **13**, 195–204.

[330] Muñoz-Castañeda, R, Díaz, D, Peris, L, Andrieux, A, Bosc, C, Muñoz-Castañeda, J. M, Janke, C, Alonso, J. R, Moutin, M. J, & Weruaga, E. (2018) Cytoskeleton stability is essential for the integrity of the cerebellum and its motor- and affective-related behaviors. *Scientific Reports 2018 8:1* **8**, 1–14.

[331] Hausrat, T. J, Janiesch, P. C, Breiden, P, Lutz, D, Hoffmeister-Ullerich, S, Hermans-Borgmeyer, I, Failla, A. V, & Kneussel, M. (2022) Disruption of tubulin-alpha4a polyglutamylation prevents aggregation of hyperphosphorylated tau and microglia activation in mice. *Nature Communications 2022 13:1* **13**, 1–18.

[332] Feng, G, Mellor, R. H, Bernstein, M, Keller-Peck, C, Nguyen, Q. T, Wallace, M, Nerbonne, J. M, Lichtman, J. W, & Sanes, J. R. (2000) Imaging neuronal subsets in transgenic mice expressing multiple spectral variants of GFP. *Neuron* **28**, 41–51.

[333] Madisen, L, Zwingman, T. A, Sunkin, S. M, Oh, S. W, Zariwala, H. A, Gu, H, Ng, L. L, Palmiter, R. D, Hawrylycz, M. J, Jones, A. R, Lein, E. S, & Zeng, H. (2010) A robust and high-throughput Cre reporting and characterization system for the whole mouse brain. *Nature neuroscience* **13**, 133–140.

[334] Brill, M. S, Lichtman, J. W, Thompson, W, Zuo, Y, & Misgeld, T. (2011) Spatial constraints dictate glial territories at murine neuromuscular junctions. *Journal of Cell Biology* **195**, 293–305.

[335] Passini, M. A & Wolfe, J. H. (2001) Widespread gene delivery and structure-specific patterns of expression in the brain after intraventricular injections of

neonatal mice with an adeno-associated virus vector. *Journal of virology* **75**, 12382–12392.

[336] Love, M. I, Huber, W, & Anders, S. (2014) Moderated estimation of fold change and dispersion for RNA-seq data with DESeq2. *Genome Biology* **15**, 1–21.

[337] Misgeld, T, Kerschensteiner, M, Bareyre, F. M, Burgess, R. W, & Lichtman, J. W. (2007) Imaging axonal transport of mitochondria in vivo. *Nature methods* **4**, 559–561.

[338] Kerschensteiner, M, Reuter, M. S, Lichtman, J. W, & Misgeld, T. (2008) Ex vivo imaging of motor axon dynamics in murine triangularis sterni explants. *Nature Protocols* **3**, 1645–1653.

[339] Berger, D. R, Seung, H. S, & Lichtman, J. W. (2018) VAST (Volume Annotation and Segmentation Tool): Efficient manual and semi-automatic labeling of large 3D image stacks. *Frontiers in Neural Circuits* **12**, 88.

[340] Goiran, T, Eldeeb, M. A, Zorca, C. E, & Fon, E. A. (2022) Hallmarks and Molecular Tools for the Study of Mitophagy in Parkinson's Disease. *Cells 2022, Vol. 11, Page 2097* **11**, 2097.

[341] Yu, Z, Wang, H, Tang, W, Wang, S, Tian, X, Zhu, Y, & He, H. (2021) Mitochondrial Ca2+ oscillation induces mitophagy initiation through the PINK1-Parkin pathway. *Cell Death and Disease 2021 12:7* **12**, 1–7.

[342] Niblack Wayne. (1986) *An introduction to image processing.* (Scientific Research Publishing, Prentice Hall, Englewood Cliffs).

[343] Jian-wu, L, Xuan-jing, S, Hui, Z, & Hai-peng, C. (2013) Adaptive Image Thresholding by Background Subtraction. pp. 116–119.

[344] Otsu, N. (1979) Threshold selection method from gray-level histograms. *IEEE Trans Syst Man Cybern* **SMC-9**, 62–66.

[345] Sato, Y, Shiraga, N, Nakajima, S, Tamura, S, & Kikinis, R. (1998) Local maximum intensity projection (LMIP): a new rendering method for vascular visualization. *Journal of computer assisted tomography* **22**, 912–917.

[346] Wallis, J. W, Miller, T. R, Lerner, C. A, & Kleerup, E. C. (1989) Three-Dimensional Display in Nuclear Medicine. *IEEE Transactions on Medical Imaging* **8**, 297–303.

[347] Schindelin, J, Arganda-Carreras, I, Frise, E, Kaynig, V, Longair, M, Pietzsch, T, Preibisch, S, Rueden, C, Saalfeld, S, Schmid, B, Tinevez, J. Y, White, D. J, Hartenstein, V, Eliceiri, K, Tomancak, P, & Cardona, A. (2012) Fiji: an open-source platform for biological-image analysis. *Nature methods* **9**, 676–682.

Acknowledgements

This work would not have been possible without the financial and scientific support of my PhD supervisors, so I would like to express my gratitude to Dr. Monika Brill and Prof. Dr. Thomas Misgeld.
I would also like to thank my Thesis Advisory Committee Prof. Dr. Carsten Janke and Prof. Dr. Conny Kopp-Scheinpflug, for their insightful comments and precious encouragement along the way. Thanks also to Dr. Shaul Yogev for agreeing to be part of my Examination Committee and correcting the thesis and our fun and insightful discussions.
I am also deeply thankful to the GSN, not only for providing the network and possibility to meet new people and experiences but also supporting me financially. Thanks in particular, to Lena and Stefanie for always being there to listen and help.
To my fellow labmates Pui Shee, Robin, Grace, Ana, Natalia, Andrian, Selin, Eleni, Roberta, Anna, Anxhela, Omar, Marlly, Sharzad, Katharina, and Mihai: the memories we made, and the experiences we shared will forever be etched in my mind. Thanks to Maurits and Sarah, but also Katharine and Theresa, I am lucky to have found such great students to supervise and even better friends.
From the Institute of Neuronal Cell Biology, thanks to Kristina Wulliman for always having such a bright and positive attitude, Manuela and Nebi for helping with the mice and having nice chats despite my broken German, and to Rosi for always being ready to share your expertise with kindness.
To my family, I simply wish to say thank you for your unconditional love and support. Faleminderit mami e babi, për tana mundsin që në keni hap me sakrificat të tuja, për besimin që keni të unë dhe per dashurin pa fundësi që keni për ne. Mundem vetëm të aspiroj me kën si ju. Marsida, Mirela e

Franci, e dini se ju dua shum.
Un immenso grazie a Giuliana and Mauro, per il vostro supporto e per essere stati una seconda casa per me.
To my dearest friends, thanks for your love, for being present and for making my life pleasant, fun and enriching in every way. Valentina, Christina, Aleli and Francescka, to me you are an immeasurable treasure.
To Alan, words cannot express how meaningful you have been to my life. Thanks for sharing this experience with me and for being there through thick and thin. You are the real mvp.
This PhD has challenged me in so many ways, and through it all, I have grown scientifically and as a person. Thus in an unconventional way, I also want to thank myself for persevering through tough times and making it until here.
Looking back, I will think of many of these moments with fondness.

Declaration of authors' contributions

Antoneta Gavoci[1], Anxhela Zhiti[1], Michaela Rusková[2], Mengzhe Wang[1], Elisabeth Graf[3], Natalia Marahori[1], Martina Schifferer[4], Magda Magiera[5], Carsten Janke[5], Mattias Kneussel[6], Martin Balastik[2], Thomas Misgeld[1,4,7] and Monika S. Brill[1,7]

[1]**Institute of Neuronal Cell Biology,** Technische Universität München, *Biedersteiner Straße 29, 80802 Munich, Germany*

[2]**Department of Molecular Neurobiology,** Institute of Physiology of the Czech Academy of Sciences, *Prague, Czech Republic*

[3]**Core Facility Next-Generation-Sequencing**, Institute of Human Genetics, Helmholtz Zentrum Muenchen, Deutsches Forschungszentrum fuer Gesundheit und Umwelt (GmbH), *Ingolstaedter Landstr. 1, 85764, Neuherberg, Germany*

[4]**German Center for Neurodegenerative Diseases (DZNE)**, *Feodor-Lynen-Straße 17, 81377 Munich, Germany*

[5]**Institut Curie,** PSL Research University, CNRS UMR3348, F-91401 Orsay, France; *Université Paris-Saclay, CNRS UMR3348, F-91401 Orsay, France*

[6]**Institute for Molecular Neurogenetics,** Center for Molecular Neurobiology (ZMNH), University Medical Center Hamburg-Eppendorf, *Falkenried 94, 20251 Hamburg, Germany*

[7]**Munich Cluster of Systems Neurology (SyNergy),** *Feodor-Lynen-Straße 17, 81377 Munich, German*

A.G designed the study, performed experiments, analysed and interpreted the data and wrote the thesis.
A.Z. conducted fixation, immunostaining and data analysis of Tuba4A experiments and βmonoE of CCP1/6$^{\mathrm{mnKO}}$; **A.G.** conducted statistical analysis.
M.R. performed TTLL1$^{\mathrm{KO}}$ CNS immunostaining and data analysis.
M.W. performed BTX injections on Spastin WT and KO models and A.Z image analysis, **A.G.** performed fixation and immunostaining and statistical analysis.
E.G. performed next-generation sequencing of Ribotagged motor neurons.
N.M. performed mito-keima injections and image acquisition of TTLL1$^{\mathrm{mnKO}}$ and mito-keima injections and transport parameter analysis of adult CCP1/6$^{\mathrm{mnKO}}$.
M.S. performed EM ultrastructural protocol.
M.K. provided Tuba4a$^{\mathrm{KI}}$ mouse line.
M.M., C.J. and M.B. contributed to study direction.
T.M. and M.S.B supervised the study, guided experimental design and interpretation and provided funding.

München / Munich
30$^{\mathrm{th}}$ May, 2023

Signature Antoneta Gavoci

Signature Prof. Dr. med. Thomas Misgeld (Supervisor)